

Micromechanical Model for Dilatant Crack Growth  
in Brittle Materials, with Applications to Rock  
Physical Properties.

by

Juan Manuel Alvarez-Tostado Sanchez

Thesis submitted for the degree of  
Doctor of Philosophy (PhD)  
of the University of London

University College London

July, 1998

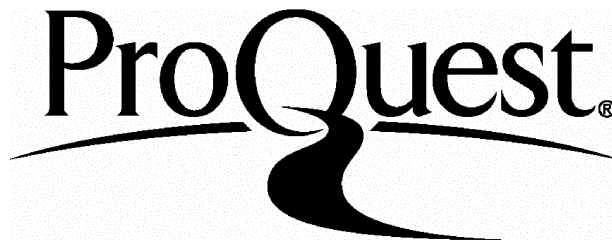
ProQuest Number: 10013917

All rights reserved

INFORMATION TO ALL USERS

The quality of this reproduction is dependent upon the quality of the copy submitted.

In the unlikely event that the author did not send a complete manuscript and there are missing pages, these will be noted. Also, if material had to be removed, a note will indicate the deletion.



ProQuest 10013917

Published by ProQuest LLC(2016). Copyright of the Dissertation is held by the Author.

All rights reserved.

This work is protected against unauthorized copying under Title 17, United States Code.  
Microform Edition © ProQuest LLC.

ProQuest LLC  
789 East Eisenhower Parkway  
P.O. Box 1346  
Ann Arbor, MI 48106-1346

## Abstract

Brittle behaviour is an important characteristic of crustal rocks, it accounts for the seismic behaviour of the crust, helps to elucidate the flow of fluids and melts, the transport of dissolved minerals and the transmission of heat in the crust.

This thesis is centred on the formulation of a theoretical model of microcrack growth to simulate the effect of cracks on deformation and the consequences on some physical properties of brittle materials subjected to external loads. The model, which is two-dimensional (using the plane theory of elasticity), is based on the formation of new dilatant cracks (NDCs) from pre-existing (Griffith type) cracks (PECs). The driving force that opens the NDCs is the intensified tensile stresses occurring near the PEC crack tips. NDCs relax the relative displacement between the crack surfaces of the PECs. The trajectories and lengths of the NDCs are calculated. They are a function of the PEC orientation. Their growth is stable over a range of applied compressive stresses, but at higher loads NDCs can become unstable. The introduction of confining pressure widens the range of stability and changes the direction of growth of the NDCs.

The formation of NDCs depends on the PEC orientation relative to the applied stress field, so that as the stress increases, PECs with a wider range of orientations create NDCs. Although the orientation of PECs is isotropic, the resulting NDC population is highly anisotropic.

Three consequences of the formation of NDCs are considered. The first of these is the cumulative acoustic emission (AE) which results from NDC formation, which is compared with experimental data. The second is the peak strength and fracture of a brittle body, and here again comparison is made with experimental data. Thirdly the effect of NDCs on elastic properties of a body is worked out. Because the theory is two-dimensional exact quantitative comparison can not be made with experimental data, which is inherently three-dimensional. However, qualitative comparison is possible.

In addition, by using the concept of crack density tensor, information about the crack orientation distribution in an actual deformed body is obtained from measurements of elastic waves velocities. The variation of crack density  $\varepsilon$  and anisotropy coefficients ( $\alpha_{11}, \alpha_{22}, \alpha_{33}$ ) with applied load is determined.

# Contents

<b>1</b>	<b>Introduction</b>	<b>12</b>
1.1	Crustal Mechanics . . . . .	12
1.1.1	Effects of pore fluid . . . . .	15
1.2	Rock Mechanics. . . . .	16
1.2.1	Brittle Rocks . . . . .	19
1.3	Brittle fracture processes . . . . .	20
1.4	Elastic properties of cracked solids . . . . .	21
1.5	Importance of a new model of crack growth based on simple assumptions.	25
<b>2</b>	<b>Fundamentals of Griffith crack model.</b>	<b>28</b>
2.1	Mathematical models of cracks. . . . .	28
2.2	Elliptical model of Griffith . . . . .	30
2.3	NDC (Wing Crack) initiation and development. . . . .	31
2.3.1	Experimental evidence of wing crack existence. . . . .	31
2.3.2	Analytical modelling of wing crack growth. . . . .	33
2.4	Pile-up model of crack nucleation. . . . .	35
<b>3</b>	<b>Growth of new dilatant crack (NDC) population.</b>	<b>37</b>
3.1	Crack model developed in this thesis. . . . .	37
3.1.1	Introduction . . . . .	37
3.1.2	Stress and strain around a pre-existing crack . . . . .	40
3.1.3	Effective stresses for closed cracks and fluid filled cracks . . . . .	43
3.1.4	Wing crack nucleation . . . . .	44
3.1.5	First PEC in nucleate wing cracks . . . . .	46
3.1.6	Stress around a wing crack . . . . .	49
3.1.7	Wing crack growth . . . . .	51

<i>CONTENTS</i>	4
3.1.8 Length of wing cracks . . . . .	54
3.1.9 Stability of wing cracks . . . . .	55
3.2 Effects of a population of Wing Cracks (NDCs) on Rock Physical Properties	58
3.2.1 Anisotropy. . . . .	58
3.2.2 Ultimate Failure of Rock. . . . .	59
3.2.3 Elastic Properties of Cracked Solids . . . . .	63
3.3 Acoustic emission. . . . .	71
<b>4 Effective elastic properties of cracked solids.</b>	<b>74</b>
4.1 Introduction . . . . .	74
4.2 The crack density tensor concept . . . . .	75
4.2.1 Calculation of $\eta_1$ and $\eta_2$ for dry cracks . . . . .	77
4.2.2 Reduced elastic potential . . . . .	80
4.2.3 $\eta$ as a function of $\epsilon$ . . . . .	81
4.2.4 Elastic Compliances . . . . .	82
4.3 Isotropic Case . . . . .	82
4.4 Transverse Isotropy . . . . .	83
4.5 Elastic properties of an isotropic uncracked medium. . . . .	84
4.6 Elastic Wave velocities in a transversely isotropic medium. . . . .	85
4.7 Orthorhombic symmetry . . . . .	86
4.8 Experimental Data . . . . .	89
4.9 Cylindrical Geometry Testing Results. . . . .	94
4.10 Cubical Geometry Testing Results. . . . .	99
4.11 Conclusions . . . . .	102
<b>5 Discussion and Conclusions</b>	<b>104</b>
<b>References</b>	<b>107</b>

# List of Figures

- 1.1 Typical stress-strain curves for rocks.
- 1.2 Penny-shaped crack with radius  $a$  and minor axis  $b$ .
- 1.3 Random distribution of cracks (RDC).
- 1.4 Cylindrical transverse isotropy (CTI).
- 1.5 Planar transverse isotropy (PTI).
- 1.6 Elastic moduli for the crack distributions considered.
  
- 2.1 Nucleation of microcrack by dislocation pile-up.
  
- 3.1 Model of Brittle material.
- 3.2 Generation of wing cracks and frames of reference used.
- 3.3 Normalised peak tangential stress at PECs' surface. Uniaxial compression case, and low coefficient of friction.
- 3.4 Normalised peak tangential stress at PECs' surface. Biaxial compression case and low coefficient of friction.
- 3.5 Normalised peak tangential stress at PECs' surface. Uniaxial compression case and high coefficient of friction.
- 3.6 Crack with a dislocation under far-field stresses.
- 3.7 Normalised tangential stress at the NDC tip.  $\mu_f = 0.5$  and  $p_0 = 0$ .
- 3.8 Normalised tangential stress at the NDC tip.  $\mu_f = 0.5$  and  $p_0 = 20K_t$ .
- 3.9 Normalised tangential stress at the NDC tip.  $\mu_f = 0.1$  and  $p_0 = 0$ .
- 3.10 Normalised wing crack length as a function of applied stress, for several confining pressures.  $\theta = 15^\circ, 30^\circ$
- 3.11 Normalised wing crack length as a function of applied stress, for several confining pressures.  $\theta = 45^\circ, 75^\circ$
- 3.12 Length and orientation of the wing crack.
- 3.13 Fracture Angle as a function of confining pressure.

- 3.14 Failure stress vs. confining pressure for 3 kinds of rocks.
  - 3.15 Failure stress vs. confining pressure for Darley Dale sandstone.
  - 3.16 Failure stress vs. confining pressure for microgranodiorite.
  - 3.17 Failure stress vs. confining pressure for Polycrystalline ice.
  - 3.18 Stress vs. axial, lateral and volumetric strain curves. Uniaxial compression.
  - 3.19 Stress vs. axial, lateral and volumetric strain curves. Biaxial compression.
  - 3.20 Number of NDC and cumulative number of AE events as functions of deviatoric stress.
- 
- 4.1 Elastic wave velocities  $V_P$  and  $V_S$  as a function of confining pressure.
  - 4.2 Compressional wave velocity versus differential stress at different confining pressures.
  - 4.3 Shear wave velocity versus differential stress at different confining pressures.
  - 4.4 Scalar crack density  $\varepsilon$  as a function of deviatoric stress using 3 methods.
  - 4.5 Variation of crack density with stress for different confining pressures  $p_0$ , using  $V_P$  and  $V_S$ .
  - 4.6 Variation of scalar crack density and anisotropy coefficients with mean stress, for hydrostatic test and for triaxial deformation.
  - 4.7 Comparison with Stuart's method.
  - 4.8 Scalar crack density  $\varepsilon$  and coefficients of the crack density tensor  $\alpha$  as functions of the applied mean stress for a triaxial test.
  - 4.9 Changes in compressional and shear wave velocities with mean stress.

## Acknowledgments

I am very grateful to my supervisor S.A.F. Murrell, whose enthusiasm, guidance and encouragement were fundamental during the writing of this thesis. I really appreciate the time he spent making numerous constructive comments and suggestions for the development of my research.

I wish to thank M.R. Ayling, P.R. Sammonds, C.E. Stuart and P. Baud of the Rock and Ice Physics group in UCL for providing experimental data as well as C. Sayers of Schlumberger Cambridge Research who provided the idea of using the crack density tensor to analyse the data.

Thanks to Ricardo Carretero, Alexandra Chávez, Raul Michel, Patrick Baud, Javier Gómez, Richard Rabe, Richard Rozanski, Mónica Pérez, Gerardo Ocaña, Vittor Bonifacio and others too numerous to mention for their friendly support.

I am grateful for the financial support of the Consejo Nacional de Ciencia y Tecnología (CONACYT) of Mexico. Thanks go to the people from Instituto de Física UNAM whom backed up my application for a scholarship. Special thanks to O. Novaro and the late J. Lomnitz-Adler.

Finally, and primarily I would like to express my gratitude to Xochitl Blanco-Cano for providing ongoing inspiration and for her constant support, concern and motivation throughout the composition of this work.

## Symbols

	First used in equation...
$a$ , distance between dislocation source $S$ and barrier $B$ .	(2.9)
$a$ , largest axis of elliptical hole.	Figure (3.1)
$\bar{a}$ , average radius of crack.	(1.2)
$a_\alpha$ , radius of the $\alpha$ th crack.	(1.6)
$A$ , area of crack.	(1.1)
$b$ , interatomic spacing.	(2.13)
$b$ , smallest axis of elliptical hole.	Figure (3.1)
$b_0$ , minor axis of the NDC.	(3.86)
$b$ , magnitude of the average Burgers vector.	(2.9)
$b_1, b_2$ , components of the Burgers vector.	(3.54)
$\mathbf{b}$ , Burgers vector.	Figure (3.6)
$C_{ijkl}$ , stiffness tensor components.	(4.61)
$c$ , semilength of a crack.	(2.3)
$c$ , semilength of the NDC.	(3.60)
$c_I, c_{II}$ , values of $c$ for which $\sigma_{\beta\beta} = T$ .	Figure (3.7)
$E^0, \nu^0$ , Young's modulus and Poisson's ratio of the uncracked solid.	(4.9)
$E$ , Young's Modulus.	(2.2)
$f_k$ , volume fraction of cracks.	(3.90)
$f(\theta)$ , angular part of the local field about the crack tip.	(2.1)
$f$ , elastic potential.	(4.2)
$F$ , magnitud of splitting forces.	(2.6)
$H^0$ , initial compliance of homogeneous material.	(1.4)
$H$ , effective compliance of cracked material.	(1.4)
$K, K_I$ , stress intensity factor.	(2.1)
$K_t$ , macroscopic tensile strength of the body.	(2.4)
$l$ , semilength of pre-existing crack.	(2.6)
$l$ , distance between foci of elliptical crack.	(3.1)
$\max \sigma_{\beta\beta}$ , maximum tangential stress.	(3.31)
$n$ , number of cracks per unit volume.	(1.1)
$n_\alpha$ , number of cracks with radius $a_\alpha$ .	(1.6)
$n$ , number of dislocations generated by a source $S$ .	(2.9)

$\hat{n}$ , normal vector.	(3.89)
$N$ , total number of cracks.	(1.5)
$P$ , perimeter of the crack.	(1.1)
$p_0$ , confining pressure.	Figure (3.3)
$r$ , radial coordinate.	(2.1)
$S$ , dislocation source; surface of cracks.	Figure (2.1)
$S_{ijkl}$ , elastic compliances tensor components.	(4.2)
$T$ , theoretical strength of the material, <i>i.e.</i> , maximum tensile interatomic force per unit area.	(2.14)
$u_i$ , displacement component.	(2.2)
$\vec{u}$ , displacement vector.	(4.5)
$U_x, U_y$ , displacement components.	(3.10)
$V$ , volume of the sample.	(3.89)
$V_P^0, V_S^0$ , compressional and shear wave velocities for an isotropic uncracked solid.	(4.70)
$V_{ij}$ , wave velocities. The first index indicates direction of propagation of the wave, and the second index the direction of particle motion (polarisation).	(4.76)
$x, y$ , cartesian coordinates.	(3.1)
$Y$ , dimensionless geometry and edge effect modification factor.	(2.3)
$z$ , complex coordinate.	(3.1)
$z$ , plane in which the hole is elliptical.	
$\alpha_0$ , aspect ratio of the PEC.	(3.4)
$\alpha_1$ , aspect ratio of the NDC.	(3.70)
$\alpha_{11}, \alpha_{22}, \alpha_{33}$ , anisotropy coefficients.	(4.45)
$\alpha$ , second order crack density tensor.	(4.1)
$\alpha, \beta$ , elliptical coordinates.	(3.1)
$(\alpha_0, \beta_c)$ , point in the surface of the ellipse where the wing crack nucleate.	(3.30)
$\delta\Omega$ , boundary of cracks.	(3.91)
$\Delta\sigma$ , deviatoric stress.	Figure (3.7)
$\Delta\vec{u}$ , crack opening displacement vector.	(3.91)
$\Delta U_x, \Delta U_y$ , relative displacements of the pre-existing crack surfaces.	(3.14)
$\epsilon, \epsilon_{ij}$ , strain tensor.	(1.4)
$\bar{\epsilon}^k$ , average strain over the $k$ th crack.	(3.90)
$\epsilon_{\text{mat}}$ , contribution of the rock matrix to strains.	(3.109)

$\epsilon'_{\text{pec}}$ , contribution of the PEC to strains, in the local coordinates of the PECs. (3.92)

$\epsilon''_{\text{wc}}$ , contribution of the NDC to strains, in the local coordinates of the NDCs. (3.94)

$\epsilon''_{\text{dis}}$ , contribution of the dislocated crack to strain, in the local coordinates of the NDCs.

(3.95)

$\epsilon_{\text{local}}, \sigma_{\text{local}}$ , strain and stress in the local coordinate system. (3.100)

$\epsilon_{\text{lab}}, \sigma_{\text{lab}}$ , strain and stress in the laboratory frame of reference. (3.100)

$\epsilon_{\text{total}}$ , total contribution of a single pre-existing crack to strains. (3.107)

$\epsilon$ , overall strains. (3.108)

$\epsilon$ , crack density parameter. (1.1)

$\epsilon_{\alpha}$ , crack density of cracks with radius  $a_{\alpha}$ . (1.5)

$\epsilon$ , angle between the major axis of the NDC and the Burgers vector  $\mathbf{b}$ . (3.71)

$\bar{\epsilon}^c$ , average strain due to cracks. (3.89)

$\eta_1, \eta_2, \omega_1, \omega_2$ , functions of the invariants of  $\alpha$ . (4.3)

$\gamma$ , angle between equivalent crack and pre-existing crack. (2.8)

$\gamma$ , angle to the slip plane. (2.11)

$\gamma_0$ , angle between the wing crack and the PEC major axis. (3.40)

$\kappa = (3 - \nu)/(1 + \nu)$ , for plane stress. (3.10)

$\kappa = (3 - 4\nu)$ , for plain strain. (3.10)

$\Lambda(\theta), \Upsilon(\theta)$ , transformation matrices for strains and stresses from local to laboratory frame of reference. (3.100)

$\mu_f$ , coefficient of friction. (2.7)

$\mu$ , shear modulus. (2.9)

$\nu$ , Poisson's ratio. (2.9)

$\omega(\xi)$ , conformal transformation. (3.3)

$\Omega_k$ , volume of the  $k$ th cavity. (3.90)

$\phi_0$ , angle between the major axis of the PEC and the Burgers vector. (3.71)

$\phi, \psi$ , elastic complex potentials. (3.8)

$\Phi$ , crack porosity.

$\rho$ , distance from the pile up point. (2.11)

$\rho$ , crack tip radius of curvature. (3.85)

$\rho^0$ , density of the uncracked solid. (4.70)

$\sigma, \sigma_{kl}$  stress tensor. (1.4)

$\sigma_{11}^0, \sigma_{22}^0$ , far field stresses. (2.4)

$\sigma_{\gamma\gamma}$ , normal tension. (2.11)

- $\sigma_{\rho\rho}, \sigma_{\beta\beta}$ , stresses in polar coordinates. (3.8)
- $\sigma_{\beta\beta}$ , tangential stress on the boundary of the crack. (3.13)
- $\sigma_{11}, \sigma_{22}, \tau_{12}$ , far field stresses in the local coordinate system of the PEC. (3.16)
- $\sigma_1, \sigma_2, \tau$ , effective stresses acting on the crack plane. (3.24)
- $\sigma_c$ , closure stress. (3.24)
- $\sigma_f$ , ultimate failure stress. (3.14)
- $\tau^*$ , local shear stress. (2.6)
- $\tau$ , shear stress. (2.9)
- $\tau_0$ , frictional resistance, Peierls' force. (2.10)
- $\theta$ , angle between far field stress and  $F$ . (2.7)
- $\theta$ , angle between major axis of a crack and far field stress. (3.11)
- $\theta_0$ , angle between the major axis of the PEC's with the principal direction  $Oy'$ . (3.35)
- $\theta_1$ , angle between the major axis of the NDC's with the principal direction  $Oy'$ . (3.72)
- $[\theta_L, \theta_U]$ , range of cracks that will nucleate wing cracks. Figure (3.3)
- $\xi$ , complex number. (3.1)
- $\xi$ , plane in which the hole becomes circular. (3.3)

### Abbreviations

- AE, acoustic emission.
- BDT, brittle-to-ductile transition.
- CTI, cylindrical transverse isotropy.
- DS, differential scheme.
- LEFM, linear elastic fracture mechanics.
- MEF, method of effective field.
- NDCs, new dilatant cracks.
- PECs, pre-existing cracks.
- PMMA, polymethylmethacrylate.
- PTI, planar transverse isotropy.
- RDC, random distribution of cracks.
- SC, self-consistent method.

# Chapter 1

## Introduction

The first section of the Introduction provides some geophysical motivation for the study of brittle fracture. We give a sketch of the crustal conditions of the Earth and the brittleness of rocks within the crust and the consequent important phenomena such as faults and earthquakes. The role of fluids in the crust is briefly discussed.

In the second section of this chapter the deformation of rocks under compressive stresses is briefly described. An interpretation of those experimental results in terms of cracks is given and experimental evidence of nucleation of wing cracks (NDCs) is outlined.

Brittle rocks are defined and brittle fracture processes are described. Some methods to calculate the overall elastic properties of cracked solids are reviewed.

Finally a review of the next chapters of this thesis is presented.

### 1.1 Crustal Mechanics

Under the relatively low pressures and temperatures at shallow depths in the Earth's crust, brittle fracture is the dominant mechanism of rock failure. The onset of fracture and the fracture itself strongly influence the physical and mechanical behaviour of the rock mass, in a way that they can be seen as premonitory events from which it may some day be possible to predict earthquakes (see Paterson, 1978; Scholz, 1990; Jaeger & Cook, 1979). The upper parts of the crust typically show evidence of widespread fracturing (faults, joints, veins), often mineralised, and in tectonically active areas earthquakes are widely believed to occur by renewed movement on existing faults. However, the latter requires that the crustal stress field is suitable oriented (Jaeger & Cook, 1979).

The knowledge of the state and magnitude of stress in the Earth's lithosphere and the

effects due to stress, are important in order to understand various geophysical problems such as the tectonic plate driving mechanism, the energy budget of the Earth, earthquake mechanisms and crustal movements (Turcotte & Schubert, 1982). A large fraction of the deformation in the upper continental crust occurs on faults. Slip movements along geological faults are usually restricted to about the upper 15 *km* of the crust in most zones of continental deformation (Scholz, 1990). This is the so-called brittle lithosphere (*schizosphere*) where most of the earthquakes occur. Beneath the brittle zone is a plastic zone (*plastosphere*) in which plastic deformation occurs. The two zones together form a strong layer known as the lithosphere that can reach depths of 100 *km* in some parts of the Earth. Where the lithosphere is subducted into the hotter mantle, the cool, strong and brittle uppermost part continues to exist to considerable depths, because of the low thermal conductivity of rocks (e.g. Murrell, 1986) and this is associated with the occurrence of deep earthquakes.

The stresses in the Earth, and in the crust in particular are normally compressive. Gravitational forces make a major contribution to these stresses, but heat from Earth's interior (by conduction and convection) is the major cause of the complex stress fields in the lithosphere. It is important to remember that in the brittle crust cracks and faults are generally filled with fluids (typically aqueous) which are under a depth-dependent pressure. Because of this, the crustal response depends on the effective stresses (the difference between the boundary stresses —generally compressive— and the internal (pore ) fluid pressures)(Scholz, 1990).

In regions of compressive stress, faulting occurs in response to shear stresses. However, in regions of crustal extension (spreading centres/mid-ocean ridges, basins, etc.) extensional or tensional fracture may also occur (joints and vein structures are evidence of this). The mechanisms of fracture are more fully discussed below.

The magnitudes of stress in the brittle lithosphere inferred from various measurements and models differ greatly. From studies of stress drop (change in the stress before and after an earthquake) in large earthquakes it seems likely that there exists a stress difference of about 1 to 10 MPa within the crust (Kanamori & Anderson, 1975), *i.e.*, many active faults are sliding in response to very low levels of shear stress. The maximum strain change associated with large earthquakes is about 2 to  $3 \times 10^{-4}$ , and therefore the Earth's crust cannot sustain a strain exceeding this value. Since the rigidity of crustal rocks is about  $3 \times 10^4$  MPa, this result suggest that the strength of the Earth's crust is about 6 to 9 MPa (Kanamori, 1980).

On the other hand, the *lithostatic* stress due to the overburden of rock should give a stress difference of 150 MPa under high topographic reliefs such as the Himalayas (Jeffreys, 1959). Such differences in the estimate of the stress might suggest either that only a small fraction of the tectonic stress is released in earthquakes or that there are weak zones (maybe generated by the presence of high temperatures), where the tectonic stress is low, and strong zones where the local stress is very high so that when integrated over the whole fault, a very low average stress drop results. Additionally, the estimated stress necessary to overcome the friction on a fault at depth, is greater than the cohesive strength of the rock. Because of this it is difficult to explain the origin of deep earthquakes (in subduction zones they may be as deep as 700km). The existence of high pore pressure may be necessary to enable deep earthquakes to occur (Murrell & Ismail 1976).

The state of stress in the lithosphere is the result of the superposition of a variety of forces (Turcotte, 1983; Hickman, 1991) . The more evident being the one produced by gravity or geostatic stress that increases with depth, although there are several assumptions regarding the horizontal stresses due to gravity (Heim's rule for instance, see Jaeger and Cook, 1979), analytical solutions for an elastic medium under gravity with an irregular surface are not available. Another important contribution to the stress field is of tectonic origin (plate-boundary forces, forces due to plate flexure and isostatically compensated uplifts). These long-range forces are transmitted over large distances within a plate. Local stresses (deviatoric stresses induced by phase changes and changes in pore pressure, stresses induced by fault-slip and strength anisotropy, stresses induced by lithological and rheological heterogeneities, and thermoelastic stresses, etc.) might dominate sometimes, although their range of influence is short. The thermal stress originating from heat transfer in the lithosphere also provides enough tensile stress to cause the fracture of upper crustal rocks (Hickman, 1991).

Because of this complex image of superposition of different stresses from different sources, the resultant stress field might have a complicated configuration. Generally, the resultant horizontal stresses are higher than the resultant vertical stress (Hast 1973; Herget 1973), although of the same order of magnitude. For depths greater than 1 Km the horizontal and vertical components tend to be similar. It is assumed for simplification that the vertical and horizontal stresses are principal stresses though this is not always the case.

Anderson (1951) classified the kind of faulting according to the relative magnitude of the vertical component of the effective stress with respect to the other two components (see Scholz, 1990):

1. Thrust Faulting, in which the vertical stress is the minimum principal compressive stress,
2. Strike-Slip Faulting, in which the vertical component of stress is the intermediate principal compressive stress, and
3. Normal Faulting in which the vertical stress is the maximum principal compressive stress.

The depth-averaged shear strengths of faults in the brittle continental crust calculated using a coefficient of friction,  $\mu$ , of 0.9 and in the absence of high pore pressures are 150, 60 and 35 MPa respectively. The coefficient of friction (ratio of shearing stress to normal stress at sliding) may be reduced significantly by the presence of elevated pore pressures or by the presence of a weaker mud-like material between the surfaces of the fault, giving as a result lower strengths (Scholz, 1990).

However, this classification defines only the simple cases and it is possible to have transitional faults when two of the stresses are approximately equal in magnitude.

Unfortunately, the information about the magnitude and orientation of the lithospheric stresses that is currently available is model dependent, and therefore it is not conclusive. Therein lies the importance of obtaining a reliable criterion of fracture.

### 1.1.1 Effects of pore fluid

Rock masses might be infiltrated with ground water. The presence of P- and S-wave anisotropy in the lower crust measured along some orthogonal profiles on the continental shelf suggest that the anisotropy might be caused by liquid-filled microcracks or pores aligned vertically along this profile. The vertical alignment of the microcracks/pores being a result of the present-day stress-field (Scholz, 1990; Crampin, 1987 ; Murrell & Ismail 1976).

The presence of water may partially stabilise the rupture process, whether in the form of slow shear crack propagation, or of deformation due to instability of a strain-weakening region or faulted zone (Scholz, 1990). Time-dependent but quasi-static processes of deformation occur within the rupturing zones, which may in some cases allow the completely aseismic completion of the rupture event, and in others lead to an accelerating creeplike progression towards seismic instability on a time scale controlled by fluid transport, tectonic loading rate and constitutive properties of the failing region.

Inelastic dilatancy is a characteristic feature of brittle rock deformation as observed in the laboratory at loadings near to failure, and is also observed to accompany shearing of rock surfaces in contact. Dilatancy is a consequence of the opening of cracks (Scholz, 1968). The effects of such processes, distributed over regions near faults, are a possible source of precursory variations in seismic and transport properties.

Dilatancy of fluid-infiltrated rocks provides another means for the stabilisation of rupture processes since the strength of brittle rock has an important-frictional component, and frictional resistance is enhanced by the suction developed in pore fluids by dilatant deformation (Ismail & Murrell, 1976).

For near-hydrostatic loading permeability decreases as the material compacts and this continues at low levels of compressive deviatoric stress. At increasing deviatoric stress levels, however, compression-induced permeability reduction may be counteracted by enlargement of additional flow channels due to shear and tensile damage to the intergranular bonds and compression-induced intragranular microcracking. The material yields in a dilatant manner. Because these stress-induced microcracks have preferred orientation quasi-parallel to the maximum load direction, permeability of the rock may become anisotropic at the macroscopic level (Gueguen & Palciauskas, 1994).

## 1.2 Rock Mechanics.

Fractures occur in rocks at all scales, from microcracks to megafaults, from the scale of dislocation planes in a single crystal to the level of major plate-bounding faults, and all of them seem related because the physical mechanism (rupture of atomic bonds) is the same, and hence fracture at macroscopic scale may be seen as a consequence of an accumulation of ruptures at smaller scales (Scholz, 1990; Lawn, 1993). The differential stresses supported by the experimentally deformed samples may be higher than those expected under geologic conditions (Turcotte & Schubert, 1982; Main et al., 1990). However, a comparison of the experimentally produced microstructures to those reported from natural fault zones suggests that similar processes are operative in the laboratory and in the Earth (Scholz, 1990; Atkinson & Meredith, 1987).

From this point of view the ultimate mechanism of brittle fracture is the nucleation and propagation of microcracks. The experimental evidence for the proliferation and growth of microcracks in rocks comes to a large degree from observations of changes of physical properties of the rock during loading, which cause dilatancy, acoustic emission, and changes

in elastic wave velocity, electrical conductivity, permeability, etc. (Paterson, 1978). Failure occurs both under tensile load and under total compression. The first case has been understood since the work of Griffith (1920) but failure under compression is less fully understood (though it was addressed by Griffith (1924)) and is the main subject of scrutiny in rock mechanics.

The failure of brittle rocks during compression is believed to be preceded by the formation, growth and coalescence of microcracks (Griffith, 1924; Murrell, 1964; Murrell & Digby, 1970; Paterson, 1978; Kranz, 1983, Ashby & Hallam, 1986). The tensile stresses necessary for microcrack growth are believed to be caused by mechanisms which include shear along pre-existing microcracks and stress concentrations (e.g. Hertzian contact stresses) around inhomogeneities. In general these microcracks may not be randomly oriented and the rock displays an elastic anisotropy determined by the shape and material content of the cracks and by the crack orientation distribution function. The change in elastic wave velocities due to cracks has been studied experimentally using ultrasound by (among others) Bonner (1974), Lockner *et al.*(1977), and Granryd *et al.*(1983) for Westerly granite, by Gupta (1973) for Indiana Limestone, by Nur & Simmons (1969) for Barre Granite, by Hadley (1975) for Westerly granite and San Marcos gabbro, by Jones (1988) and Jones & Murrell (1989) for a variety of rocks (Darley Dale sandstone, Solenhofen limestone, Penmaenmawr microgranodiorite, Nottinghamshire gypsum, Kimmeridge dolomite, Westerly granite, and Oulx serpentinite), by Sammonds *et al.*(1989) and Stuart *et al.*(1993) for Darley Dale sandstone, and by Sayers *et al.*(1990) and Sayers & van Munster (1990) for Berea sandstone.

The deformation history of an experimentally compressed brittle rock can be characterised by several stages (e.g. Paterson, 1978, Aves, 1995) (see Figure 1.1a). In the first stage, the material compacts, suitably oriented pre-existing cracks (PECs) and pores not previously closed by the application of confining pressure are closed further. This results in an increase in the stiffness of the rock. In the case when cracks are almost fully closed, the rock deforms essentially in a linear elastic way (stage II). In stages I and II deformation is essentially reversible. In the third stage the onset of stable new dilatant crack initiation and growth occurs, and the deformation becomes irreversible. In the fourth stage the interaction and linkage of growing cracks begins and deformation becomes conspicuously inelastic. At the peak stress macroscopic fracture begins, and spreads through the sample under decreasing load (stage V). Finally, in stage VI the sample is macroscopically fractured and deformation occurs by displacement on the fractures (faults), the strength is then

determined by friction on these faults (see Murrell 1965). At low confining pressures the rock loses all cohesion and fails by axial splitting (Figure 1.1b). At intermediate confining pressures strain softening occurs, leading to localisation of damage and the rock fails by shear along a single fault plane. Under high confining pressure, strain hardening occurs, leading to non-localised cataclastic flow (Ashby & Hallam, 1986; Paterson, 1978).

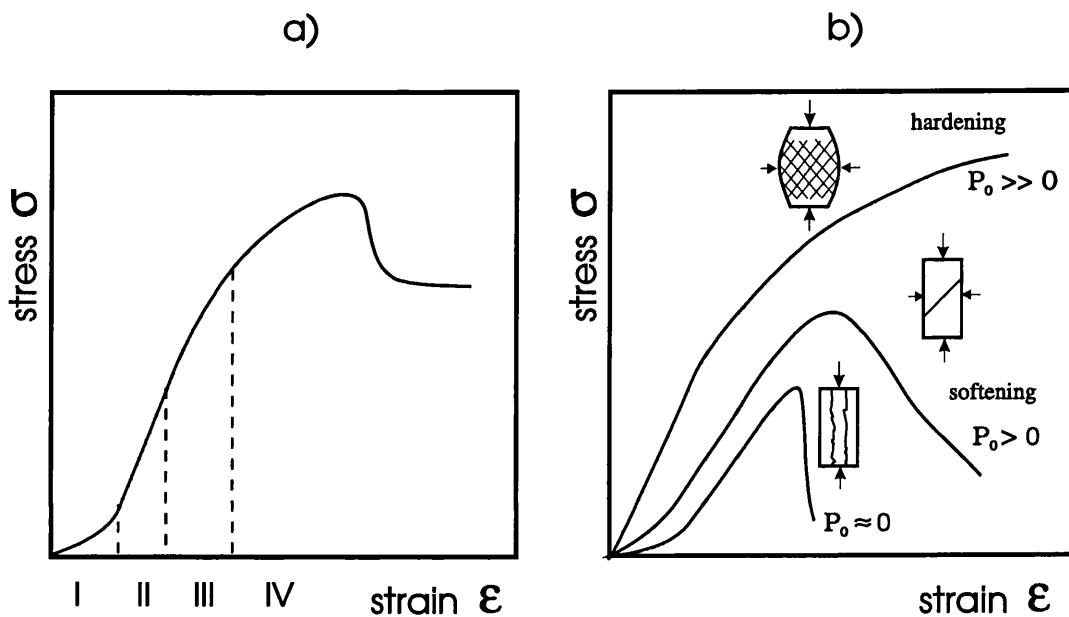


**Figure 1.1:** Typical stress-strain curves. In a) the four distinguishable stages appearing during the loading of a rock are displayed. In b) the influence of confining pressure on the behaviour of a rock is shown; from brittle behaviour with axial splitting, to semi-brittle with shearing failure, and finally to ductile behaviour with strain hardening.

The phenomenon of the brittle-to-ductile transition (BDT) is believed to be controlled (Murrell, 1990) by the competition between cleavage fracture and dislocation activity at crack tips. The brittle-plastic transition in the continental crust occurs over a relatively wide range of conditions (Scholz, 1990). The brittle-plastic transition in rocks involves at least three transitions in deformation mechanism that occur with increasing temperature and/or pressure. The transition from cataclastic faulting to semibrittle faulting is due to the activation of dislocations. Blunting of cracks makes the faulting process stable in the semibrittle regime. The transition from semibrittle faulting to semibrittle flow corresponds to a change from localised to distributed deformation. Microcracks nucleate in response to stress concentrations at dislocation pile-ups in the semibrittle flow regime. The transition to semibrittle flow occurs when the stress intensity at crack tips is insufficient to allow

propagation across grain boundaries. There is a transition from semibrittle flow to dislocation creep occurring as a result of an increase in grain boundary mobility with increasing temperature. In addition, a transition from dominantly mode I (axial) to mode II (shear) microcracking occurs with an increase in confining pressure regardless of temperature.

The brittle compressive failure of fresh-water, columnar ice under biaxial loading, shows similar behaviour and was investigated by Smith & Schulson (1993). The failure mode changes from splitting along the columns along the loading direction at zero confinement to shear faulting in the loading plane at moderate confining pressure to a combined mode of splitting across the columns and shear faulting out of the loading plane at greater confinement.

Batto & Schulson (1993), studying fresh-water ice under uniaxial compression, found that secondary cracks (wing cracks) emerging from pre-existing cracks form within both the brittle and the ductile regimes, but that individual wing cracks propagate only within the brittle regime. Using artificial cracks Batto & Schulson (1993) found that when individual wing cracks propagate, brittle behaviour is generally observed; when individual cracks do not propagate, ductile behaviour is generally observed. When cracked samples are crept under a small load, wing crack propagation is suppressed. These observations may indicate that damage in ice in the semibrittle regime is mainly due to the nucleation of new, grain-sized cracks, rather than the propagation of those already present.

Macroscopic fracture, therefore, is to be interpreted in terms of microscopic processes. In such situations, an understanding of the behaviour of a basic single crack is very important. The main goal at this level is to establish a relationship between the dimensions and orientation of the growing crack as a function of the applied loads. Having achieved this objective it is convenient to consider a distribution function that represents a population of these cracks in order to obtain the crack density and average strains that will allow us to evaluate the amount of damage due to the cracks, and how they will affect the physical properties of the rock as functions of the deviatoric stress.

### 1.2.1 Brittle Rocks

In the above section we have mentioned 'brittle' fracture and 'plastic' deformation without defining these terms. Now we will try to clarify this point. 'Brittleness' measures the competition between non-elastic deformation and fracture. An ideally brittle solid deforms elastically until the cohesive bonds break in a conservative way, i.e. the breaking process

is reversible, and the strength of the atomic bonds alone determines the resistance to fracture. But in reality this process of breaking is accompanied by irreversible processes at the tips of growing cracks, in some cases by the emission of dislocations that deforms the material in a permanent way without total destruction of the lattice integrity (this is called plastic deformation). When widespread plastic deformation occurs before crack nucleation is possible, materials are classified as ductile. Those materials which fall between these two end-members are called semi-brittle solids, and might constitute most of the solid materials that we know. Brittle solids are much stronger in compression than in tension, but in semi-brittle materials the difference between compressive and tensile strength tends to diminish (Paterson, 1978; Murrell, 1990).

Although undoubtedly the intrinsic elastic properties of the material are of the most importance to determine if a solid will be brittle or plastic, the external physical conditions (stress, temperature, strain rate, etc.) are the ones that will determine the behaviour of the rock. In that sense one should speak more of brittle or plastic *states* rather than brittle or plastic *materials*. It is believed that in rocks at sufficiently high pressures and temperatures there is a gradual transition from fracture to cataclastic flow and then to plastic flow. Brittleness is basically associated with the formation of cracks, plasticity with the formation of dislocations, and clearly both kinds of defects might coexist in a material and even one of them can nucleate the other (e.g., dislocation pile-up causing crack formation). The growth of cracks may be favoured under low pressures and low temperatures but large confining pressures or suitably high temperatures may suppress the growth of microcracks and promote plastic flow, making it the dominant mechanism of the overall deformation (Murrell, 1990).

### 1.3 Brittle fracture processes

In this work we focus on the brittle regime and aim to explain and describe brittle fracture from a simple model of crack growth.

The stages of fracture as we know them are:

- 1 Nucleation of cracks.
- 2 Growth of individual microcracks which may be stable or unstable.
- 3 Coalescence of stable microcracks to form macroscopic cracks.

4 Unstable growth of a macroscopic crack will lead to complete fracture. In stable growth, the macrocrack might coalesce with other macrocracks before fracture.

These stages may be repeated at different size scales. Nucleation of cracks at a certain scale might be seen as the result of stages 2 and 3 applied to microcracks at a smaller scale. Under those circumstances the ultimate mechanism of failure might be the result of the progression of very small microcracks originated from forces of mechanical, chemical, electromagnetic and thermal nature (Lawn, 1993). An ideal strong material is that one that does not have any flaw. In the present thesis we start from Griffith's standpoint (1920, 1924) by assuming that brittle material (e.g. rocks) contains a homogeneous population of pre-existing cracks (PECs).

## 1.4 Elastic properties of cracked solids

In a linear elastic solid containing a population of microcracks, the cracks are generally characterised by a nondimensional crack density parameter  $\varepsilon$  (Bristow, 1960; Walsh, 1965; Budiansky & O'Connell, 1976), which depends on their geometry:

$$\varepsilon = \frac{2 * n}{\pi} \left\langle \frac{A^2}{P} \right\rangle \quad (1.1)$$

where  $n$  is the number of cracks per unit volume, and  $A$  and  $P$  are the area and perimeter of the crack respectively. The brackets denote an average. This formula is only valid in the 3-dimensional case.

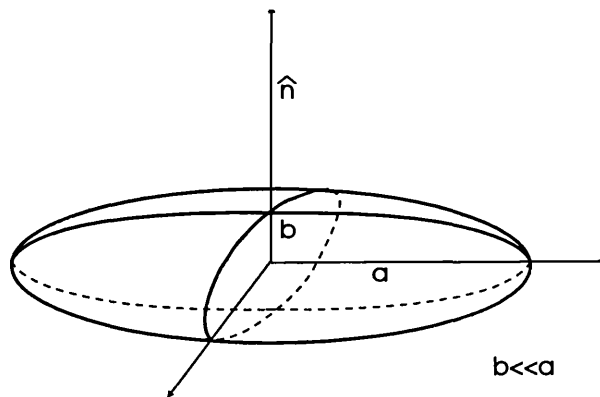


**Figure 1.2:** Penny-shaped crack with radius  $a$  and minor axis  $b$ .

Typically a 3-D crack is regarded as an ellipsoid with its minor axis considerable smaller than the other two and whose orientation is given by the unit normal  $\hat{n}$  (Figure 1.2). In

the case of a penny shaped crack of these characteristics, the crack density parameter  $\varepsilon$  (equation 1.1) becomes:

$$\varepsilon = n \langle \bar{a}^3 \rangle \quad (1.2)$$

where  $n$  is the number of cracks per unit volume and  $\bar{a}$  is their average radius. In the two-dimensional case the crack density parameter is defined as:

$$\varepsilon = n \langle \bar{a}^2 \rangle, \quad (1.3)$$

some authors (Davis & Knopoff, 1995) include a multiplier  $\pi$  in the above equation in order to have  $\varepsilon$  representing the relative area of circles with cracks as diameters.

A number of solutions have been reported in the literature for the changes in elastic moduli as a function of the crack density parameter, geometry and orientation. They predict degradation of stiffness, development of anisotropy and changes in wave speeds caused by microcracking, however, they differ substantially from intermediate to high concentrations of cracks.

For an elastic, homogeneous material with compliance  $\mathbf{H}^0$ , the volume average of strain can be written in terms of the volume average stress as;

$$\langle \epsilon_{ij} \rangle = (H^0 + \Delta H)_{ijkl} \langle \sigma_{kl} \rangle = H_{ijkl} \langle \sigma_{kl} \rangle \quad (1.4)$$

where  $\Delta H$  is the change in compliance due to cracks and  $H$  is the effective compliance of the cracked material.

In the approximation of non-interacting cracks (Walsh, 1965, 1969), the crack locations and their sizes are assumed to be random, each crack is regarded as isolated and does not experience any influence of other cracks, therefore the overall strain due to the presence of cracks is the weighted sum of the isolated cracks' contributions,

$$\langle \epsilon_{ij} \rangle^{cracks} = \sum_{\alpha=1}^N \varepsilon_{\alpha} \langle \epsilon_{ij} \rangle^{\alpha} \quad (1.5)$$

where  $\langle \epsilon_{ij} \rangle^{\alpha}$  is the average strain over each individual crack,  $N$  is the total number of cracks,  $\varepsilon_{\alpha}$  is the density of cracks with radius  $a_{\alpha}$ , i.e.,

$$\varepsilon_{\alpha} = n_{\alpha} \langle \bar{a}_{\alpha}^3 \rangle \quad (1.6)$$

$n_{\alpha}$  is the number of cracks of radius  $a_{\alpha}$  per unit volume. The total crack density and the total number of cracks per unit volume are

$$\varepsilon = \sum_{\alpha=1}^N \varepsilon_{\alpha}, \quad n = \sum_{\alpha=1}^N n_{\alpha}. \quad (1.7)$$

We will see in Chapter 4 that the average strain over each individual crack can be calculated from the crack opening displacement on the surface of the crack and integrated over the orientations. The result is that the components of the strain  $\langle \epsilon_{ij} \rangle^\alpha$  is proportional to the far-field stresses  $\sigma_{ij}^\infty$ , and therefore the total change in compliance  $\Delta H$  due to the presence of a population of cracks is linear in the crack density parameter  $\epsilon$ .

The problem of effective elastic moduli for non-interacting cracks has been solved for different orientational distributions (random or nonrandom) by a number of authors (Bristow, 1960; Walsh, 1965; Sayers & Kachanov, 1991; Nemat-Nasser & Hori, 1993).

There are various approximate schemes to take into account, to a certain extent, interaction between cracks. In some of them a *typical* crack is placed into a medium with *effective* moduli already affected by the presence of other cracks (Budiansky & O'Connell, 1976; Bruner, 1976; Hoenig, 1979). In others schemes a crack is placed into an undamaged matrix, but subjected to a self-consistent *effective* stress field which not necessarily coincide with the remotely applied stress (Kanaun, 1980, 1983).

The self-consistent method (SC) (O'Connell & Budiansky, 1974; Budiansky & O'Connell, 1976; Hoenig, 1979) was used originally for predicting the effective properties of isotropic composites (Hill, 1965; Budiansky, 1965). In this method the crack is inserted in an isotropic medium assumed to have the same elastic properties as the cracked body. The result is a system of algebraic equations that can be solved for the moduli as functions of the crack density  $\epsilon$ . This scheme overestimates interaction and therefore predicts a point where the Poisson's ratio vanishes (Bruner, 1976; Kemeny and Cook, 1986).

The differential scheme (DS) (Bruner, 1976; Henyey & Pomphrey, 1982) makes the assumptions of the SC method, but the crack density is changed incrementally and the effective compliances are calculated at each step, i.e. cracks are added one at a time so that the moduli of the solid is changing each time. This procedure results in a set of coupled differential equations for the moduli. In this scheme there is no vanishing of the Poisson's ratio.

Both schemes (SC and DS) predict a softening effect on the effective moduli, and none of them take into account the mutual positions of the cracks.

As an illustration, some representative results of the differential scheme applied to 3 different crack systems are given in Figures 1.3-1.5. It is found that the relative values of different moduli are strongly dependent on the crack orientation distribution. For a random distribution of penny shaped cracks (RDC) (Figure 1.3) the changes in the 3 relative moduli  $E/E_0$ ,  $G/G_0$  and  $\nu/\nu_0$  as functions of crack density  $\epsilon$  are almost the same. In the case of

cylindrical transverse isotropy (CTI) (Figure 1.4), the shear modulus  $G$  in the  $z$ -direction is less affected by the presence of cracks than in the other directions. In the planar transverse isotropy case (PTI) (Figure 1.5) the variations in the three moduli are completely different between them, being the Poisson ratio the most affected by the presence of cracks.

Both CTI and PTI distributions have symmetry in the  $x - y$  plane. In the first case all the cracks have their normals lying in that plane, and in PTI all the crack planes are in the  $x - y$  plane. As seen from Figure 1.6, cracks with PTI distribution have more impact in the moduli than the other distributions.

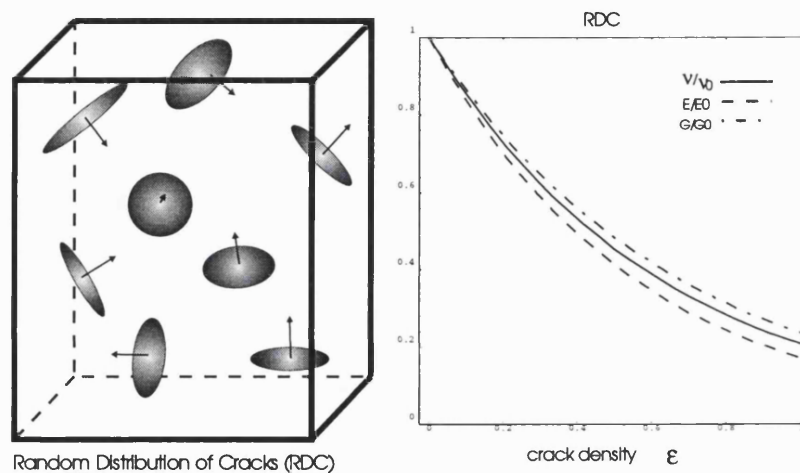


**Figure 1.3:** Random distribution of cracks (RDC) where the penny-shaped cracks can have any orientation within the material. The relative Young's Modulus  $E/E_0$ , shear modulus  $G/G_0$  and Poisson's ratio  $\nu/\nu_0$  as functions of crack density  $\epsilon$  are almost equal for this distribution of cracks.

The calculations were done by myself following Bruner's paper of 1976.

The methods of effective field (MEF) (Kanaun, 1980, 1983) incorporates the actual mechanics of interaction between cracks and take into account the mutual positions of cracks. MEF not always predict reduction in the stiffness, but in the case of random locations of cracks, the predicted effective moduli coincide with the moduli given by the non-interacting cracks scheme (Kachanov, 1992).

There is another approach, the method of smoothing, that calculates the effective stiffnesses including a second order term in crack density (Hudson, 1980, 1981, 1986, 1990), it covers crack populations with a variety of orientations, arbitrary distributions and a variety of interior conditions on the crack. This method appears to be very accurate at low values of the crack density, but from moderate to high crack densities it shows an unexpected behaviour, i.e., that stiffness increases with increasing crack density (Sayers & Kachanov,

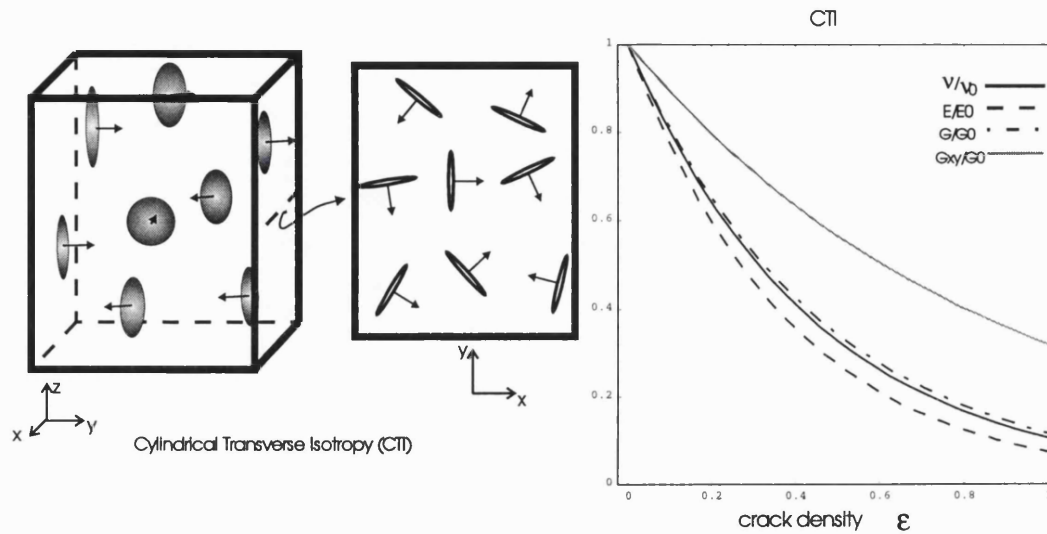


**Figure 1.4:** Distribution of cracks with cylindrical transverse isotropy (CTI). The normals of the cracks always lie in the plane perpendicular to the  $z$ -axis. The relative Young's Modulus  $E/E_0$ , Poisson's ratio  $\nu/\nu_0$  and shear modulus  $G/G_0$  (in the  $z$  direction) as functions of crack density  $\varepsilon$  again are almost equal for this distribution of cracks, but in this case the shear moduli  $G^{xy}/G_0$  in the directions  $x$  and  $y$  are less affected by the presence of cracks than in the  $z$  direction.

The calculations were done by myself following Bruner's paper of 1976. (1991).

Comparison between various schemes can be found in Kemeny & Cook (1986), Sayers & Kachanov (1991). Computer experiments for some 2 dimensional crack arrays with a small number of cracks (Kachanov, 1982) and with a large number of randomly distributed, strongly interacting cracks (Davis & Knopoff, 1995) have shown that the simple approximation of non-interacting cracks gives a very good fit to the numerical solution even at high values of crack density. The reason for this accuracy seems to be that the competing effects of stress shielding and stress amplification cancel each other. This cancellation may not be complete for certain ordered crack arrays and either amplification (softening) is favoured or shielding (stiffening) is favoured.

## 1.5 Importance of a new model of crack growth based on simple assumptions.

An understanding of the growth behaviour of a basic single pre-existing crack is very important. It is desirable to establish a relationship between the dimensions and orientation of the growing crack as a function of the applied loads. Having achieved this objective it is convenient then to consider a distribution function that represents a population of these

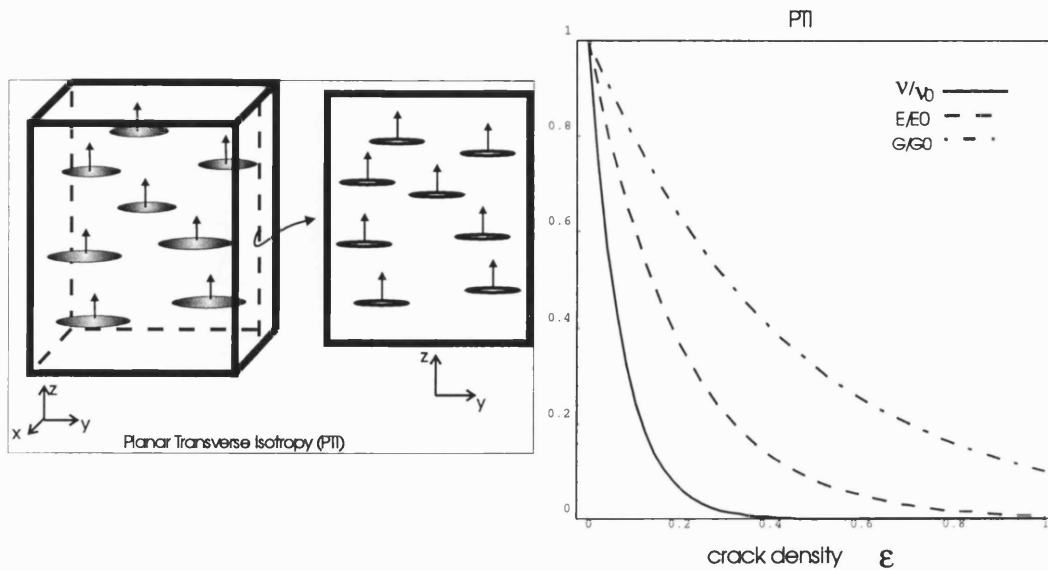


**Figure 1.5:** Distribution of cracks with planar transverse isotropy (PTI). The normals of the cracks are always parallel to the  $z$ -axis. In this case the 3 relative moduli are perfectly split. Note the sharp fall of the Poisson's ratio due to the alignment of the cracks.

The calculations were done by myself following Bruner's paper of 1976.

cracks in order to obtain the crack density and average strains that will allow us to evaluate the amount of damage due to the cracks, and how they will affect the physical properties of the rock as functions of the deviatoric stress.

In Chapter 2 we make a brief review of some important concepts on crack modelling focusing on Griffith's models. We present some experimental evidence of wing crack existence, and mention some models to describe the wing crack growth. A model of pre-existing crack initiation is presented.

In Chapter 3 the initiation and growth of wing cracks in a body, under external loads, is modelled using the maximum local tensile stress criterion. The orientation and size of the wing crack is found by modelling the pre-existing crack as a dislocation that wedge open the wing crack. The Burgers vector of this "dislocation" depends on the elastic properties of the material, the size of the pre-existing crack and the applied stresses. With this model it is possible to study the system under both tensile and compressive stress fields. In the tensile case, the growth of the crack is unstable, so once the crack extension or wing crack is formed, it continues to grow until failure of the specimen occurs. In the compressive case, initiation of the wing crack is followed by a period of stable propagation where increasing loads are necessary to make the crack extend further. At higher level of stress the crack might be unstable, even under confining pressure. One of the more remarkable changes

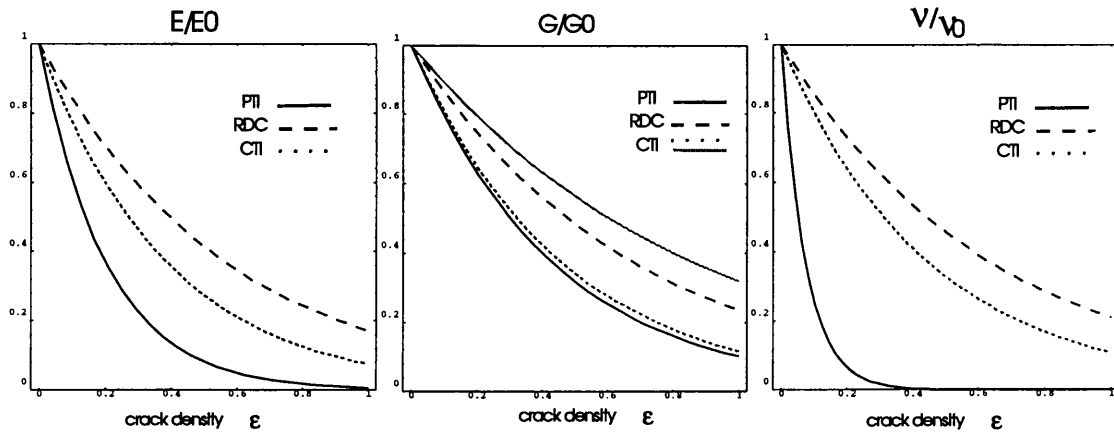


**Figure 1.6:** The Young's modulus  $E/E_0$ , the shear modulus  $G/G_0$ , and the Poisson ratio  $\nu/\nu_0$  as a function of crack density  $\epsilon$  for the 3 distributions of cracks considered.

The calculations were done by myself following Bruner's paper of 1976.

that occurs is the anisotropy of the resultant cracked material, this is due to the growing of wing cracks at certain preferred orientations.

In Chapter 4 we will see that within a proper mathematical framework it is possible to calculate the elastic properties of solids containing crack populations, and a new analysis of experimental data is introduced. Using the crack density tensor concept we can estimate the crack density and crack distribution from elastic wave velocity measurements. We explain some of the results in terms of the model of Chapter 3.

Finally in Chapter 5 we summarise the results and consider future work.

## Chapter 2

# Fundamentals of Griffith crack model.

Chapter Two introduces the concept of a Griffith crack with a discussion about the validity of his approach. The initiation of new dilatant cracks (NDCs) from pre-existing cracks (PECs) is discussed, and a model of pre-existing crack nucleation is presented. (Note: in the literature NDCs are sometimes referred to as wing cracks).

### 2.1 Mathematical models of cracks.

Pre-existing defects of whatever origin can act as stress concentrators and produce flaws that eventually will propagate and produce failure. These defects may be pores, grain boundaries, inclusions, microcracks, crystal dislocations, etc. Each one of these is a potential source of local tensile stress concentration even for all-round compressive loads.

In 1913, Inglis calculated the stresses around an elliptical hole within a plate in a state of plane stress. He found that any hole under external stresses produces a stress-concentration, and that the increase in local stress depends strongly on the shape of the hole. For an elliptical hole with small aspect ratio ( $b/a$ , where  $b$ =smallest axis,  $a$ =largest axis of the ellipse), the stress concentration is high, and such holes can be used to model cracks (Griffith 1920; Murrell 1964; Murrell & Digby 1970).

Based on experiments on glass, Griffith (1920) found that this material fractures in an apparently elastic manner at tensile stresses very much less than its theoretical atomic bond strength. Griffith explained this fact by the existence of crack-like flaws contained inherently in the glass. At tensile stress concentrations these flaws may begin to grow, and

when the flaw begins to grow the increase in length could exaggerate the stress concentration yet further leading to an unstable propagation as long as the material is in tension. The strength of a material is dependent on the size of the pre-existing cracks in it (Griffith, 1920; Murrell, 1964).

Griffith (1920) was able to do a theoretical study of the stress field due to an elliptical slot embedded in a body under tensile loading conditions. According to Griffith (1920) the surfaces of a solid possess a 'surface tension (energy)' and when a crack propagates, the decrease in the strain energy is balanced by an increase in the potential energy due to this surface energy and by the work done by the loading tractions. An increase in the size of the crack leads to a diminution of the total free energy, the system becomes unstable and the crack spreads. Griffith deduced this change in energy for a narrow elliptical crack for which the near-tip stresses are highly concentrated. These stresses can exceed the intrinsic strength of the material (the cohesive strength, which depends on atomic bonding, and is related to the intrinsic surface energy). With these simple ideas he was able to explain the weakness of real materials and provided the tools for the quantitative treatment of tensile fracture in brittle solids.

Based on the previous investigations by Griffith (1920), Orowan (1944) showed that the propagation of a crack was not only accompanied by the formation of new surfaces, with their intrinsic surface energy ( $\gamma_i$ ), but that processes of microscopic damage formation close to the margin (tip) of a crack led to the formation of a thin damage layer at the new crack surface so that the fracture surface energy  $\gamma_f$  was much larger than  $\gamma_i$  ( $\gamma_f \gg \gamma_i$ ). Orowan's discovery became the foundation for modern fracture mechanics (Orowan, 1952; Irwin, 1957; Lawn, 1993).

The principles of linear elastic fracture mechanics (LEFM) were developed in the 1950s by George Irwin (1957). If the elliptical crack is reduced to a flat crack of zero thickness the stress at the tip of the crack becomes singular. Irwin (1957) demonstrated that the amplitude of the stress ahead of a crack could be expressed in terms of a scalar quantity known as stress intensity factor,  $K$ . The components of stresses and displacements fields at the crack tip are (Lawn, 1993),

$$\sigma_{ij} = \left( \frac{K_m f_{ij}(\theta)}{\sqrt{2\pi r}} \right) \quad (2.1)$$

$$u_i = \left( \frac{K_m}{2E} \right) \sqrt{\left( \frac{r}{2\pi} \right)} f_i(\theta) . \quad (2.2)$$

The  $K_m$  factors depend only on the applied loading and specimen geometry, and determine the intensity of the local field about the crack tip. The subscript  $m$  denotes one of three modes of crack surface displacement - I (opening mode), II (sliding mode), III (tearing mode). The remaining factors depend only on the spatial coordinates about the tip and determine the distribution of the field,  $r$  is the radial coordinate (distance from the crack tip), and  $\theta$  is the angular component. For a crack of length  $2c$  embedded in a material under uniform remote applied loadings,  $\sigma^m$  in modes I, II and III the stress intensity factors are,

$$K_m = Y \sigma^m \sqrt{c} \quad (2.3)$$

where  $Y$  is a dimensionless geometry and edge effect modification factor. Conditions for crack propagation are met when the stress intensity factor exceeds a critical value  $K_c$  (fracture toughness).

The irregular structure of the surface of a real crack may also be taken into account. Goldshtein (1992) obtained asymptotic expressions for describing the stress field and displacements near the crack tip of fractal-like cracks. Fractal geometry of the crack leads to a change in the singular behaviour of the stress fields at the crack tip, and to the appearance of a dimensionally dependent factor in the expression for the stress intensity factor.

In this thesis we will take Griffith's model of pre-existing cracks (PECs) and take it a step further in order to understand fracture in compression. We will not modify his criteria but use it again to model the growth of new dilatant cracks (NDCs).

## 2.2 Elliptical model of Griffith

Griffith's energy balance concept although appropriate for tensile fracture proved to be difficult to apply for compressive fracture. Griffith (1924) formulated another elliptical crack model to describe brittle behaviour in both tension and compression. He considered elliptical cracks obliquely oriented to the main applied stresses, and allowed the external loads to be either tensile or compressive. Griffith considered a 2-dimensional material that contains a large number of randomly oriented identical open flaws elliptical in shape. The material is assumed to be loaded under plane stress/strain conditions by principal stresses  $\sigma_{22}^0$  and  $\sigma_{11}^0$ . He assumed that fracture initiates from the boundary of an open flaw when the tensile stress on this boundary exceeds the local tensile cohesive strength of the material (a physical property of the material). He calculated then the tangential stress at the edge of the crack and found that "the presence of cracks can give rise to (local) tensile stresses large

enough to cause fracture, even when the applied tractions are both compressive, provided that they are unequal” Griffith (1924). He found that these local (tensile) stresses are very near the ends of the major axis of the crack and then assumed that the propagation of the crack would take place in its own plane and that the propagation would be immediately unstable, leading to a surface of rupture oblique to the main stresses even for uniaxial compression. As we will see, this is not the case but his ideas indeed provided the starting point for the understanding of fracture in general.

The form of the Griffith criterion for fracture is

$$\left(\sigma_{11}^0 - \sigma_{22}^0\right)^2 - 8K_t \left(\sigma_{11}^0 + \sigma_{22}^0\right) = 0 \text{ if } 3\sigma_{11}^0 + \sigma_{22}^0 \leq 0, \text{ compression,} \quad (2.4)$$

$$\sigma_{11}^0 = K_t \quad \text{if } 3\sigma_{11}^0 + \sigma_{22}^0 \geq 0, \text{ tension,} \quad (2.5)$$

where  $K_t$  is the tensile strength of the body. This criterion predicts a compressive strength to tensile strength ratio of 8:1, which is less than that found experimentally.

Extending Griffith’s model, Murrell (1964) analysed elliptical cracks, and the effect of fluid pressures, leading to the effective stress principle. Murrell & Digby (1970) made a 3D model of a Griffith crack based on Eshelby (1957), and showed the effect of the intermediate principal stress in fracture, which is relevant to Anderson’s theory of faulting. This extended Griffith criterion gives a more realistic *compressive : tensile* strength ratio of 12:1. The Griffith theory considered only open cracks, but in reality, cracks close under moderate confining pressure, Murrell (1964) calculated the crack closure stress for the 2D case and Murrell & Digby (1970) did it for the 3D case.

All these models dealt only with initiation of new developed cracks (NDCs) from pre-existing cracks, but did not consider the growth or stability of NDCs and ultimate failure. The generation of meta-stable NDCs is thought to be central to the macroscopically inelastic (and dilatant) deformation of brittle rocks tested under compression. In the literature NDCs are frequently named as Wing Cracks.

## 2.3 NDC (Wing Crack) initiation and development.

### 2.3.1 Experimental evidence of wing crack existence.

The first evidence of the existence of tensile cracks in a brittle material under all-around compressive loads comes from the experiments of Bridgman (1931) (see Jaeger and Cook, 1963). He submerged a sealed cylindrical ring of a brittle material, that is tightly fitted

over a solid steel cylinder, in a fluid bath which is then pressurised. He observed that axial tension cracks develop from the interior surface of the ring in the radial direction, growing axially in a stable manner, and never reaching the exterior surface of the tube (Nemat-Nasser & Hori, 1993).

Scholz *et al.* (1986) repeated Bridgman experiments using pyrex glass tubes and observed, with scanning electron micrographs, those axial tension cracks emanating from pre-existing cracks of about  $20\mu m$ . Scholz *et al.* (1986) explained the existence of these tensile cracks in terms of model calculations of Nemat-Nasser and Horii (1982). These extensions from the PEC are called NDCs or wing cracks.

Cannon *et al.* (1990) performed uniaxial compression experiments on plates of fresh-water columnar ice, and observed that stable wing cracks develop on inclined cracks which are nucleated at grain boundaries during loading.

Brace and Bombolakis (1963) and others have found that in compressive tests on thin plates of brittle material containing artificially made flaws, there is a tendency for the newly nucleated wing cracks to grow in the direction of the maximum compressive applied stress. They observed that, at least when there is a lateral tension, once a critical crack extension length is attained, the crack may become unstable. However with no lateral tension the wing cracks remained stable. It is important to note here that the fact that these experiments failed to show crack instability in the purely compressive state does not mean that such cracks will be stable always, but instead that the critical crack length was not attained for the particular conditions of the experiments (*i.e.*, crack-size to plate-size ratio, aspect ratio of the crack, stress level, etc.). It is fair to say that the concept of wing cracks was first postulated by Brace and Bombolakis (1963), to explain dilatancy in rocks.

Studying pre-existing oblique open slots in PMMA (polymethylmethacrylate) plates Barquins *et al.*, (1992) found that branching always initiates perpendicular to the local plane tangent to the slot edge at the branch crack root while the distance of the initiation point to the tip of the crack increases with the inclination angle of the slot to the main loading axis, all in accordance with Griffith's idea of a maximum tensile stress at the edge of the crack. Under combined mode conditions the cracks show nonplanar growth. The crack begins to propagate at an angle for which the tangential stress is a maximum. It then follows a curved path which is one for which pure tensile mode I conditions prevail locally at the tip.

It is our belief that these kinds of experiments in which artificial slits are cut in an otherwise homogeneous material (e.g. polymethylmethacrylate (PMMA)), should be treated

with caution when extrapolated to rocks. One has to ask whether the crack size (with respect to the size of the plate and of the material microstructure), and aspect ratio used are similar to the ones that one expects to find naturally in rocks.

### 2.3.2 Analytical modelling of wing crack growth.

In the sliding crack models for fracture under compression (Brace and Bombolakis, 1963; Kachanov, 1982; Horii & Nemat-Nasser, 1985,1986; Ashby & Hallam, 1986), it is assumed that pre-existing cracks (PECs) are already closed and that at a certain level of differential stress (enough to overcome friction) the walls of these cracks start to slide while experiencing frictional resistance, and a shear stress concentration is developed at the ends of the cracks. As a consequence of this concentration of stress, new dilatant cracks (NDCs) appear and propagate, driven by the shearing of the pre-existing cracks (PECs), towards the major principal stress direction. The relationships between the compressive stress, the length of the growing crack (NDC) and deformation due to the formation of cracks are then established. The mathematical model adopted is based on the infinitesimal flat crack model proposed by Irwin (1957),.

Horii & Nemat-Nasser (1986) write an expression for the stress intensity factor at the tips of a representative tension crack of length  $2c$  (equivalent to 2 wing cracks) subjected at its centre to a pair of collinear splitting forces of equal magnitude  $F$  which make an angle  $\theta$  with the far field stress  $\sigma_2^0$ . These forces represent the effect on the representative crack of the sliding of the pre-existing closed crack under the local shear stress  $\tau^*$ , so

$$F = 2l\tau^* \quad (2.6)$$

where  $2l$  is the length of the pre-existing crack, and

$$\tau^* = -\frac{1}{2}(\sigma_2^0 - \sigma_1^0) \sin 2\theta - \tau_c + \mu_f \frac{1}{2} [\sigma_1^0 + \sigma_2^0 - (\sigma_2^0 - \sigma_1^0) \cos 2\theta] \quad (2.7)$$

$\tau_c$  is the cohesive stress,  $\mu_f$  is the coefficient of friction and  $\sigma_1^0, \sigma_2^0$  are the far field stresses. The stress intensity factor solution at the tip of the equivalent crack is

$$K_I = \frac{2l\tau^* \sin \gamma}{\sqrt{\pi(c+c^*)}} + \frac{\sqrt{\pi c}}{2} [\sigma_1^0 + \sigma_2^0 - (\sigma_2^0 - \sigma_1^0) \cos 2(\theta - \gamma)] \quad (2.8)$$

$\gamma$  is the angle between the equivalent crack and the pre-existing crack,  $c^* = 0.27 * l$ .

A good review of fracture initiation models is provided by Kemeny and Cook (1991) who also calculate the stress intensity factor associated with each mechanism.

A more refined constitutive model for brittle rocks was developed by Li & Nordlund (1993). The total deformation caused by the closure and fracture of cracks was obtained by the sum of the components of individual cracks. The non-linear behaviour of deformation results either from the closure of open cracks at low stress levels, or from the fracture of microcracks at high stress levels. They are able to obtain realistic stress-strain curves for loading and unloading cycles. Although their model includes open and closed cracks, they postulate that the NDCs will be always parallel to the major principal stress and basically the driving force that opens these NDCs is a central wedge force very similar in form to the one used by Horii & Nemat-Nasser (1985).

Nemat-Nasser and Deng (1994) showed that the experimentally observed change in the compressive failure stress with increasing strain rate, may be considered to be a consequence of the generation and dynamic growth of interacting, compression-induced, tensile microcracks.

Due to the apparent different behaviour of the cracks under tensile or compressive loads, there has been a tendency to adopt physically different models to study the two cases. However, the elliptical crack model has the advantage of being able to describe a material under either tensile or compressive loads, and its mathematical formulation is capable of dealing with both open and closed cracks. Using Griffith's approach without assuming a priori that a crack propagates in its own plane, it is possible to calculate the points on the surface of an elliptical PEC where an NDC forms and starts to propagate, and the direction of propagation, that in general is out of the original plane of the crack. The direction of fracture propagation and the critical stress which causes the fracture initiation for different pre-existing crack inclinations deduced from this theory are consistent with experimental data (Wu and Chang, 1978; Chang, 1981; Barquins & Petit, 1992).

Maugis (1992) writes the correct expression for the complex elastic potentials, in elliptical coordinates, for the angled elliptical crack problem. He depicts the stress tensor by drawing contours of principal stresses, isopach, isochromatic lines, the von Mises criterion and stress trajectories for both elliptical cavities and cracks under uniaxial or biaxial loading. He shows that published experimental results on angled cracks are in agreement with the slope of the stress trajectory starting from the crack tip or the more stressed point of the cavity.

## 2.4 Pile-up model of crack nucleation.

It was suggested by Zener (1948) that dislocations (in metals) pile up behind a barrier (obstacle, grain boundaries, etc), and could cause stress concentrations high enough to break the cohesive bonds between the atoms in the vicinity of the pile-up.

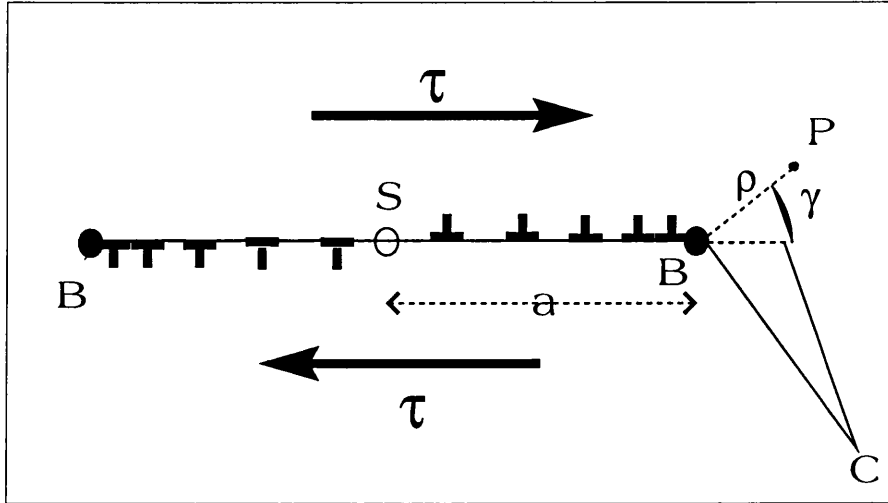


**Figure 2.1:** Nucleation of microcrack by dislocation pile-up. Under shear stress  $\tau$  source  $S$  generates dislocation loops which pile up at barriers  $B$  and  $B'$  in the slip plane. Stress concentration at point  $B$  nucleates microcrack  $BC$ .

Suppose that there is a dislocation source  $S$  which produces equal numbers of positive and negative dislocations, and that  $S$  is located at the middle of a grain of diameter  $2a$ , *i.e.*, at  $x = 0$ . Under the action of an external shear stress  $\tau$ , the positive dislocations move to the right and pile up at  $x = a$ , while the negative dislocations move to the left and pile up at  $x = -a$ . The source stops producing dislocations when the shear stress acting on it is reduced to zero by the field of the two piled-up arrays. The number of dislocations pairs generated by the source  $S$  in this way is:

$$n = 2\tau a \frac{(1 - \nu)}{\mu b} \quad (2.9)$$

where  $\mu$  is the shear modulus,  $\nu$  is the Poisson's ratio and  $b$  is the magnitude of the average Burgers vector, that could be equated to the smallest possible Burgers vector, *i.e.* the interatomic spacing. If 'frictional resistance' (Peierls' force)  $\tau_0$  is present then

$$n = 2(\tau - \tau_0)a \frac{(1 - \nu)}{\mu b} \quad (2.10)$$

The normal tension acting across the radial element  $BP$  (at an angle  $\gamma$  to the slip plane)

at P,  $\sigma_{\gamma\gamma}$ , is obtained as

$$\sigma_{\gamma\gamma} = -3\tau \left(\frac{a}{2\rho}\right)^{\frac{1}{2}} \sin\left(\frac{\gamma}{2}\right) \cos^2\left(\frac{\gamma}{2}\right) \quad (2.11)$$

$\rho$  is the length BP, the maximum value of  $\sigma_{\gamma\gamma}$  is obtained for  $\gamma = 70.5^\circ$ , *i.e.*, the microcrack might start at an angle of 70.5 degrees to the slip-plane direction, in this plane

$$\sigma_{\gamma\gamma} = -\frac{2}{\sqrt{3}}\tau \left(\frac{a}{2\rho}\right)^{\frac{1}{2}}. \quad (2.12)$$

The criterion for a crack to nucleate is that at a distance  $\rho = b$ , the interatomic spacing, from the pile-up point  $B$ , the stress should reach the value of the cohesive strength,  $T \simeq E/\pi$ .

Therefore the stress of nucleation is

$$\tau = \tau_0 + \left(\frac{3}{2}\right)^{\frac{1}{2}} \sqrt{\frac{b}{a}} T. \quad (2.13)$$

Substituting in 2.10 we obtain the number of dislocations that are sufficient to initiate fracture,

$$n = \sqrt{\frac{6a}{b} \frac{(1-\nu)}{\mu}} T. \quad (2.14)$$

Therefore equation 2.13 gives the strength of the material. As we can see the strength of the body decreases as the grain size increases. This model can therefore explain the grain-size dependence of the strength of semibrittle materials if we assume that nucleation of cracks is a critical event that causes failure.

If a given number  $n$  of dislocations run into the microcrack, it is possible to calculate the length of the crack. It turns out that the crack can exist with a stable length under the influence of external stresses and within a range of applied loads, as we shall see in the next chapter. Preliminary results, using a particular set of material parameters, show that the size of the cracks generated in this way, for the uniaxial compression case, are bigger for the bigger grains, but they become unstable at approximately the same level of applied stress  $\sim 9.1Kt$  and at the same orientation as the cracks generated from smaller grains, hence giving a strength independent of grain size.

## Chapter 3

# Growth of new dilatant crack (NDC) population.

In this Chapter the modelling of the NDCs is developed. First, the nucleation of NDCs is obtained using Griffith's ideas, then the properties of these NDCs are examined. The effect of NDCs on the physical properties of rocks is investigated. A comparison with experimental data on failure stress (strength) and acoustic emission is carried out. The equations describing the strains in terms of NDCs and PECs are obtained.

### 3.1 Crack model developed in this thesis.

#### 3.1.1 Introduction

Cracks can be studied theoretically by making some idealisations about crack geometry, the media that surround them and the external conditions on this media. We will assume that the material is isotropic and homogeneous and that the external stresses are uniform. Of course whenever there is a crack, there is a disturbance of the stress field in its near-field neighbourhood that makes the material locally anisotropic, but we can assume that on average over the whole body the isotropy holds, at least at the beginning of the process of deformation. In fact, we have found that macroscopic anisotropy arises naturally from our simple model, depending on the external stress conditions imposed on the material.

Consider a two-dimensional (plane-state), linear elastic, isotropic and homogeneous material that contains a number of randomly oriented open identical cracks of elliptical shape (Figure 3.1). The material is assumed to be loaded by principal stresses  $\sigma_{22}^0$  and  $\sigma_{11}^0$ . In order to obtain the stresses and displacements around the boundary of the elliptical

crack we make the assumption initially that a single crack is not affected by the field of the adjacent flaws. However, a self-consistent approximation could be introduced later by placing the single crack in a material with mean properties of the cracked solid. We will assume that the system can be treated two dimensionally within the limits of linear plane elasticity theory.

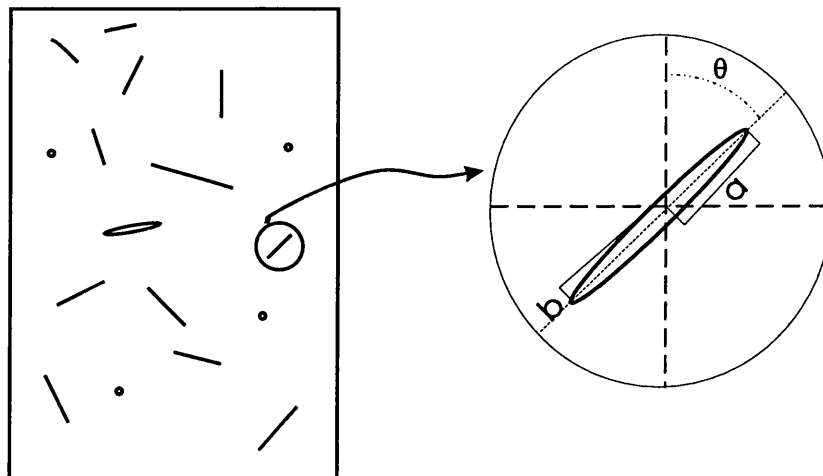


**Figure 3.1:** The Brittle material is modelled as a solid consisting of an isotropic linear elastic matrix containing randomly distributed and oriented identical elliptical microcracks. Each crack is characterised by its inclination  $\theta$  with respect to the main compressive stress, its length  $2a$  and its aspect ratio  $\alpha = b/a$ .

The criterion for the growth of the crack is that fracture initiates in its boundary when the tensile stress on the crack's boundary exceeds the theoretical strength  $T$  of the material (Griffith, 1924; Murrell, 1964) ( $T$  is a physical property of the material, the maximum tensile interatomic force per unit area). From the microscopic point of view fracture must involve the breaking of atomic bonds, so the theoretical strength of a solid is the stress required to separate and break the atomic bonds. In crystals with distinctive cleavage planes the crystal strength depends on the bonds holding atoms of pairs of cleavage planes together.

From the points on the surface of the original crack where there is rupture new secondary cracks appear (this set of two, symmetrically placed cracks are labelled new dilatant cracks, NDCs). Therefore, the initial crack configuration has changed and a new boundary value problem is generated. In fact, with each growth increment of a NDC and its changing crack trajectory the boundary value problem may change. These changes of structure make the

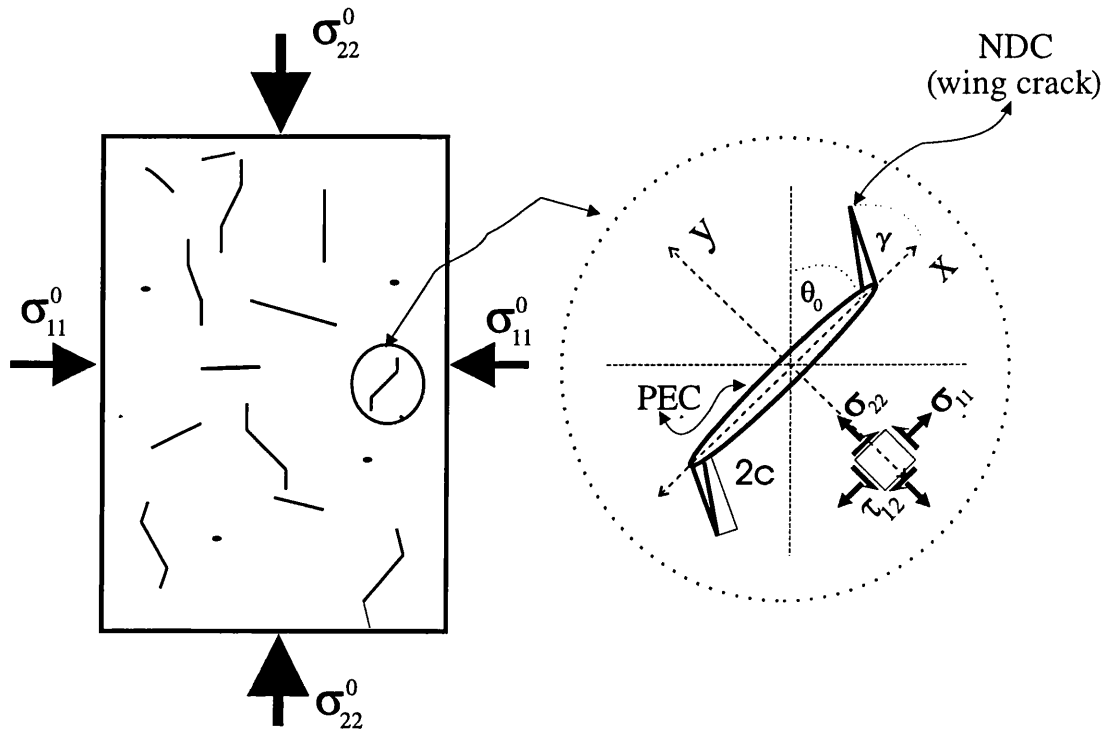


**Figure 3.2:** Under application of external stresses, there is a point when the tangential tensile stress  $\sigma_T$  on the surface of the crack becomes equal to the bond strength between the atoms and then a new crack (NDC) grows from the pre-existing crack (PEC), and propagates in a different plane from the PEC. The newly initiated wing cracks tend to grow in the direction of the major principal compressive stress.

problem of crack propagation modelling a particularly difficult one. Several attempts have been made by other authors to solve this problem, but always some simplifying assumptions need to be done (Brace and Bombolakis, 1963; Nemat-Nasser and Horii, 1982; Steif, 1984; Ashby and Hallam, 1986).

The most important assumption of our model is that the relative displacements of the faces of the original crack (pre-existing crack, PEC) will eventually wedge open a new dilatant wing crack (NDC) in the same way as a dislocation, with Burgers vector  $\mathbf{b} = (\Delta U_x, \Delta U_y)$ , does in the pile-up model described in chapter 2.  $\Delta U_x$  and  $\Delta U_y$  are the components of the crack opening displacement for the PEC, and are taken to be equal to the average relative displacement of points on opposite surfaces of the pre-existing cracks (PECs). In other words, we assume that the formation of NDCs completely relaxes the relative elastic displacements of the surfaces of the PECs. The stress concentration at the tip of the PEC is relaxed gradually through the increase of the NDC's length or, if preferred the stress concentration at the tip of the PEC is transferred to the tip of the NDC though

altered in magnitude due to the different orientation of the NDC.

The next important simplification of our model is the substitution of curved wing cracks by equivalent straight ones (Figure 3.2). This approach has been tested by Horii & Nemat-Naser (1986) giving good results over the entire range of crack lengths and orientations when compared to numerical calculations of the singular integral equation of a model with curved new developed cracks.

### 3.1.2 Stress and strain around a pre-existing crack

In 1921, Pöschl was the first to give an explicit expression for the stress function of an elliptical hole making an arbitrary angle with the direction of the applied tensile stress. He used elliptical coordinates  $(\alpha, \beta)$  derived from the transformation

$$z = x + iy = l \cosh(\alpha + i\beta) = l \cosh(\xi) \quad (3.1)$$

applied to the Cartesian coordinate system  $(x,y)$ , so that

$$x = l \cosh(\alpha) \cos(\beta) ; y = l \sinh(\alpha) \sin(\beta) , \quad (3.2)$$

where  $l$  is the distance between the foci of the elliptical crack,  $\alpha \geq 0$ , and  $0 \leq \beta \leq 2\pi$ . At constant  $\alpha$  or  $\beta$ , these coordinates describe, respectively, homofocal ellipses or hyperbolas. The elliptical cavity is defined by  $\alpha = \alpha_0$ , with semi-axis  $a = l \cosh(\alpha_0)$  and  $b = l \sinh(\alpha_0)$ . For  $\alpha_0 \ll 1$ ,  $\alpha_0$  coincides with the aspect ratio of the ellipse. Pöschl considered that the stress function must fulfil certain asymptotic conditions and that both  $\sigma_{\alpha\alpha}$  and  $\sigma_{\alpha\beta}$  must vanish over the surface of the crack ( $\alpha = \alpha_0$ ).

Muskhelishvili (1953) gives the complex stress functions for a stress-free elliptical hole in an homogeneous and isotropic material when it is subjected to an external load  $\sigma_{11}^0$  along  $Ox'$ . The major axis  $Ox$  of the cavity makes an angle  $\theta + \pi/2$  with the  $x'$  direction.

He makes a conformal transformation from the  $z$  plane in which the hole is elliptical, on to the  $\xi$  plane, in which the hole becomes circular, through the relationship

$$z = x + iy = \omega(\xi) = R \left( \frac{m}{\xi} + \xi \right) \quad (3.3)$$

where  $R > 0$  and  $0 \leq m < 1$ . A point outside the hole in the  $\xi$  plane is described by the coordinates  $\rho \geq 1$  and  $0 \leq \beta \leq 2\pi$ , so  $\xi = \rho e^{i\beta}$ . On the boundary of the hole  $\rho = 1$ , and this corresponds to a unit circle in the  $\xi$  plane and to an elliptical hole in the  $z$  plane, having semi-axes  $a = R(1 + m)$ ,  $b = R(1 - m)$ . The following relations holds between the

two planes,

$$\rho = e^{\alpha - \alpha_0} ; m = e^{-2\alpha_0} ; R = \frac{l}{2} e^{\alpha_0} \quad (3.4)$$

where  $l$  is the distance between the foci of the elliptical crack, and  $\alpha_0$  is the aspect ratio of the crack. The boundary conditions at infinity are

$$\sigma_{x'} = \sigma_{11}^0 \quad (3.5)$$

$$\sigma_{y'} = \tau_{x'y'} = 0, \quad (3.6)$$

whereas on the stress-free-cavity the boundary conditions are

$$\sigma_\alpha = \tau_{\alpha\beta} = 0. \quad (3.7)$$

The stresses and displacements in terms of complex potentials are

$$\sigma_{\rho\rho} + \sigma_{\beta\beta} = 4\text{Re}(\Phi(\xi)) \quad (3.8)$$

$$\sigma_{\beta\beta} - \sigma_{\rho\rho} + 2i\sigma_{\rho\beta} = \frac{2\xi^2}{\bar{\omega}'(\xi)\rho^2} (\bar{\omega}(\xi)\Phi'(\xi) + \omega'(\xi)\Psi(\xi)) \quad (3.9)$$

$$2\mu(U_x + iU_y) = \kappa\phi(\xi) - \frac{\omega(\xi)}{\bar{\omega}'(\xi)} \bar{\phi}'(\xi) - \bar{\psi}(\xi) \quad (3.10)$$

where  $\Phi = \phi'/\omega'$  and  $\Psi = \psi'/\omega'$ .  $\kappa = (3 - \nu)/(1 + \nu)$  for plane stress,  $\kappa = (3 - 4\nu)$  for plain strain and the primes indicate differentiation with respect  $\xi$ .

The complex potentials are given by (Maugis, 1992; Jaeger and Cook, 1979; Timoshenko and Goodier, 1970),

$$\phi(\xi) = \frac{\sigma_{11}^0 R}{4} \left( \frac{2e^{2i\theta} - m}{\xi} + \xi \right) \quad (3.11)$$

$$\psi(\xi) = -\frac{\sigma_{11}^0 R}{2} \left( \frac{e^{2i\theta}}{m\xi} + e^{-2i\theta} \xi - \frac{(e^{2i\theta} - m)(1 + m^2)\xi}{m(\xi^2 - m)} \right) \quad (3.12)$$

If we have in addition another uniform stress  $\sigma_{22}^0$  applied at large distance from the crack and making an angle  $\theta$  with the major axis of the crack, we can derive the corresponding equations by superposition of the two cases.

We are interested in the tangential stress at the boundary of the hole, which is,

$$\sigma_{\beta\beta} = \frac{-(\sigma_{22}^0 - \sigma_{11}^0)(-e^{2\alpha_0} \cos(2(\beta - \theta)) + \cos(2\theta)) + (\sigma_{22}^0 + \sigma_{11}^0) \sinh(2\alpha_0)}{-\cos(2\beta) + \cosh(2\alpha_0)} \quad (3.13)$$

and in the relative displacements of the faces of the hole, given by

$$\Delta U_x = -\left( \frac{1 + \kappa}{2\mu} \right) R (\sigma_{22}^0 - \sigma_{11}^0) \sin(\beta) \sin(2\theta) \quad (3.14)$$

$$\Delta U_y = \left( \frac{1 + \kappa}{4\mu} \right) R \left( 2 \left( \sigma_{22}^0 - \sigma_{11}^0 \right) \cos(2\theta) + \left( \sigma_{22}^0 + \sigma_{11}^0 \right) (1 + m) \right) \sin(\beta). \quad (3.15)$$

For our purpose it is convenient to express the tangential stress  $\sigma_{\beta\beta}$  in terms of the stresses acting on the plane containing the major axis of the elliptical crack (Figure 3.2). The normal stress and shear stress generated by the remote stresses  $\sigma_{11}^0$  and  $\sigma_{22}^0$  are:

$$2 \sigma_{22} = \sigma_{22}^0 + \sigma_{11}^0 + \left( \sigma_{11}^0 - \sigma_{22}^0 \right) \cos(2\theta) \quad (3.16)$$

$$2 \tau_{12} = - \left( \sigma_{11}^0 - \sigma_{22}^0 \right) \sin(2\theta), \quad (3.17)$$

and the stress acting parallel to the crack plane is,

$$2 \sigma_{11} = \sigma_{22}^0 + \sigma_{11}^0 - \left( \sigma_{11}^0 - \sigma_{22}^0 \right) \cos(2\theta). \quad (3.18)$$

The tangential stress is then

$$\sigma_{\beta\beta} = \frac{2 \sigma_{22} \sinh(2\alpha_0) + 2 \tau_{12} \left( -e^{2\alpha_0} \cos(2(\beta - \theta)) \csc(2\theta) + \cot(2\theta) (1 + \sinh(2\alpha_0)) \right)}{-\cos(2\beta) + \cosh(2\alpha_0)}. \quad (3.19)$$

For a complete analysis of the above equations see Maugis (1992).

It can be assumed that in rocks the elliptical cracks will be very flat in shape, *i.e.*, that  $\alpha_0$  is very small. This means that the maximum tensile stress will occur near the tip of the elliptical flaw, where  $\beta$  is small. So neglecting terms of the second order and higher in  $\alpha_0$  and  $\beta$ , the tangential stress near the tip of the crack will be,

$$\sigma_{\beta\beta} = \frac{2 (\alpha_0 \sigma_{22} - \beta \tau_{12})}{\alpha_0^2 + \beta^2}. \quad (3.20)$$

We can generalise this result identifying the stresses  $\sigma_{22}$  and  $\tau_{12}$  with effective stresses  $\sigma_2$  and  $\tau$  acting on the crack plane, and  $\sigma_{11}$  with effective stress  $\sigma_1$  acting parallel to that plane. These effective stresses will have different values for different boundary conditions. Therefore, with the help of this concept of effective stresses we can obtain the tangential stress near the tip of the crack and the relative displacements of the faces of the crack for different boundary conditions at the crack surface, namely

$$\sigma_{\beta\beta} = \frac{2 (\alpha_0 \sigma_2 - \beta \tau)}{\alpha_0^2 + \beta^2}, \quad (3.21)$$

and

$$\Delta U_x = \left( \frac{1 + \kappa}{\mu} \right) R \sin(\beta) \tau \quad (3.22)$$

$$\Delta U_y = \left( \frac{1 + \kappa}{4\mu} \right) R \left( 2 (\sigma_2 - \sigma_1) + (\sigma_2 + \sigma_1) (1 + m) \right) \sin(\beta). \quad (3.23)$$

If we consider firstly the problem of open empty cracks, the effective stresses are then simply the components of the farfield stresses on a plane parallel to the major axis of the crack, and  $\sigma_2 = \sigma_{22}$  and  $\tau = \tau_{12}$ , substituing in (3.21), (3.22) and (3.23), we recover equations (3.20), (3.14) and (3.15)

For the idea of effective stresses see Murrell (1977) and Scholz (1990).

### 3.1.3 Effective stresses for closed cracks and fluid filled cracks

If an open crack closes, the stress normal to the plane of the crack in excess of that required for closure is transmitted across the crack faces and thus is not concentrated at the tips. The normal stress  $\sigma_2$  acting across the faces of a closed crack is equal to the applied normal stress  $\sigma_{22}$  reduced by the value of the normal stress  $\sigma_c$  needed to close it, i.e.,

$$\sigma_2 = \sigma_{22} - \sigma_c . \quad (3.24)$$

The effective shear stress in the plane of the crack  $\tau$  will be the shear stress in the plane of the crack minus the frictional resistance, (Walsh, 1965; Scholz, 1990),

$$\tau = \tau_{12} + \mu_f (\sigma_{22} - \sigma_c) \frac{\tau_{12}}{|\tau_{12}|} , \quad (3.25)$$

where the coefficient of friction between the crack faces is denoted  $\mu_f$ . Note that if  $\tau_{12}$  is greater than the frictional resistance then the closed crack will slide, otherwise will be locked.

The effective stress parallel to the crack plane is simply the stress acting parallel to the crack plane;

$$\sigma_1 = \sigma_{11} . \quad (3.26)$$

Substituing in (3.21), (3.22) and (3.23), we obtain the expressions for the local maximum tensile stress around the tip of the closed crack and the relative displacements of the crack faces.

It should be noted that although  $\Delta U_x$  can have any value,  $\Delta U_y$  can not have all negative values, because there is a closure stress  $\sigma_c$  for which the faces of the crack are in contact. Therefore, in this case

$$\Delta U_y = -2x_2; \text{ where } x_2 = a \sinh(\alpha_0) \sin(\beta) \quad (3.27)$$

equating with equation 3.23, we obtain the closure stress

$$\sigma_c = \frac{-4 \mu \alpha_0}{\kappa + 1} \quad (3.28)$$

which agrees with the value reported in the literature (Murrell, 1964; Berg, 1965; Murrell and Digby, 1970).

In the case when the crack is open and there is a fluid pressure  $p_f$  in its interior, the effective stresses are;  $\sigma_1 = \sigma_{11} - p_f$ ,  $\sigma_2 = \sigma_{22} - p_f$ , and  $\tau = \tau_{12}$ . Again we need to substitute in (3.21), (3.22) and (3.23), [see Murrell (1977) and Scholz (1990)].

### 3.1.4 Wing crack nucleation

The maximum tangential stress on the boundary of a crack with any particular orientation  $\theta$  occurs when (Murrell, 1964),

$$\frac{\partial \sigma_{\beta\beta}}{\partial \beta} = 0 \quad (3.29)$$

and this gives a quadratic equation for  $\beta$  whose solutions are,

$$\beta_c = \frac{\alpha_0 (\sigma_2 \pm \sqrt{\sigma_2^2 + \tau^2})}{\tau}. \quad (3.30)$$

Substituting these solutions in (3.21), we obtain

$$\max \sigma_{\beta\beta} = \mp \frac{\tau^2 \sqrt{\sigma_2^2 + \tau^2}}{\alpha_0 (\sigma_2^2 + \tau^2 \pm \sigma_2 \sqrt{\sigma_2^2 + \tau^2})} \quad (3.31)$$

Adding and subtracting from the right-hand side's numerator the quantity

$$\sigma_2 (\sigma_2^2 + \tau^2 \pm \sigma_2 \sqrt{\sigma_2^2 + \tau^2}) \quad (3.32)$$

and factorising the quantity

$$(\sigma_2^2 + \tau^2 \pm \sigma_2 \sqrt{\sigma_2^2 + \tau^2}) \quad (3.33)$$

we finally obtain a simple expression for the maximum tangential stress on the boundary of the pre-existing crack,

$$\max \sigma_{\beta\beta} = \frac{1}{\alpha_0} (\sigma_2 \mp \sqrt{\sigma_2^2 + \tau^2}). \quad (3.34)$$

The stress with the minus sign is always compressive and the one with the plus sign is always tensile.

In the case of uniaxial stress this equation simplifies further,

$$\max \sigma_{\beta\beta} = \frac{\sigma_{11}^0 (-1 + \sin(\theta_0)) \sin(\theta_0)}{\alpha_0} \quad (3.35)$$

where  $\sigma_{11}^0$  is the far field stress and  $\theta_0$  is the angle that the pre-existing crack makes with the applied stress.

The criterion for fracture initiation is that a crack will propagate when the tangential stress  $\sigma_{\beta\beta}$  is tensile and reaches a critical value equal to the maximum tensile interatomic force per unit area  $T$ . So taking the maximum tensile stress solution and making it equal to  $T$  we obtain

$$\alpha_0 T = \sigma_2 + \sqrt{\sigma_2^2 + \tau^2}, \text{ or} \quad (3.36)$$

$$\alpha_0^2 T^2 - 2\alpha_0 \sigma_2 T - \tau^2 = 0 \quad (3.37)$$

This equation is very important, because it relates the external stresses at fracture with a material property,  $T$  and with the crack parameters (aspect ratio, orientation). In particular, if we write  $T = 2K_t/\alpha_0$ , with  $K_t$  being the macroscopic tensile strength of the body, we obtain a parabola in the  $\sigma_2 - \tau$  plane, (Murrell, 1964)

$$\tau^2 = 4K_t(K_t - \sigma_2), \quad (3.38)$$

that defines the relation between  $\sigma_2$  and  $\tau$  at which fracture will occur, *i.e.*, the Mohr envelope.

Wing cracks (NDCs) will nucleate in compression from either open or closed flaws under shear if the tangential stress ( $\sigma_{\beta\beta}$ ) at the PEC surface is high enough.

As the maximum tension is parallel to the crack surface at the point  $(\alpha_0, \beta_c)$ , where

$$\beta_c = \frac{\alpha_0}{\tau} \left( \sigma_2 - \sqrt{\sigma_2^2 + \tau^2} \right), \quad (3.39)$$

the crack extension, or wing crack, will start to grow at that point and the direction of growth will be given by the normal to the surface at that point. This normal makes an angle  $\gamma_0$  with the major axis of the ellipse, which is given by, (for small  $\alpha_0, \beta_c$ ),

$$\tan(\gamma_0) = \coth(\alpha_0) \tan(\beta_c) = \frac{\sigma_2 - \sqrt{\sigma_2^2 + \tau^2}}{\tau}. \quad (3.40)$$

The peak tangential stress of PECs (from equation 3.34) is shown in Figures (3.3), (3.4) and (3.5) as a function of the flaw orientation and for several values of the applied deviatoric compressive stress. Each figure shows results for different values of confining pressure  $p_0$  and friction coefficient  $\mu_f$ . When the normalised stress ( $\frac{\sigma_{\beta\beta}}{T}$ ) is  $> 1$  then PECs of the corresponding orientation will produce wing cracks (NDCs). It is apparent from these figures that PECs with an increasing range of orientations ( $\theta_L \leq \theta \leq \theta_U$ ) nucleate wing cracks (NDCs) as the external stress ( $\Delta\sigma$ ) is increased. From this result, it is straightforward to obtain a distribution function that will describe the number of wing cracks (NDCs) as a function of the applied stress. The region of open and closed cracks is also shown.

The effect of confining pressure can be seen comparing Figures (3.3) and(3.4). A higher stress is needed to nucleate NDCs when a confining pressure is present. This means that the elastic region of a stress-strain curve is longer for higher confining pressures, or in other words the initiation of dilatancy is delayed. Also the confining pressure closes a big proportion of PECs except the ones that are quasi-parallel to the maximum compressive stress. The range of PECs ( $\theta_L \leq \theta \leq \theta_U$ ) nucleating wing cracks is reduced with confining pressure.

The effect of friction can be seen comparing Figures (3.3) and(3.5). The range of PECs ( $\theta_L \leq \theta \leq \theta_U$ ) nucleating wing cracks is reduced notoriously with increasing coefficient of friction. This is due to the locking of closed cracks, i.e., the majority of them can not overcome friction and consequently they can not slide.

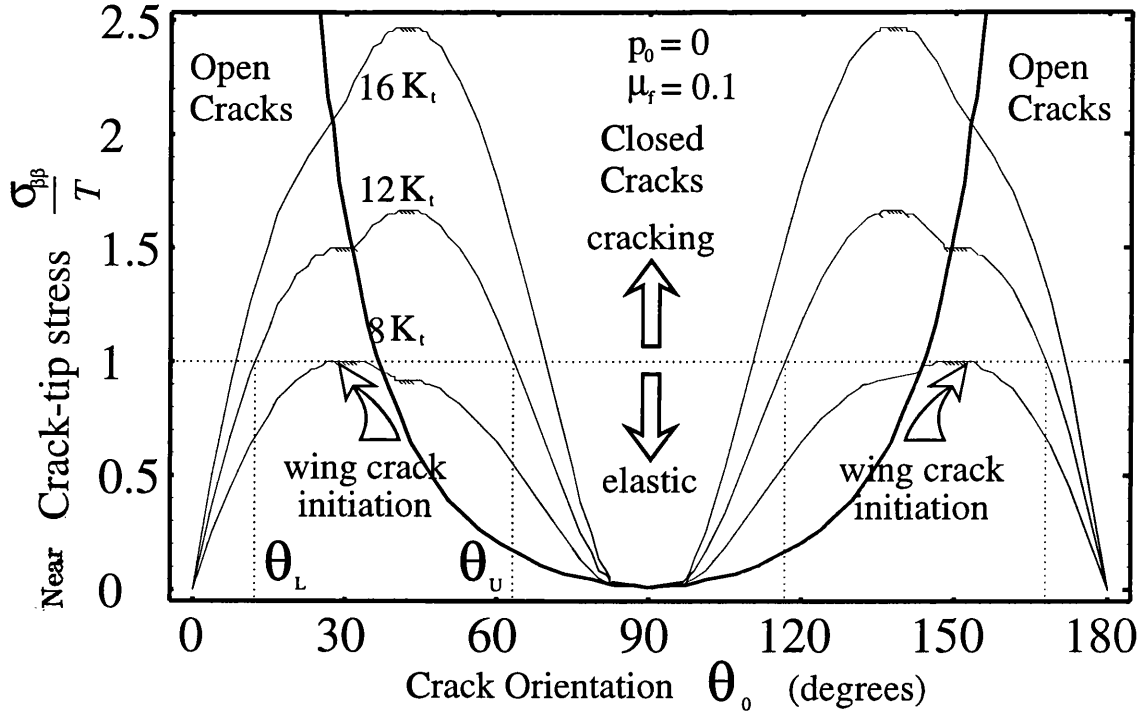


**Figure 3.3:** Normalised peak tangential stress at PECs' surface as a function of the pre-existing crack orientation  $\theta_0$ , where  $T$  is the interatomic cohesive strength of the matrix. The onset of propagation is reached when  $\sigma_T/T$  is greater than 1. For a higher level of stress, there is a whole range of cracks ( $\theta_L < \theta_0 < \theta_U$ ) that will nucleate wing cracks, from which it is possible to obtain the proportion of cracks that are propagating as a function of the applied stress. The thick parabolic line delimits the region of open and closed cracks. Uniaxial compression case, and low coefficient of friction.

### 3.1.5 First PEC in nucleate wing cracks

From equation 3.34 we can obtain the orientation  $\theta_0$  of the first crack to nucleate wing cracks see Murrell (1964).



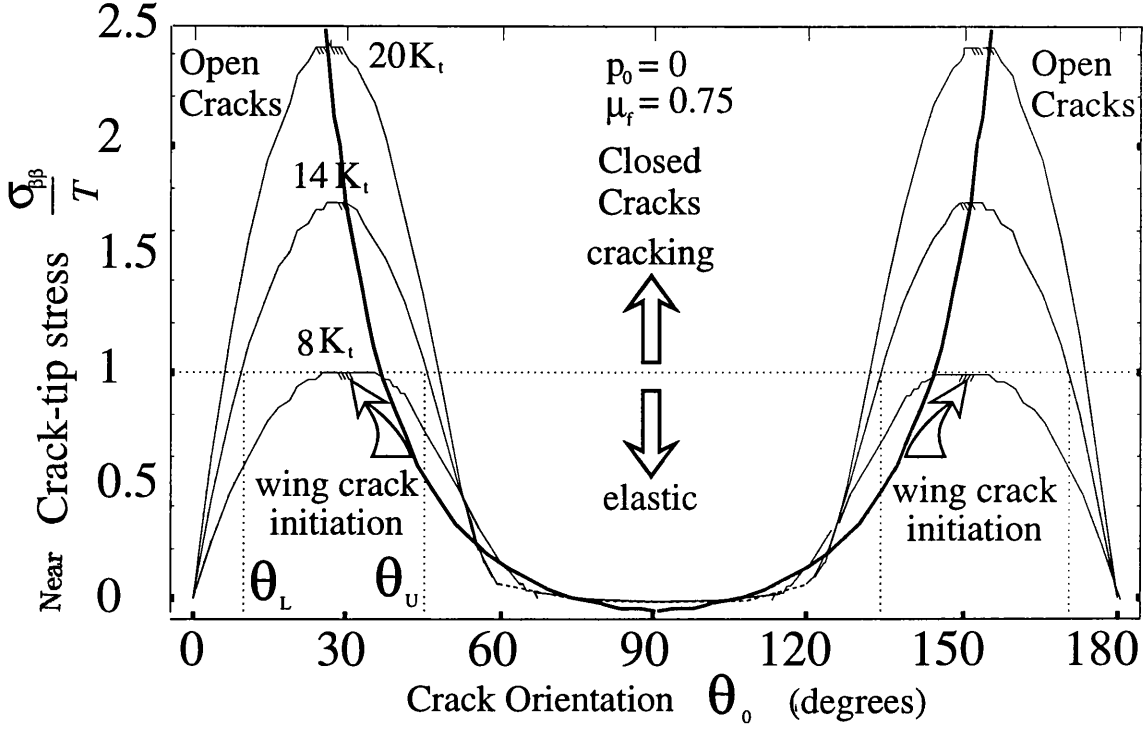


**Figure 3.5:** Normalised peak tangential stress at PECs' surface as a function of the pre-existing crack orientation  $\theta_0$ . The onset of propagation is reached when  $\sigma_T/T$  is greater than 1. For a higher level of stress, there is a whole range of cracks ( $\theta_L < \theta_0 < \theta_U$ ) that will nucleate wing cracks, from which it is possible to obtain the proportion of cracks that are propagating as a function of the applied stress. The thick parabolic line delimits the region of open and closed cracks. Uniaxial compression case and high coefficient of friction.

After simplifications, this equation can be reduced to

$$\cos(2\theta_0) = \frac{-(\sigma_{22}^0 - \sigma_{11}^0)}{2(\sigma_{22}^0 + \sigma_{11}^0)}. \quad (3.44)$$

This equation is true only if  $|\cos(2\theta_0)| \leq 1$ ; i.e., only if

$$-1 \leq \frac{-(\sigma_{22}^0 - \sigma_{11}^0)}{2(\sigma_{22}^0 + \sigma_{11}^0)} \leq 1. \quad (3.45)$$

The above inequalities may be expressed in the form

$$\sigma_{22}^0 + 3\sigma_{11}^0 \geq 0 \quad (3.46)$$

$$3\sigma_{22}^0 + \sigma_{11}^0 \geq 0 \quad (3.47)$$

If these inequalities are violated, then the solutions  $\theta_0 = 0$  or  $\theta_0 = \pi/2$  should be used.

In this thesis we will consider that  $\sigma_{22}^0 < \sigma_{11}^0$ , taking compressive stresses as negative.

As a result we obtain the following two cases;

I) If  $3\sigma_{11}^0 + \sigma_{22}^0 \geq 0$ , then  $\theta_0 = \pi/2$ ,  $\sigma_2 = \sigma_{11}^0$  and  $\tau_0 = 0$ , and

$$\max \sigma_{\beta\beta} = 2\sigma_{11}^0 / \alpha_0 \quad (3.48)$$

This is a pure Mode I failure, *i.e.*, tensile. The direction of growth of the crack is  $\gamma_0 = 0$ .

II) If  $3\sigma_{11}^0 + \sigma_{22}^0 \leq 0$ , then

$$\cos(2\theta_0) = \frac{-(\sigma_{22}^0 - \sigma_{11}^0)}{2(\sigma_{22}^0 + \sigma_{11}^0)}, \quad (3.49)$$

and the local stresses are:

$$\sigma_2 = \frac{(\sigma_{22}^0)^2 + 6\sigma_{22}^0\sigma_{11}^0 + (\sigma_{11}^0)^2}{4(\sigma_{22}^0 + \sigma_{11}^0)}, \quad (3.50)$$

$$\tau = \frac{(-\sigma_{22}^0 + \sigma_{11}^0) \sqrt{3(\sigma_{22}^0)^2 + 10\sigma_{22}^0\sigma_{11}^0 + 3(\sigma_{11}^0)^2}}{4(\sigma_{22}^0 + \sigma_{11}^0)} \quad (3.51)$$

Therefore, this is a mixture of Modes I and II failure for a general compressive state. The direction of growth of the wing crack (NDC) (equation 3.40) is given by,

$$\tan(\gamma_0) = \frac{\sigma_{22}^0 - \sigma_{11}^0}{\sqrt{3(\sigma_{22}^0)^2 + 10\sigma_{22}^0\sigma_{11}^0 + 3(\sigma_{11}^0)^2}}. \quad (3.52)$$

In the case when the applied stresses are enough to close the cracks, crack propagation depends on the friction between the closed crack surfaces, and the orientation of the first crack that propagates is:

$$\theta_0 = \frac{1}{2} \arctan\left(\frac{1}{\mu_f}\right), \quad (3.53)$$

where  $\mu_f$  = coefficient of friction, see Murrell (1977).

Therefore, it is found that under a general system of loads, a crack (open or closed) does not grow in its own plane. Instead, it will develop wing cracks (NDCs) emerging symmetrically from near its tips, that extend in a direction quasi-parallel to the maximum compressive stress, as shown in figure 3.2.

### 3.1.6 Stress around a wing crack

At this point we can see that for given far-field stresses  $\sigma_{22}^0$  and  $\sigma_{11}^0$  acting on a material with cracks of aspect ratio  $\alpha_0$  and random orientations, we can predict which cracks will propagate, if they will, and in which direction they will grow, but we can not yet say if the NDC (wing crack) will have a length of finite value.

In order to estimate the wing crack length, we will make use of the following stratagem. The relative displacements of the faces of the original crack will control the wing crack in the same way as a dislocation, with Burgers vector  $\mathbf{b} = (\Delta U_x, \Delta U_y)$ , that wedges open the wing crack.  $\Delta U_x$  and  $\Delta U_y$  are the components of the crack opening displacement of the pre-existing crack.

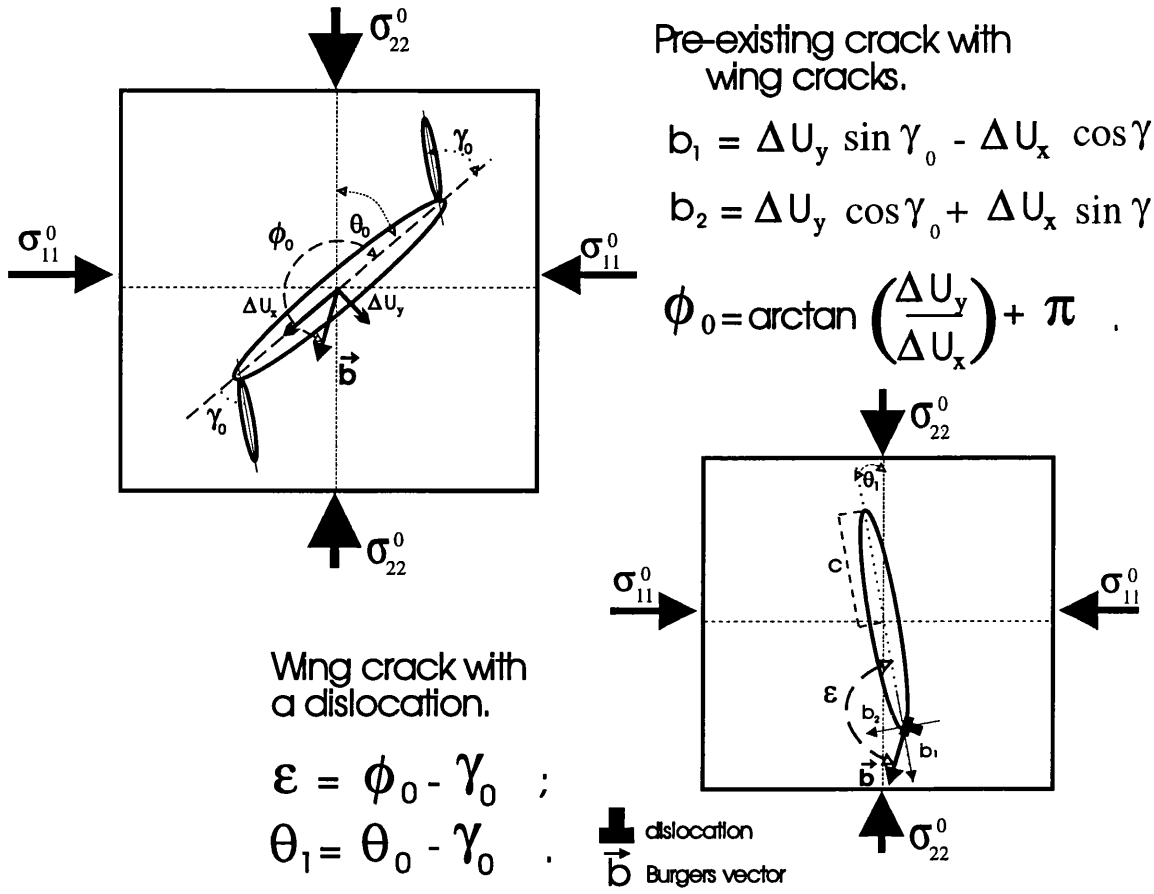


**Figure 3.6:** The wing crack growth can be modelled assuming that the effect of the original crack on the wing crack is analogous to the effect on a crack due to a dislocation with Burgers vector  $\vec{b}$  in one of its tips.

Following Murrell's work (Murrell, 1964), we calculated analytically the tangential stress and displacements on the surface of an elliptical crack of length  $2c$  and aspect ratio  $\alpha_1$ , that has an edge dislocation  $\vec{b} = (b_1, b_2)$  at one of its ends, and which is making an angle  $\epsilon$  with the major axis of the ellipse, being under external stresses  $\sigma_{11}^0$  and  $\sigma_{22}^0$ , see figure 3.6. We will solve first the problem of the elliptical crack with a dislocation, and then superpose this solution with the solution of the elliptical crack under external stresses that has already been obtained before.

The stress functions for the dislocation are:

$$\phi(z) = \frac{-\mu(ib_1 + b_2)\zeta}{(\kappa + 1)\pi} \quad (3.54)$$

and

$$\psi(z) = \frac{\mu}{(\kappa + 1)\pi} ((ib_1 - b_2)\zeta + (ib_1 + b_2) \cosh(2\alpha_1) \coth(\zeta)), \quad (3.55)$$

where  $z = c \cosh(\zeta)$  and  $\zeta = \alpha + i\beta$ .

The stresses and displacements in terms of these complex elastic potentials are given by

$$\sigma_{\rho\rho} + \sigma_{\beta\beta} = 4\text{Re}(\phi'(z)) \quad (3.56)$$

$$\sigma_{\beta\beta} - \sigma_{\rho\rho} + 2i\sigma_{\rho\beta} = 2(\bar{z}\phi''(z) + \psi'(z)) \quad (3.57)$$

$$2\mu(U_x + iU_y) = \kappa\phi(z) - z\bar{\phi}'(z) - \bar{\psi}(z) \quad (3.58)$$

The solution of these equations has to be superposed to the solution of an elliptical crack under far field stresses  $\sigma_{11}^0, \sigma_{22}^0$ . For  $\alpha$  and  $\beta$  small the total tangential stress is:

$$\sigma_{\beta\beta} = \frac{\alpha_1 (\sigma_{22}^0 + \sigma_{11}^0 + (\sigma_{11}^0 - \sigma_{22}^0) \cos(2\theta_1) + B \sin(\epsilon)) + \beta (-B \cos(\epsilon) + (\sigma_{22}^0 - \sigma_{11}^0) \sin(2\theta_1))}{\alpha_1^2 + \beta^2} \quad (3.59)$$

where

$$B = \frac{4\mu \sqrt{b_1^2 + b_2^2}}{c(\kappa + 1) \pi} \quad (3.60)$$

$\theta_1$  is the orientation of the major axis of the crack with respect to the load  $\sigma_{22}^0$  and  $c$  is the separation between the foci of the elliptical crack. It is very easy to see that if we define the effective stresses acting in the crack plane as

$$2\sigma_2 = \sigma_{22}^0 + \sigma_{11}^0 + (\sigma_{11}^0 - \sigma_{22}^0) \cos(2\theta_1) + B \sin(\epsilon) \quad (3.61)$$

$$2\tau = B \cos(\epsilon) - (\sigma_{22}^0 - \sigma_{11}^0) \sin(2\theta_1) \quad (3.62)$$

then we obtain again an equation with the same form as equation 3.21;

$$\sigma_{\beta\beta} = \frac{2(\alpha_1\sigma_2 - \beta\tau)}{\alpha_1^2 + \beta^2}. \quad (3.63)$$

### 3.1.7 Wing crack growth

The maximum tangential stress on the boundary of a crack (wedged open by a dislocation) with any particular orientation  $\theta$  occurs when, see Murrell (1964),

$$\frac{\partial\sigma_{\beta\beta}}{\partial\beta} = 0 \quad (3.64)$$

and this gives a quadratic equation for  $\beta$  whose solutions are,

$$\beta_c = \frac{\alpha_1 (\sigma_2 \pm \sqrt{\sigma_2^2 + \tau^2})}{\tau}. \quad (3.65)$$

Substituting these solutions in 3.63, we obtain

$$\max\sigma_{\beta\beta} = \mp \frac{\tau^2 \sqrt{\sigma_2^2 + \tau^2}}{\alpha_1 (\sigma_2^2 + \tau^2 \pm \sigma_2 \sqrt{\sigma_2^2 + \tau^2})} \quad (3.66)$$

Adding and subtracting from the right-hand side's numerator the quantity

$$\sigma_2 \left( \sigma_2^2 + \tau^2 \pm \sigma_2 \sqrt{\sigma_2^2 + \tau^2} \right) \quad (3.67)$$

and factorising the quantity

$$\left( \sigma_2^2 + \tau^2 \pm \sigma_2 \sqrt{\sigma_2^2 + \tau^2} \right) \quad (3.68)$$

we finally obtain a simple expression for the maximum tangential stress on the boundary of the crack wedged open by a dislocation,

$$\max \sigma_{\beta\beta} = \frac{1}{\alpha_1} (\sigma_2 \mp \sqrt{\sigma_2^2 + \tau^2}) \quad (3.69)$$

The stress with the minus sign is always compressive and the one with the plus sign is always tensile.

Therefore, we will have the same equations as before (Eqs. 3.21 -3.37) but with different effective stresses and with  $\alpha_1$  instead of  $\alpha_0$ . In particular, we will have the result that the NDC will propagate when the maximum tensile stress reaches the critical value  $T$ , then

$$\alpha_1^2 T^2 - 2 \alpha_1 \sigma_2 T - \tau^2 = 0 . \quad (3.70)$$

If we take this wedged open crack as a model for the NDC (i.e. the wing crack formed from the PEC), we find that (See Figure 3.6)

$$\epsilon = \phi_0 - \gamma_0 ; \phi_0 = \arctan\left(\frac{\Delta U_y}{\Delta U_x}\right) + \pi \quad (3.71)$$

$$\theta_1 = \theta_0 - \gamma_0 \quad (3.72)$$

The orientation  $\theta_1$  of this wing crack with respect to the major principal stress  $\sigma_{22}^0$  is determined by the orientation  $\theta_0$  of the original crack and the point on the surface of this crack where it starts to grow.

In the case of an external uniaxial tensile stress, the first PEC to nucleate wing cracks is the one that is oriented at  $\theta_0 = 0$ , and it will grow in the direction  $\gamma_0 = 0$  when the applied stress  $\sigma_{11}^0$  reaches the value  $\alpha_0 T/2$ . The equivalent edge dislocation will be perpendicular ( $\phi_0 = \pi/2$ ) to the main axis of the wing crack, and  $B$  in this case will be

$$B = \frac{2a\sigma_{11}^0}{\pi c} . \quad (3.73)$$

The case of external compressive stresses is more complicated. Note that the only part in equations 3.61–3.62 that will be affected by the closure of the crack is the one that depends on both  $B$  and  $\epsilon$ . We can rewrite the local stresses as;

$$\sigma_2 = a_1 + \frac{b'_2}{c} ; \tau = a_2 + \frac{b'_1}{c} \quad (3.74)$$

where

$$a_1 = \frac{\sigma_{22}^0 + \sigma_{11}^0 + (\sigma_{11}^0 - \sigma_{22}^0) \cos(2\theta_1)}{2}, \quad (3.75)$$

$$a_2 = \frac{-(\sigma_{22}^0 - \sigma_{11}^0) \sin(2\theta_1)}{2}, \quad (3.76)$$

$$b'_1 = \frac{B}{2} c \cos(\epsilon) = \frac{2\mu b_1}{(\kappa + 1)\pi} \text{ and } b'_2 = \frac{B}{2} c \sin(\epsilon) = \frac{2\mu b_2}{(\kappa + 1)\pi}. \quad (3.77)$$

The quantities  $a_1$ ,  $a_2$ ,  $b'_1$  and  $b'_2$  depend on the effective stresses on the original crack. Then, they depend on whether the PEC is open or closed at the particular level of stress (and also whether a fluid pressure exists in the crack). Explicitly, the dislocation components are:

$$b_1 = \Delta U_y \sin \gamma - \Delta U_x \cos \gamma, \quad (3.78)$$

$$b_2 = \Delta U_x \sin \gamma + \Delta U_y \cos \gamma. \quad (3.79)$$

$\Delta U_x$  and  $\Delta U_y$  are given by equations (3.22) and (3.23) respectively.

It is important to notice that if we assume that the wing crack propagates in its own plane, i.e.,  $\beta = 0$ , and that the pre-existing crack is a perfectly closed sharp slit, equation 3.21 for the PEC becomes

$$\sigma_{\beta\beta} = \lim_{\alpha_0 \rightarrow 0} \frac{2 * \sigma_2}{\alpha_0} \quad (3.80)$$

which is singular and is similar to equation (2.1). Therefore we can calculate the mode I stress intensity factor as: (Lawn, 1993)

$$K_I = \sqrt{\pi c} \sigma_2 \quad (3.81)$$

and  $\sigma_2$  is given in equation 3.74 which after the substitutions becomes,

$$\sigma_2 = \frac{1}{2} \left[ \sigma_{11}^0 + \sigma_{22}^0 + (\sigma_{11}^0 - \sigma_{22}^0) \cos 2(\theta - \gamma) \right] + \frac{4\mu}{(\kappa + 1)\pi c} \Delta U_x \sin \gamma. \quad (3.82)$$

For a closed crack the relative displacement on the PEC's plane is (Nemat-Nasser and Hori, 1993),

$$\Delta U_x = \left( \frac{1 + \kappa}{\mu} \right) \frac{l}{2} [\tau - \mu(\sigma)]. \quad (3.83)$$

$\Delta U_y = 0$  because we are talking about a closed sharp slit.

After multiplying  $\sigma_2$  by  $\sqrt{\pi c}$  we obtain the same expression for the stress intensity factor  $K_I$  (mode I) at the tip of the wing crack as that obtained by Horii and Nemat-Nasser (1986) (see equation (2.8)), except by the term  $c^*$  that was introduced *ad hoc* by them. Therefore we have obtained the sliding crack model as a limit case.

While Horii and Nemat-Nasser (1986) and Wong (1990) make the assumption that the wing crack propagates in its own plane, we are actually calculating the direction of growth of this wing crack using the same criteria that we use for the growth of the original crack. This criteria led us to equations 3.21 and 3.63, which tell us that in the process of growth of wing cracks, both the mode I and mode II displacements are important, and therefore both modes or stress intensity factors should be taken into account. The procedure that we followed is therefore more complete than the previous models.

### 3.1.8 Length of wing cracks

Substituting 3.74 into 3.70 we can obtain several versions of the equation for the wing crack length  $c$  depending on how the aspect ratio  $\alpha_1$  of the wing crack depends on  $c$  itself.

If we take  $\alpha_1$  as independent of  $c$ , i.e. scale independent, we obtain a quadratic equation for  $c$ ,

$$-b_2'^2 + c(-2 a_2 b_2' - 2 \alpha_1 b_1' T) + c^2(-a_2'^2 - 2 \alpha_1 a_1' T + \alpha_1^2 T^2) = 0 \quad (3.84)$$

where  $a_1$ ,  $a_2$ ,  $b_1'$  and  $b_2'$  are given by equations (3.75-3.77). The solution of this equation is straightforward.

If we take  $\alpha_1 = \sqrt{\frac{\rho}{c}}$ , where  $\rho$  is the crack tip radius of curvature, and keep  $\rho$  fixed, we obtain a quartic equation,

$$-b_2'^2 - 2 a_2' b_2' c - a_2'^2 c^2 - 2 b_1' \sqrt{c} \sqrt{\rho} T - 2 a_1' c^{\frac{3}{2}} \sqrt{\rho} T + c \rho T^2 = 0 \quad (3.85)$$

(no solution is available at this moment). **This aspect ratio was used by Murrell (1964).**

If we take  $\alpha_1 = b_0/c$ , where  $b_0$  is the minor axis of the branching crack and is constant, we obtain again a quadratic equation,

$$-b_2'^2 - a_2'^2 c^2 - 2 b_0 b_1' T + b_0^2 T^2 + c(-2 a_2' b_2' - 2 a_1' b_0 T) = 0. \quad (3.86)$$

In the following we will make use of the first of these equations (eq. 3.84). Thus, we are making the assumption that the wing-crack aspect ratio is scale independent. We will also make this aspect ratio equal to that of the pre-existing crack.

### 3.1.9 Stability of wing cracks

The length  $c$  from which we can deduce whether or not the wing crack is stable, is obtained from the physical conditions imposed on the original crack. The only external parameters in our model are: Young's modulus  $E$ , Poisson's ratio  $\nu$ , the friction coefficient  $\mu_f$ , the orientation  $\theta_0$ , the aspect ratio  $\alpha_0$  and the length  $2a$  of the original crack, the confining pressure  $p_0$  ( $= -\sigma_{11}^0$ ) and the deviatoric stress  $\Delta\sigma$  ( $= \sigma_{11}^0 - \sigma_{22}^0$ ).

Unstable crack growth implies that crack length grows without limit leading to failure of the specimen, but stability may be favoured by a superimposed confining pressure  $p_0$ , or by the blunting of the microcrack before it reaches an unstable length, etc. In any case, under a given applied stress, macroscopic fracture will not occur while the wing crack has a stable length. As previously noted, under uniaxial tensile stress NDCs are always unstable.

In order to consider the problem of NDC stability, we calculate the peak tensile stress ( $\sigma_{\beta\beta}$ ) in the surface of an NDC as a function of the NDC length. The peak value of  $\sigma_{\beta\beta}$  for a crack of any given orientation  $\theta$  is given by **equation (3.69)**,

$$\max\sigma_{\beta\beta} = \frac{1}{\alpha_1}(\sigma_2 \mp \sqrt{\sigma_2^2 + \tau^2}) \quad (3.87)$$

with  $\sigma_2$  and  $\tau$  given by equation 3.74.

Contributions to this peak stress come from the far-field stress and from the near field dislocation stresses. As the NDC grows the far-field component increases and the near field component decreases. In Figures 3.7 to 3.9 we show the peak value of  $\sigma_{\beta\beta}$  as a function of NDC length for several values of compressive deviatoric far field stress  $\Delta\sigma$ . Each figure shows the results for different values of confining pressure and coefficient of friction. In each case, the orientation  $\theta_0$  of the PEC was chosen to correspond to the PEC that produces the first unstable wing crack, i.e., the most dangerous pre-existing crack.

In figures 3.7 to 3.9 it should be noted that an NDC only exists if  $\sigma_{\beta\beta} \geq T$ , and that growth of the NDC will not occur if  $\sigma_{\beta\beta} < T$ . NDCs first nucleate under a uniaxial compressive far field stress when  $\Delta\sigma = 8K_t$  (Griffith, 1924; Murrell, 1964), and they are clearly stable (the equation for  $\sigma_{\beta\beta}$  as a function of  $c(a)$  has only one real root,  $c_I^0$ ). When  $\Delta\sigma$  is increased above this value there are two finite values for  $c$ . Consider, for example, the case when  $\Delta\sigma = 12K_t$ . The curve in this case intersects the line  $\sigma_{\beta\beta} = T$  at two points: at  $c = c_I$  the wing crack is stable; and at  $c = c_{II}$  the crack is potentially unstable. Further increments in  $\Delta\sigma$  cause the stable NDC length lower value of  $c(a)$ ,  $c_I$ , to increase stably and the larger value  $c_{II}$  to decrease until  $c_I = c_{II}$ , when the NDC becomes unstable. The value of  $\Delta\sigma$  for which this happens is the ultimate failure stress of the body. This result

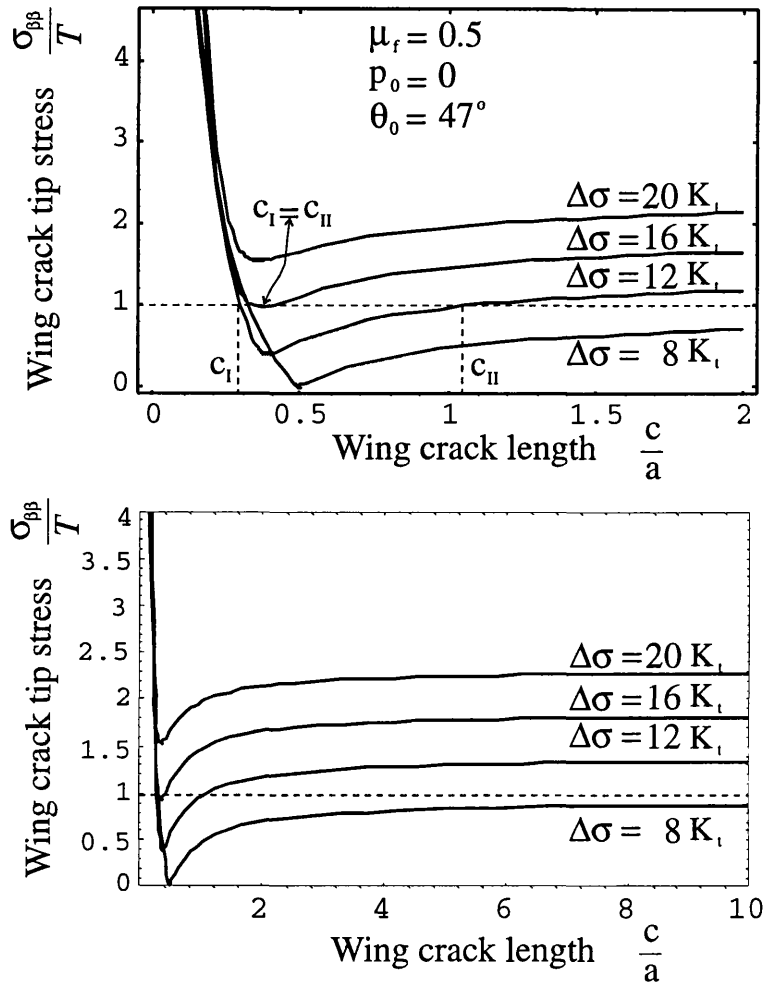


**Figure 3.7:** Normalised tangential stress (where  $T$ = "atomic" strength of solid) as a function of normalised wing crack length for uniaxial compression. If  $\sigma_T/T < 1$  there is no propagation at all. When the tangential stress decreases with crack length, the growth is stable, and when it increases with crack length the growth is unstable. It can be seen that at a stress of  $16 K_t$  the growth becomes unstable leading to the fracture of the specimen.

is completely new for models dealing with crack growth under compression and note that crack-crack interactions have not yet been included.

Comparing figures (3.7) and (3.8) we can appreciate the effect of confining pressure on stability of the NDCs. In presence of confining pressure not only the NDCs have become more stable, but the NDC's lengths have been reduced considerably. Then we can anticipate that this NDCs will not have a strong impact on the compliances of a elastic body subjected to high confining pressures.

Comparing figures (3.7) and (3.9) we can see the effect of different friction coefficients on NDC's length. It is apparent that less friction produces more unstable cracks, though in the regime of stability the lengths are more or less of the same size.

Figures 3.10-3.11 show that for a given PEC with orientation  $\theta_0$ , the corresponding

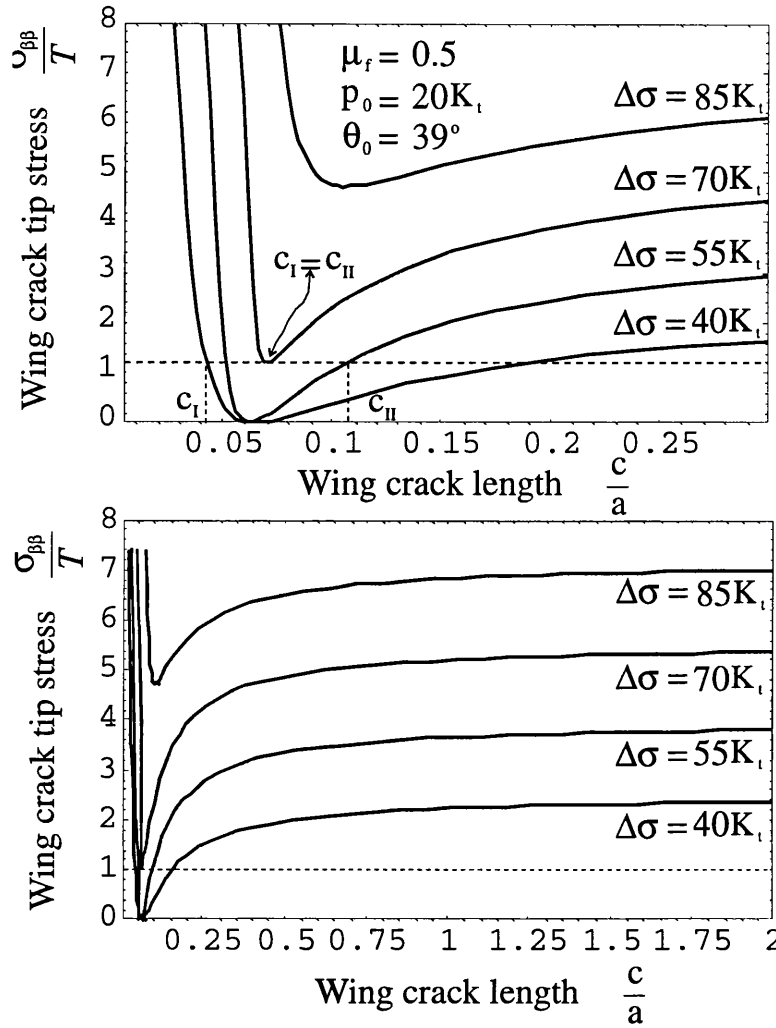


**Figure 3.8:** Normalised tangential stress (where  $T$ = "atomic" strength of solid) as a function of normalised wing crack length for uniaxial compression. If  $\sigma_T/T < 1$  there is no propagation at all. When the tangential stress decreases with crack length, the growth is stable, and when it increases with crack length the growth is unstable. It can be seen that at a stress of  $70 K_t$  the growth becomes unstable leading to the fracture of the specimen.

NDCs grow quite stably until the peak stress is reached. The stabilising effect of the confining pressure can also be seen. It is seen as well that the point of NDC initiation is higher for higher confining pressures, which is an indication that the body has a larger elastic regime in presence of confining pressure. Another feature is that elevated confining pressure appear to suppress crack growth by reducing the size of NDCs. This should have an impact in the coalescence of cracks which will not be favoured by the small wing crack lengths.

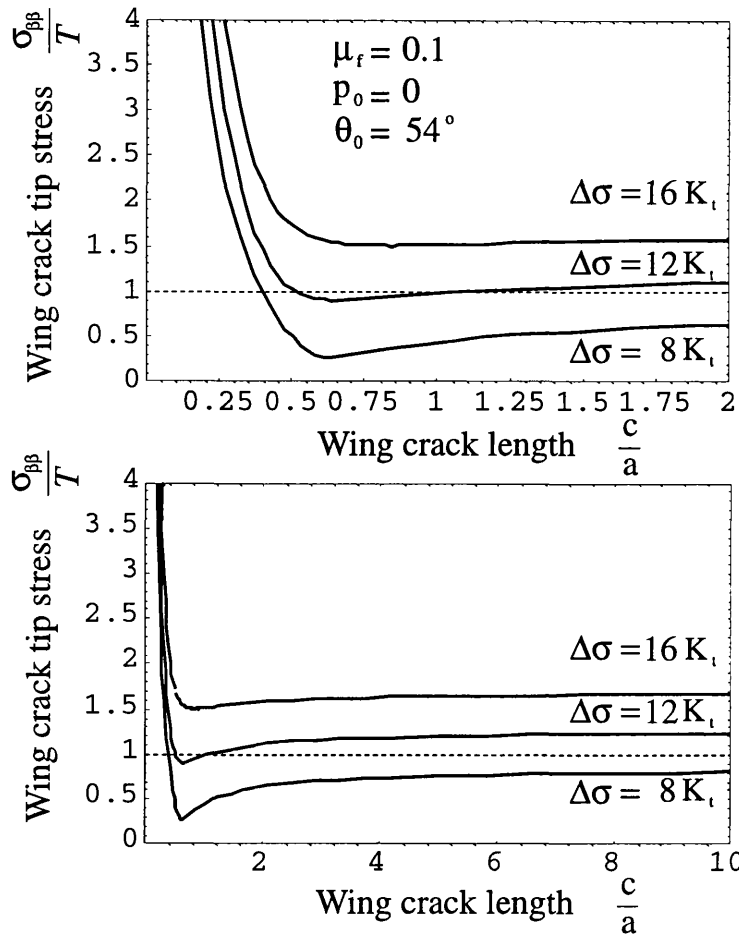


**Figure 3.9:** Normalised tangential stress (where  $T$ = "atomic" strength of solid) as a function of normalised wing crack length for uniaxial compression. If  $\sigma_T/T < 1$  there is no propagation at all. When the tangential stress decreases with crack length, the growth is stable, and when it increases with crack length the growth is unstable. It can be seen that at a stress greater than  $12 K_t$  the growth becomes unstable leading to the fracture of the specimen.

### 3.2 Effects of a population of Wing Cracks (NDCs) on Rock Physical Properties

#### 3.2.1 Anisotropy.

In the top panel of Figure 3.12 the dependence of  $c = c_I$  with the orientation of the original crack is plotted for the uniaxial compression case, we can see that the cracks with  $30^\circ < \theta_0 < 57^\circ$  develop longer wing cracks than any other, and that these wing cracks are orientated between  $30^\circ$  and  $11^\circ$  with respect to the maximum compressive stress (Bottom panel Figure 3.12). Thus, the wing crack (NDC) population is highly anisotropic. The theoretical treatment and analysis of anisotropic crack populations and their elastic effects is discussed in detail in Chapter 4 of this thesis. However, this approach has not yet been

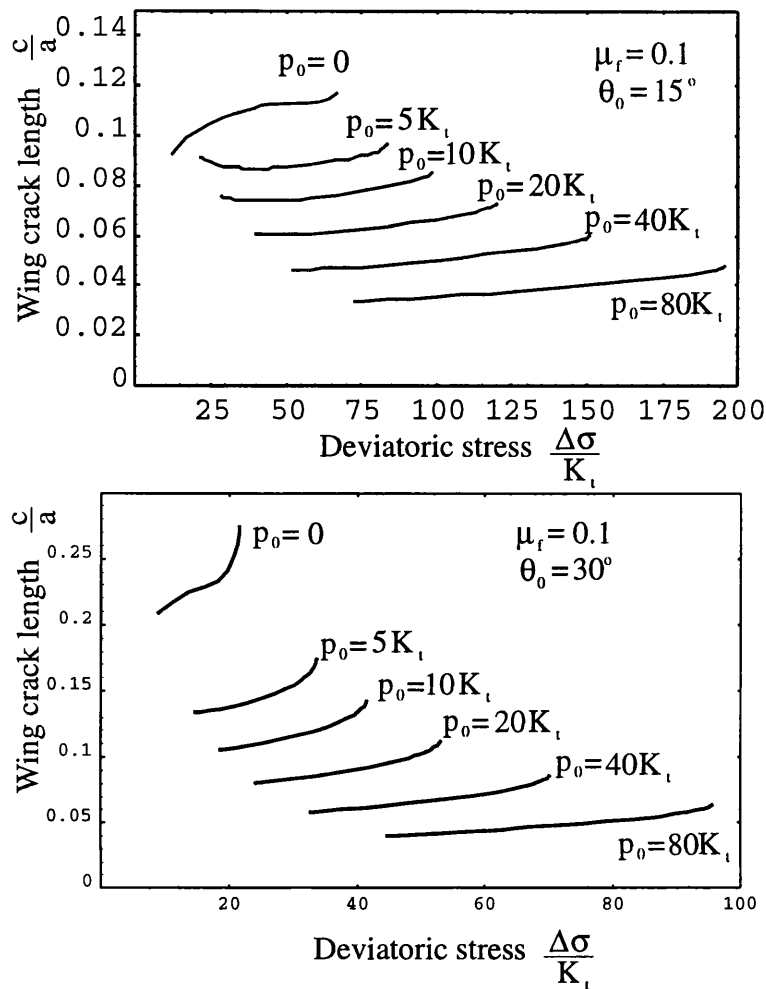


**Figure 3.10:** Normalised wing crack length as a function of applied stress, for several confining pressures.  $c$  is the length of the wing crack and  $a$  the pre-existing crack length. Clearly there is a regime of stability where the crack has a finite length, and there is a critical point where the crack becomes unstable.  $\Delta\sigma$  is the differential stress and  $K_t$  is the tensile strength of the body.  $c$  is the length  $c_l$  of Figure 3.7.

applied to the crack model considered in this section, due to lack of time, and remains for future work.

### 3.2.2 Ultimate Failure of Rock.

The strength is defined as the maximum differential stress a rock can support. The strength increases dramatically with increasing confining pressure. The increase is non-linear, and is faster at lower confining pressures. High confining pressures also promote larger deformation prior to eventual brittle failure. As pressure is increased further, rock samples eventually go through a brittle-ductile transition. Above a certain confining pressure the rock is completely ductile and macroscopic fracture does not occur. (See Paterson (1978)).

At low confining pressure samples tend to fail by axial splitting, presumably due to a

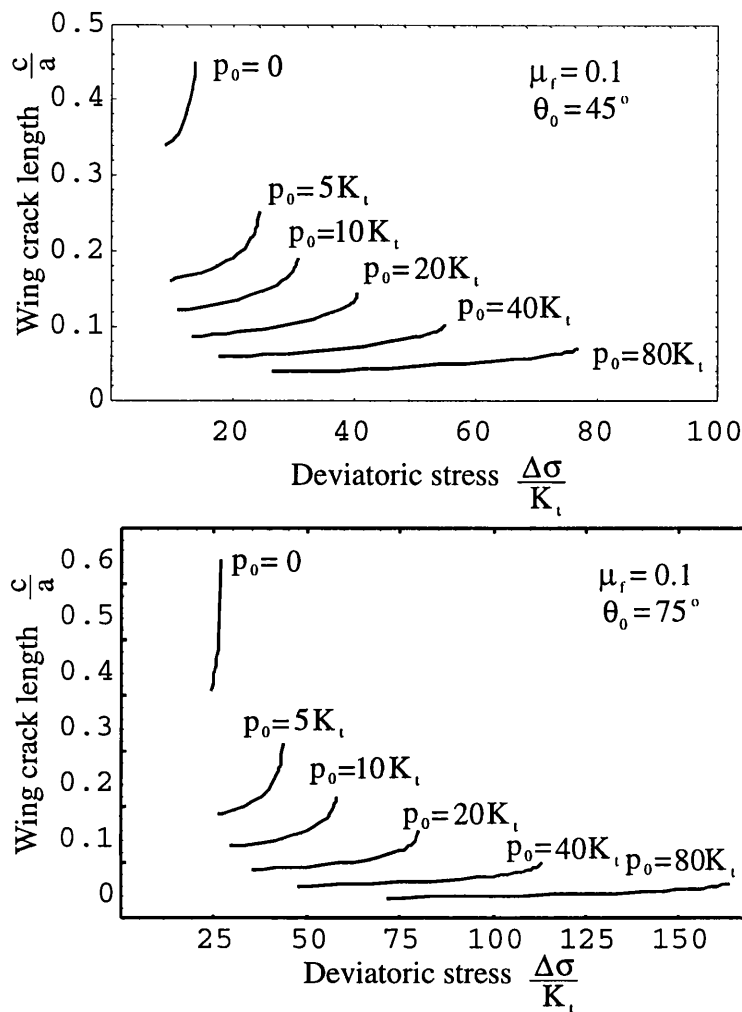


**Figure 3.11:** Normalised wing crack length as a function of applied stress, for several confining pressures.  $c$  is the length of the wing crack and  $a$  the pre-existing crack length. Clearly there is a regime of stability where the crack has a finite length, and there is a critical point where the crack becomes unstable.  $\Delta\sigma$  is the differential stress and  $K_t$  is the tensile strength of the body.

$c$  is the length  $c_I$  of Figure 3.7.

few cracks. As pressure is increased the sample fails along well defined shear faults, these faults broaden with increasing pressure into zones of intense crack initiation, where the crack density is big enough to allow crack interaction to be important. **Evans et al. (1990).**

The orientation  $\theta_1$  of the first unstable wing crack at the ultimate stress  $\sigma_f$  tends to increase with the confining pressure  $p_0$ , in agreement with the experimental measurements of the shear failure surface orientation at different confining pressures, (see Paterson, 1978). Therefore, the fracture angle  $\theta_1$  may help to determine possible directions of faulting as is shown in Figure 3.13. At low confining pressures the theoretical curves match the data very well, but the rate at which the experimental fracture angle increases with confining pressure is more abrupt at moderate pressures. The plotted data for Westerly Granite are from Mogi (1966), for Berea Sandstone are from Bernabe and Brace (1990), for Daye

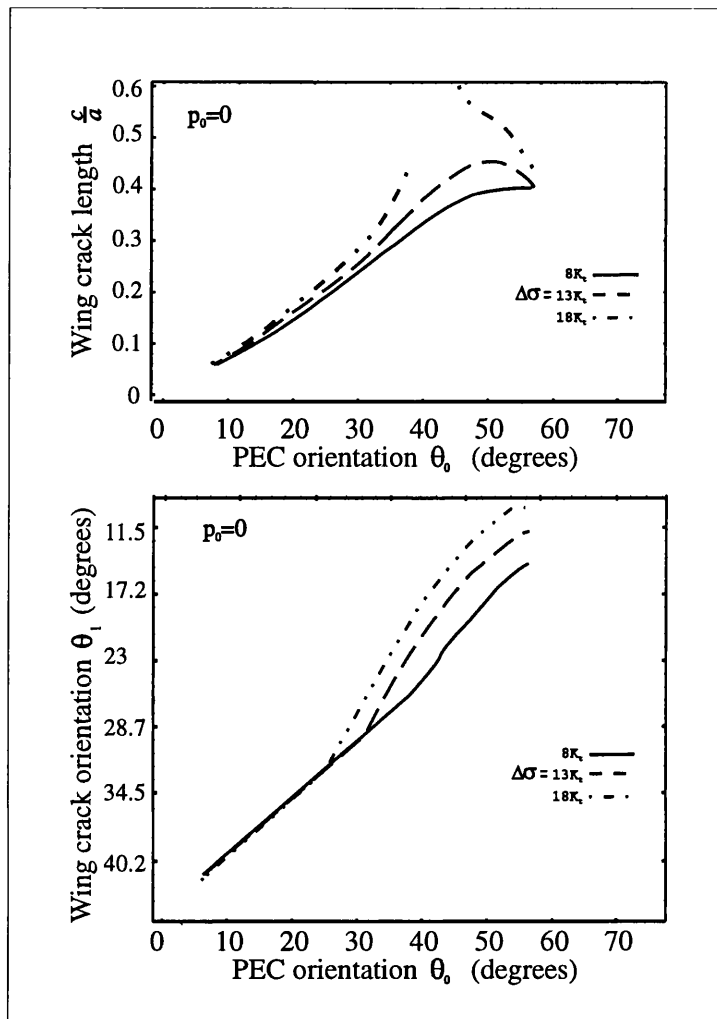


**Figure 3.12:** Length and orientation of the wing crack as a function of the original crack orientation for 3 different deviatoric stresses. Uniaxial compression case.  $\mu_f = 0.1$ .

Marble are from Ouyang and Elsworth (1991), and for Darley Dale Sandstone are from Murrell (1965). However, before ultimate failure, when fractures are formed, wing cracks of other orientations are also formed.

The stability of the wing cracks and consequently their lengths, will depend on several factors. Unstable crack growth implies failure of the specimen, but stability may be favoured by a superimposed hydrostatic pressure  $p_0$ , as well as by the blunting of the microcrack before it reaches an unstable length, etc. Anyway, under a given applied stress, macroscopic fracture will not occur if the wing crack reaches a stable length. As shown in Figures 3.7-3.9, the stress at which  $c_I = c_{II}$  is the ultimate failure stress  $\sigma_f$  for that particular stress-state.

In Figure 3.14, the variation of the calculated ultimate failure stress  $\sigma_f$  as a function of

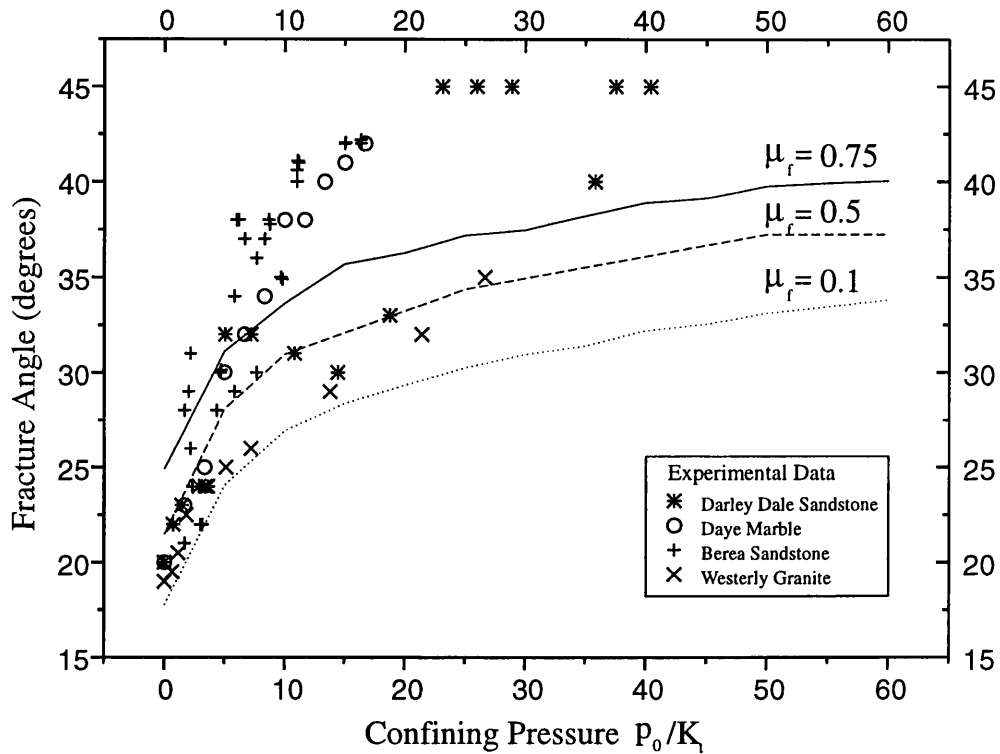


**Figure 3.13:** Orientation of the first unstable wing crack at the ultimate stress as a function of confining pressure. Lines are the theoretical values for 3 different values of friction coefficient. Points are experimental data of failure surface orientation for several kind of rocks (see text for references).

the confining pressure  $p_0$  is shown. Three different values for the friction coefficient were used. This Figure also shows experimental values of failure stress obtained by Edmond and Murrell (1972) for microgranodiorite rock; by Murrell (1965) for Darley Dale sandstone; and by Rist and Murrell (1994) for polycrystalline ice. Note that the experimental points for each particular rock can match with the theoretical  $\sigma_f$  if we choose the right coefficient of friction. Thus, the polycrystalline ice fracture stress follows the curve corresponding to a friction of 0.1, the microgranodiorite points match very closely the curve corresponding to a friction of 0.5, and finally the sandstone follows the curve for  $\mu_f = 0.75$  with certain deviation at high confining pressure.

In Figures 3.15-3.17 we show separately the variation of the calculated ultimate failure stress  $\sigma_f$  and the stress ( $\sigma_i$ ) for the initiation of NDCs as functions of the confining pressure  $p_0$  for each type of rock and for the corresponding friction coefficient. In the 3 figures, it can be seen the apparent increasing gap between  $\sigma_f$  and  $\sigma_i$  as  $p_0$  is raised, this is due to the stabilising effect of the confining pressure. Note that  $\sigma_f$  fits the experimental points very well specially at low confining pressures. The discrepancy at higher  $p_0$ , in the cases of polycrystalline ice and sandstone, may be due to the occurrence of interaction and linkage

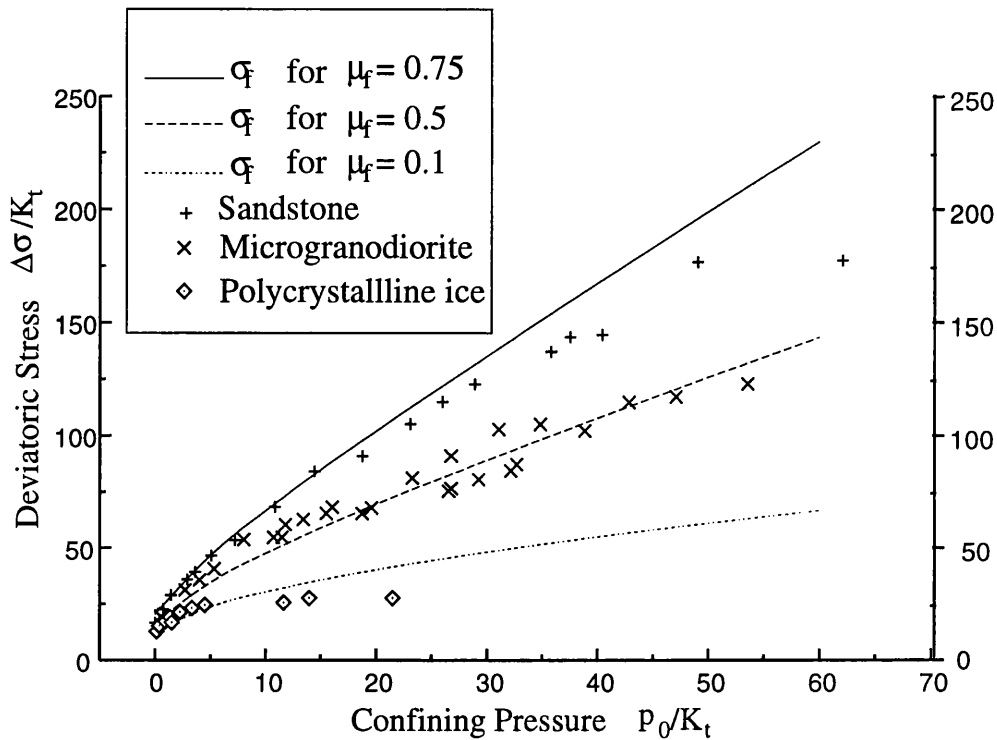


**Figure 3.14:** Deviatoric stress  $\Delta\sigma/K_t$  for which the first unstable wing crack appears, and leads to ultimate failure  $\sigma_f$ , shown as a function of normalised confining pressure  $p_0/K_t$ ; The points correspond to experimental data for different rocks, see text.

between cracks.

From Figure 3.3 we can calculate the proportion of PECs which nucleate NDCs at any given level of stress  $\Delta\sigma$ . For example, in the case when  $\Delta\sigma = 12K_t$ , the proportion is

$$(\theta_U - \theta_L) / \left(\frac{\pi}{2}\right) \tag{3.88}$$

if we assume an isotropic distribution of identical PECs.

The dashed line in Figure 3.15 corresponds to a proportion of 35% of PEC's having nucleated wing cracks. Interestingly the experimental points at high confining pressure are closely scattered about this line, suggesting that fracture occurs at a critical density of NDCs that is independent of the confining pressure. Of course at that level of NDC density one expects that the assumption of non-interacting cracks may no longer be valid and one has to consider the possibility of interaction between neighbouring cracks.

### 3.2.3 Elastic Properties of Cracked Solids

**Expressions for the effects of cracks on elastic properties of a solid.**

It is possible to calculate the exact form of the effect of cracks on elastic properties of a solid treating the cracks on a (non-interacting) individual basis . The average strain  $\bar{\epsilon}^c$  due

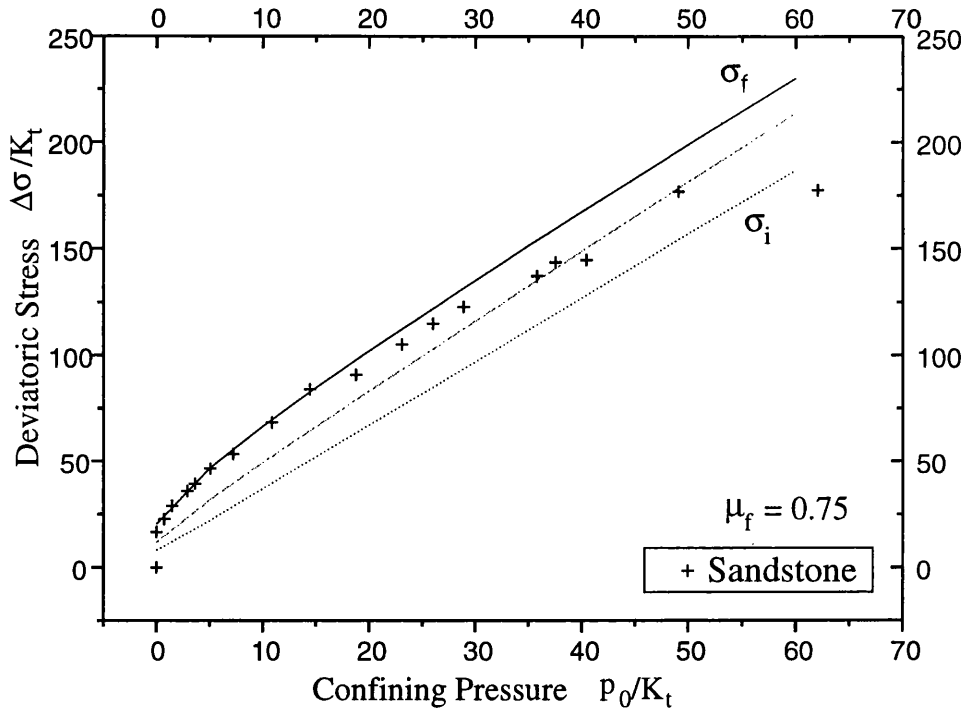


**Figure 3.15:** Deviatoric stress  $\Delta\sigma/K_t$  shown as a function of normalised confining pressure  $p_0/K_t$  for which i) wing cracks are first initiated  $\sigma_i$  (corresponding to the onset of AE), and ii) the first wing crack becomes unstable and initiates failure  $\sigma_f$ ; The coefficient of friction was taken as 0.75. Between these two extremes, crack damage accumulates continuously. The middle line shows the case when 35% of the pre-existing cracks have nucleated wing cracks. The crosses correspond to experimental points for Darley Dale sandstone, see text.

to the presence of cavities is given by

$$\bar{\epsilon}_{ij}^c = \frac{1}{V} \int_{\delta\Omega} \frac{1}{2} (n_i u_j + n_j u_i) dS \quad (3.89)$$

where  $\hat{n}$  is the exterior unit normal of the cavity,  $\vec{u}$  denote the displacement,  $V$  is the total volume of the sample and the integration is along the boundary  $\delta\Omega$  of the cracks. If the cavity has a simple form, e.g. elliptical, the integration can be performed analytically. We can rewrite this equation in terms of the average strain over each individual cavity  $\gamma$ , then if there are  $N$  cavities in  $V$

$$\bar{\epsilon}_{ij}^c = \sum_{k=1}^N f_k \left( \frac{1}{\Omega_k} \int_{\delta\Omega_k} \frac{1}{2} (n_i u_j + n_j u_i) dS \right) = \sum_{k=1}^N f_k \bar{\epsilon}^k, \quad (3.90)$$

where  $f_k \equiv \frac{\Omega_k}{V}$  is the volume fraction of the cracks, and  $\Omega_k$  represents the volume or the “influence” volume of the  $k$ th cavity.

In general, a crack is identified by two surfaces (identical in the simplest cases) which are separated by the crack opening displacement  $\Delta \vec{u}$ , representing the relative displacements of corresponding points on the two crack faces in the undeformed state. The boundary

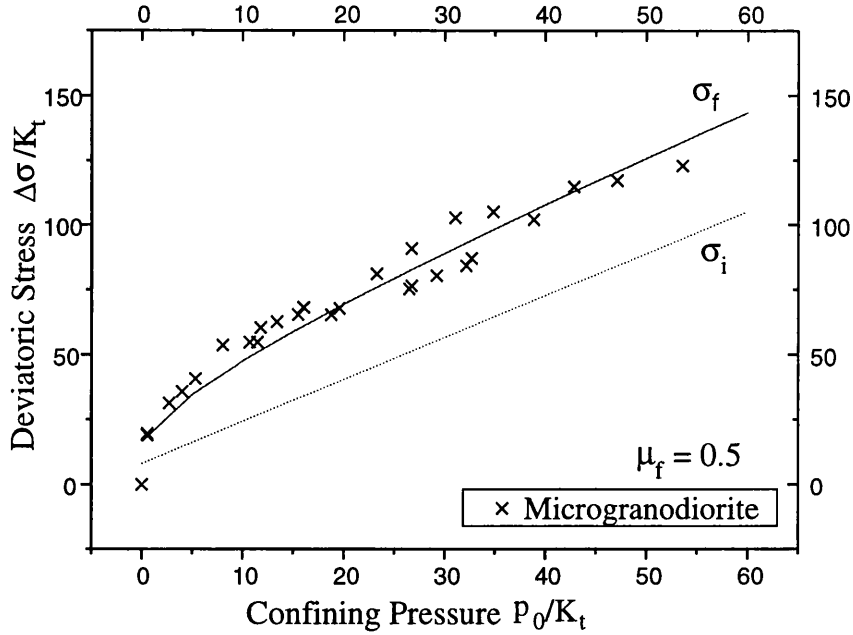


**Figure 3.16:** Deviatoric stress  $\Delta\sigma/K_t$  shown as a function of normalised confining pressure  $p_0/K_t$  for which i) wing cracks are first initiated  $\sigma_i$  (corresponding to the onset of AE), and ii) the first wing crack becomes unstable and initiates failure  $\sigma_f$ ; The coefficient of friction was taken as 0.5. Between these two extremes, crack damage accumulates continuously. The crosses correspond to experimental points for microgranodiorite, see text. In this case  $\sigma_f$  corresponds approximately to 45% of PECs nucleating NDCs.

$\delta\Omega_k$  of the  $k$ th cavity is divided into  $\delta\Omega_k^+$  (upper face) and  $\delta\Omega_k^-$  (lower face). The surface integral of a function  $f(x)$ , over the entire  $\delta\Omega_k$  can be reduced to the integral over  $\delta\Omega_k^+$  of the function  $\{f(x^+) - f(x^-)\}$  where  $x^+$  and  $x^-$  are points on  $\delta\Omega_k^+$  and  $\delta\Omega_k^-$ , respectively.

Then the average strain over the  $k$ th cavity is given by (for almost flat cracks),

$$\bar{\epsilon}^k = \left( \frac{1}{\Omega_k} \int_{\delta\Omega_k^+} \frac{1}{2} (n_i \Delta u_j + n_j \Delta u_i) dS \right). \quad (3.91)$$

This expression is valid for both open or closed cracks, with or without friction, as long as the  $\Delta \vec{u}$  is a linear and homogeneous function of the overall prescribed macrostress  $\sigma^0$ .

This result can be used for both 2-dimensional and 3-dimensional models. In

the next chapter results are derived for the case of 3-dimensional models, and in the chapter 4 the results are applied to the analysis of some experimental data, in the framework of the crack-density tensor concept of Sayers & Kachanov (1991).

### Application to the case of an evolving crack population with NDCs

In this case, the crack is considered to be 2-dimensional and elliptical in shape, so the normal to the surface is given by  $\hat{n} = (\cos \gamma_0, \sin \gamma_0)$ , where  $\gamma_0 = \arctan \left( \frac{\tan \beta}{\tanh \alpha_0} \right)$ , the

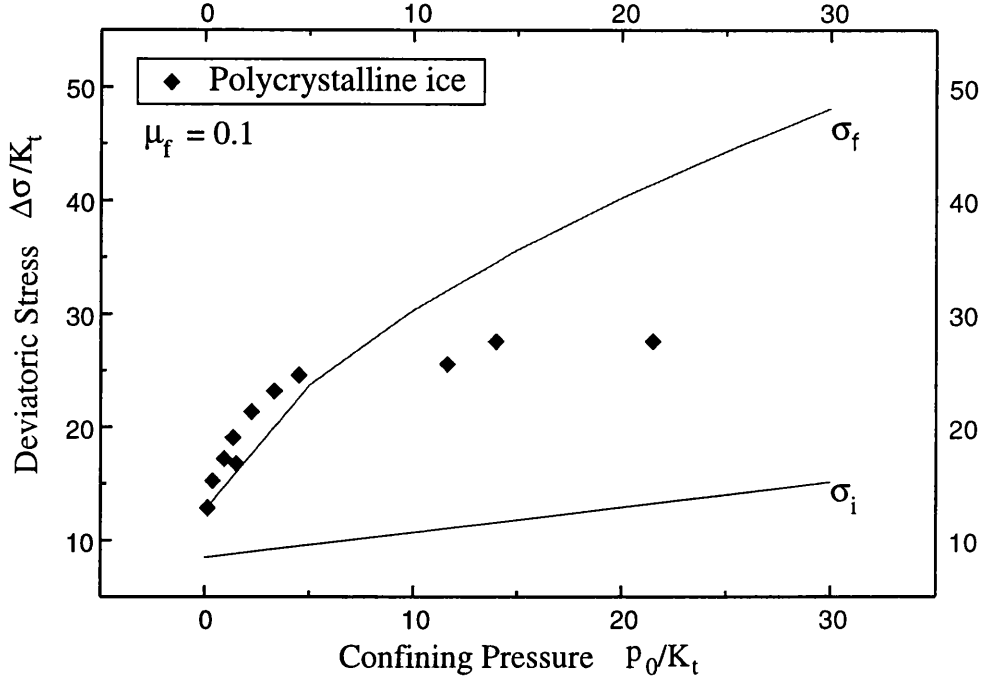


**Figure 3.17:** Deviatoric stress  $\Delta\sigma/K_t$  shown as a function of normalised confining pressure  $p_0/K_t$  for which i) wing cracks are first initiated  $\sigma_i$  (corresponding to the onset of AE), and ii) the first wing crack becomes unstable and initiates failure  $\sigma_f$ ; The coefficient of friction was taken as 0.1. Between these two extremes, crack damage accumulates continuously. The diamonds correspond to experimental points for Polycrystalline ice, see text. The line  $\sigma_f$  corresponds approximately to 68% of PECs generating NDCs, but the experimental data passes from 68% at uniaxial compression to 50% at  $p_0 = 20K_t$ .

surface element is given by  $dS = c_k \sqrt{\sinh^2 \alpha_0 + \sin^2 \beta} d\beta$ , and the relative displacement components are given by equations (3.14) and (3.15).  $c_k$  is the half length of the  $k$ th cavity and  $\alpha_0$  its aspect ratio. We calculate the contributions to the strain due to the pre-existing cracks (PECs) and to the dislocated elliptical wing cracks (NDCs).

After performing the integrals, these contributions are:

- i) Pre-existing cracks (PECs). In the local coordinates  $S'$  of these cracks;
  - a) Open cracks. The strains are (using Voight's notation);

$$\begin{aligned} \vec{\epsilon}'_{\text{pec}} &= \begin{pmatrix} \bar{\epsilon}_{11}^k \\ \bar{\epsilon}_{22}^k \\ \frac{\bar{\epsilon}_{12}^k}{2} \end{pmatrix}_{\text{pec}} = (H'_0)_{\text{open}} \cdot \vec{\sigma}'_{\text{pec}} \\ &= \frac{(1 + \kappa)\pi (c_k)^2 \exp 2\alpha_0}{4\mu\Omega_k} \begin{pmatrix} \frac{(3-m_0)}{4} \frac{\sinh \alpha_0}{\exp \alpha_0} & \frac{-(m_0+1)}{4} \frac{\sinh \alpha_0}{\exp \alpha_0} & 0 \\ \frac{-(m_0+1)}{4} \frac{\sinh \alpha_0}{\exp \alpha_0} & \frac{(3+m_0)}{4} \frac{\cosh \alpha_0}{\exp \alpha_0} & 0 \\ 0 & 0 & 1 \end{pmatrix} \cdot \begin{pmatrix} \sigma_{11}^k \\ \sigma_{22}^k \\ \tau_{12}^k \end{pmatrix}_{\text{pec}} \end{aligned} \quad (3.92)$$

where  $m_0 = \exp(-2\alpha_0)$ .

b) Closed cracks;

$$\begin{aligned} \vec{\epsilon}'_{\text{pec}} &= \begin{pmatrix} \bar{\epsilon}_{11}^k \\ \bar{\epsilon}_{22}^k \\ 2\bar{\epsilon}_{12}^k \end{pmatrix}'_{\text{pec}} = \frac{(1 + \kappa)\pi (c_k)^2 \exp 2\alpha_0}{4\mu\Omega_k} \times \\ &\left[ \begin{pmatrix} \frac{(3-m_0) \sinh \alpha_0}{4 \exp \alpha_0} & 0 & 0 \\ \frac{-(m_0+1) \sinh \alpha_0}{4 \exp \alpha_0} & 0 & 0 \\ 0 & \text{sign}[\tau^k]\mu_f & 1 \end{pmatrix} \cdot \begin{pmatrix} \sigma_{11}^k \\ \sigma_{22}^k \\ \tau_{12}^k \end{pmatrix}'_{\text{pec}} + \begin{pmatrix} \frac{-(m_0+1) \sinh \alpha_0}{4 \exp \alpha_0} \\ \frac{(3+m_0) \cosh \alpha_0}{4 \exp \alpha_0} \\ -\text{sign}[\tau^k]\mu_f \end{pmatrix} \sigma_c \right] \\ &= (H'_0)_{\text{closed}} \cdot \vec{\sigma}'_{\text{pec}} + \vec{m}_c \sigma_c \end{aligned} \quad (3.93)$$

The local stresses are given by equations 3.16 to 3.18 with  $\theta = \theta_0$ .

ii) Wing cracks. In the local frame  $S''$  of the wing crack, the strain due to the wing crack is the sum of the strain due to an elliptical crack of major semi-axis  $c_k^w(\sigma_{\text{lab}}, \theta_0)$  and aspect ratio  $\alpha_1$ , which is inclined by an angle  $\theta_1$  with respect to the most compressive external stress,

$$\begin{aligned} \vec{\epsilon}''_{\text{wc}} &= \begin{pmatrix} \bar{\epsilon}_{11}^k \\ \bar{\epsilon}_{22}^k \\ 2\bar{\epsilon}_{12}^k \end{pmatrix}''_{\text{wc}} = H''_1 \cdot \vec{\sigma}''_{\text{wc}} \\ &= \frac{(1 + \kappa)\pi (c_k^w)^2 \exp 2\alpha_1}{4\mu (\Omega_k)^w} \begin{pmatrix} \frac{(3-m_1) \sinh \alpha_1}{4 \exp \alpha_1} & \frac{-(m_1+1) \sinh \alpha_1}{4 \exp \alpha_1} & 0 \\ \frac{-(m_1+1) \sinh \alpha_1}{4 \exp \alpha_1} & \frac{(3+m_1) \cosh \alpha_1}{4 \exp \alpha_1} & 0 \\ 0 & 0 & 1 \end{pmatrix} \cdot \begin{pmatrix} \sigma_{11}^k \\ \sigma_{22}^k \\ \tau_{12}^k \end{pmatrix}''_{\text{wc}} \end{aligned} \quad (3.94)$$

and that of the dislocated crack,

$$\epsilon''_{\text{dis}} = \begin{pmatrix} \bar{\epsilon}_{11}^k \\ \bar{\epsilon}_{22}^k \\ 2\bar{\epsilon}_{12}^k \end{pmatrix}''_{\text{dis}} = \frac{c_k^w \cosh \alpha_1}{(\Omega_k)^w} \begin{pmatrix} 0 & 0 & 0 \\ 0 & 1 & 0 \\ 0 & 0 & -1 \end{pmatrix} \cdot \begin{pmatrix} 0 \\ b_2 \\ b_1 \end{pmatrix} \quad (3.95)$$

where  $m_1 = \exp(-2\alpha_1)$ . Again, the local stresses are given by equations 3.16 to 3.18, but this time with  $\theta = \theta_1$ . The Burgers vector of the dislocation  $(b_1, b_2)$  is given in the wing crack frame of reference but depends on the local stresses on the pre-existing crack. It can be shown that

$$b_1 = \frac{8(1 + \kappa)c \exp(\alpha_0)}{3\mu\pi\sqrt{2}} Z\tau_0; \quad b_2 = -\frac{8(1 + \kappa)c \exp(\alpha_0)}{3\mu\pi Z} \tau_0 \sqrt{\left(\frac{\sigma_0}{\tau_0}\right)^2 + 1} \quad (3.96)$$

where

$$Z = \sqrt{2} \sqrt{1 + \left(\frac{\sigma_0}{\tau_0}\right)^2} - \frac{\sigma_0}{\tau_0} \sqrt{\left(\frac{\sigma_0}{\tau_0}\right)^2 + 1}, \quad (3.97)$$

and  $\sigma_0, \tau_0$  are the effective stresses on the pre-existing crack as defined before. Then  $\epsilon''_{dis}$  can be rewritten as

$$\begin{aligned} \vec{\epsilon}''_{dis} &= \left(H_2''\right)_{open} \cdot \vec{\sigma}'_{pec} \\ &= \frac{8(1+\kappa)c \exp(\alpha_0) c_k^w \cosh \alpha_1}{6\mu\pi (\Omega_k)^w} \begin{pmatrix} 0 & 0 & 0 \\ 0 & 0 & -\frac{1}{Z} \sqrt{\left(\frac{\sigma_0}{\tau_0}\right)^2 + 1} \\ 0 & 0 & -Z/\sqrt{2} \end{pmatrix} \cdot \begin{pmatrix} \sigma_{11}^k \\ \sigma_{22}^k \\ \tau_{12}^k \end{pmatrix}'_{pec} \end{aligned} \quad (3.98)$$

if the original crack remains open, or as

$$\begin{aligned} \vec{\epsilon}''_{dis} &= \frac{8(1+\kappa)c \exp(\alpha_0) c_k^w \cosh \alpha_1}{6\mu\pi (\Omega_k)^w} \times \\ &\left[ \begin{pmatrix} 0 & 0 & 0 \\ 0 & -\frac{\text{sign}(\tau)\mu_f}{Z} \sqrt{\left(\frac{\sigma_0}{\tau_0}\right)^2 + 1} & -\frac{1}{Z} \sqrt{\left(\frac{\sigma_0}{\tau_0}\right)^2 + 1} \\ 0 & -\text{sign}(\tau)\mu_f Z/\sqrt{2} & -Z/\sqrt{2} \end{pmatrix} \cdot \begin{pmatrix} \sigma_{11}^k \\ \sigma_{22}^k \\ \tau_{12}^k \end{pmatrix}'_{pec} + \begin{pmatrix} 0 \\ \frac{\text{sign}(\tau)\mu_f}{Z} \sqrt{\left(\frac{\sigma_0}{\tau_0}\right)^2 + 1} \\ \text{sign}(\tau)\mu_f Z/\sqrt{2} \end{pmatrix} \sigma_c \right] \\ &= \left(H_2''\right)_{closed} \cdot \vec{\sigma}'_{pec} + \vec{m}_{dis} \sigma_c \end{aligned} \quad (3.99)$$

if the original crack closes.

To obtain the overall strain due to cracks of different orientations, we have to transform these equations in the local crack reference frame into equations in a fixed (laboratory) reference frame and integrate over all the orientations.

The transformation matrices for strains and stresses from the local axes inclined by  $\theta$ , to the laboratory frame of reference are:

$$\vec{\epsilon}'_{lab} = \begin{pmatrix} \bar{\epsilon}_{11} \\ \bar{\epsilon}_{22} \\ \bar{2\epsilon}_{12} \end{pmatrix}_{lab} = \begin{pmatrix} \cos^2\theta & \sin^2\theta & \frac{\sin 2\theta}{2} \\ \sin^2\theta & \cos^2\theta & -\frac{\sin 2\theta}{2} \\ -\sin 2\theta & \sin 2\theta & \cos 2\theta \end{pmatrix} \cdot \begin{pmatrix} \bar{\epsilon}_{11} \\ \bar{\epsilon}_{22} \\ \bar{2\epsilon}_{12} \end{pmatrix}_{local} = \Lambda(\theta) \cdot \vec{\epsilon}'_{local} \quad (3.100)$$

for the strains and

$$\vec{\sigma}'_{lab} = \begin{pmatrix} \sigma_{11} \\ \sigma_{22} \\ \sigma_{12} \end{pmatrix}_{lab} = \begin{pmatrix} \cos^2\theta & \sin^2\theta & \sin 2\theta \\ \sin^2\theta & \cos^2\theta & -\sin 2\theta \\ -\frac{\sin 2\theta}{2} & \frac{\sin 2\theta}{2} & \cos 2\theta \end{pmatrix} \cdot \begin{pmatrix} \sigma_{11} \\ \sigma_{22} \\ \sigma_{12} \end{pmatrix}_{local} = \Upsilon(\theta) \cdot \vec{\sigma}'_{local}. \quad (3.101)$$

for the stresses.

The contribution of a pre-existing crack with inclination  $\theta_0$  to the overall strain in the laboratory frame of reference is

$$\vec{\epsilon}_{\text{pec}} = \Lambda(\theta_0) \cdot \vec{\epsilon}'_{\text{pec}} = \Lambda(\theta_0) \cdot H'_0 \cdot \vec{\sigma}'_{\text{pec}} = \Lambda(\theta_0) \cdot \left(H'_0\right)_{\text{open}} \cdot \Upsilon(\theta_0)^{-1} \cdot \vec{\sigma}_{\text{lab}} \quad (3.102)$$

if the crack remains open, and

$$\vec{\epsilon}_{\text{pec}} = \Lambda(\theta_0) \cdot \left(H'_0\right)_{\text{closed}} \cdot \Upsilon(\theta_0)^{-1} \cdot \sigma_{\text{lab}} + \Lambda(\theta_0) \cdot \vec{m}_c \sigma_c \quad (3.103)$$

if the crack closes.

The contribution of an elliptical wing crack with inclination  $\theta_1(\theta_0)$  to the overall strain in the laboratory frame of reference is

$$\vec{\epsilon}_{\text{wc}} = \Lambda(\theta_1) \cdot \vec{\epsilon}''_{\text{wc}} = \Lambda(\theta_1) \cdot H''_1 \cdot \vec{\sigma}''_{\text{wc}} = \Lambda(\theta_1) \cdot H''_1 \cdot \Upsilon(\theta_1)^{-1} \cdot \vec{\sigma}_{\text{lab}} \quad , \quad (3.104)$$

and that of the dislocated wing crack is:

$$\vec{\epsilon}_{\text{dis}} = \Lambda(\theta_1) \cdot \vec{\epsilon}''_{\text{dis}} = \Lambda(\theta_1) \cdot \left(H''_2\right)_{\text{open}} \cdot \vec{\sigma}'_{\text{pec}} = \Lambda(\theta_1) \cdot \left(H''_2\right)_{\text{open}} \cdot \Upsilon(\theta_0)^{-1} \cdot \vec{\sigma}_{\text{lab}} \quad (3.105)$$

if the original crack remains open, and

$$\vec{\epsilon}_{\text{dis}} = \Lambda(\theta_1) \cdot \left(H''_2\right)_{\text{closed}} \cdot \Upsilon(\theta_0)^{-1} \cdot \vec{\sigma}_{\text{lab}} + \Lambda(\theta_1) \cdot \vec{m}_{\text{dis}} \sigma_c \quad (3.106)$$

if the original crack closes.

Then the contribution of a single active pre-existing crack with orientation  $\theta_0$  will be the sum of all these contributions,

$$\vec{\epsilon}_{\text{total}}(\vec{\sigma}_{\text{lab}}, \theta_0) = \vec{\epsilon}_{\text{pec}} + 2\vec{\epsilon}_{\text{wc}} + 2\vec{\epsilon}_{\text{dis}} \quad (3.107)$$

If we have a distribution of pre-existing active crack orientations  $F(\theta_0)$ , then we can obtain the overall strain due to the presence and growing of cracks in the material, as

$$\vec{\epsilon}(\sigma_{\text{lab}}) = \vec{\epsilon}_{\text{mat}} + \int \vec{\epsilon}_{\text{total}}(\vec{\sigma}_{\text{lab}}, \theta_0) F(\theta_0) d\theta_0, \quad (3.108)$$

where  $\vec{\epsilon}_{\text{mat}}$  is the contribution of the rock matrix for the plane strain case, and is given by

$$\vec{\epsilon}_{\text{mat}} = \begin{pmatrix} \frac{(1-\nu^2)}{E} & -\frac{\nu(1+\nu)}{E} & 0 \\ -\frac{\nu(1+\nu)}{E} & \frac{(1-\nu^2)}{E} & 0 \\ 0 & 0 & \frac{2(1+\nu)}{E} \end{pmatrix} \begin{pmatrix} \sigma_{11}^0 \\ \sigma_{22}^0 \\ \sigma_{12}^0 \end{pmatrix}. \quad (3.109)$$

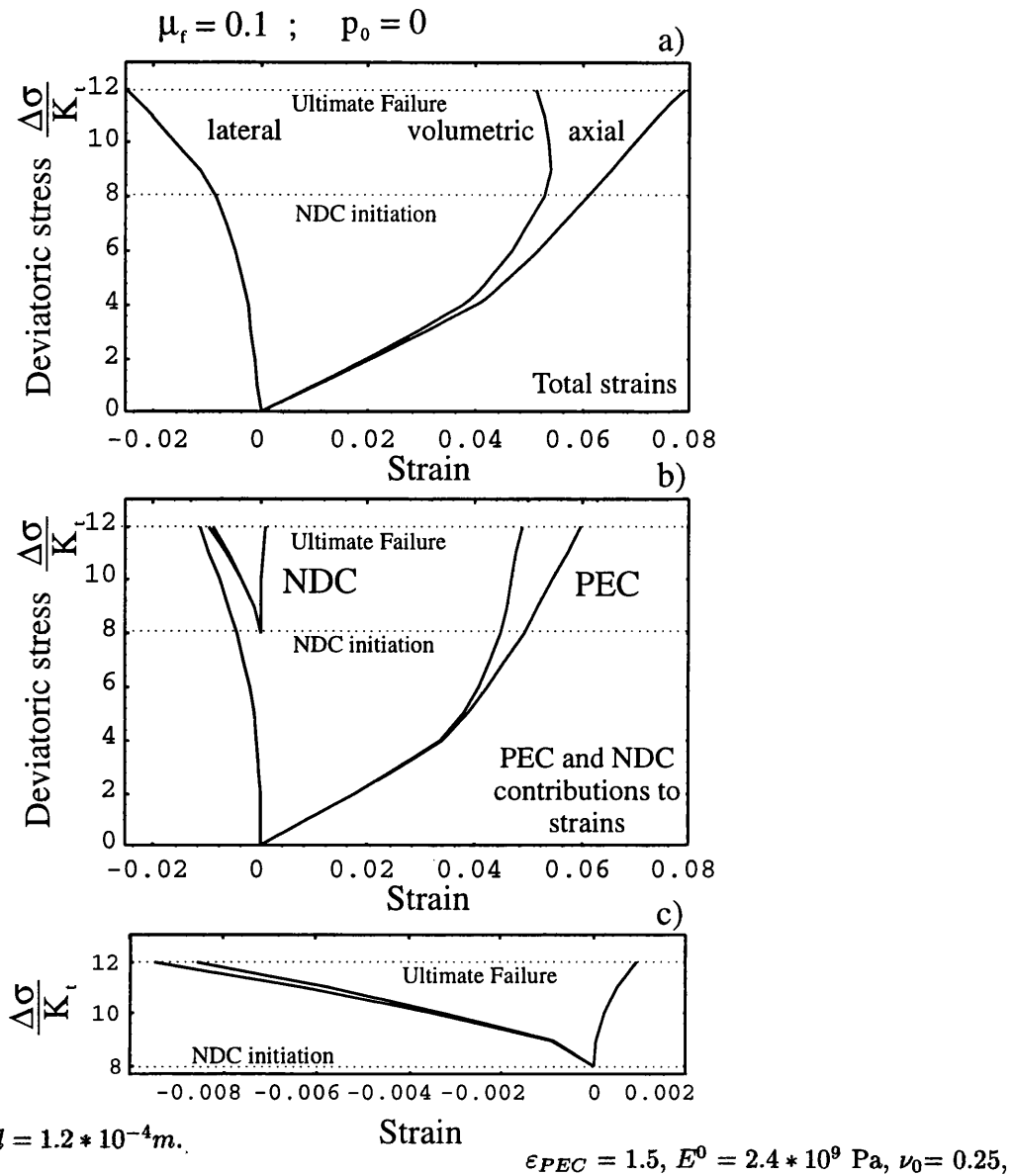


**Figure 3.18:** Stress vs. axial, lateral and volumetric strain curves calculated under uniaxial compression. The figures were calculated for  $\theta = 45^\circ$ . In b) the separate contributions of PECs and NDCs are shown. In c) the NDC contribution is shown amplified.

The changes in compliances due to the presence of the crack can be calculated from these equations\*. Lack of time has prevented any extensive numerical calculations based on these equations. The results that have been obtained are presented in Figures 3.18-3.19 where axial, lateral and volumetric strains are plotted for uniaxial and biaxial compression. Separate contributions from PECs and NDC are also shown. The PEC density  $\epsilon$  was taken equal to 1.5 to exaggerate the features of these curves and appreciate more the effect of cracks on the elastic behaviour of the body. At least 3 regions of deformation that were shown in Figure (1.1) are shown by these curves.

\* For instance, the effective Poisson's ratio is the ratio of the lateral strain increment to the axial strain increment, and the Young's modulus is the derivative of axial stress with respect to the axial strain. See for instance Li and Nordlund (1993).

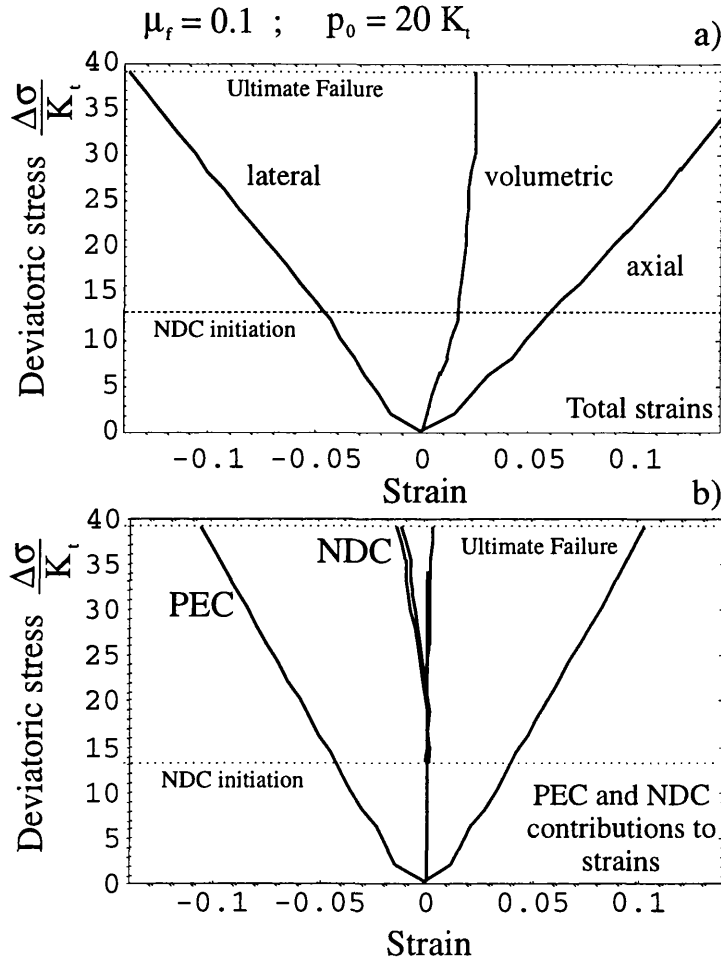


**Figure 3.19:** Stress vs. axial, lateral and volumetric strain curves calculated under biaxial compression.

### 3.3 Acoustic emission.

Advancing cracks emit elastic waves due to the sudden relaxation of stress in a localised part of the stressed material. These elastic waves are detectable, and are usually observed as acoustic pulses, hence the name of acoustic emission (AE). (Lockner, 1993).

On loading, the initial compaction is related to the closure of cracks and pores and is reflected in the upward curvature of the stress-strain curve and the low level of acoustic activity. This is followed by a period of relative acoustic emission (AE) inactivity and linear elastic behaviour. (Scholz, 1968; Stuart, 1993).

Eventually, acoustic emission activity recommences accompanied by dilatation and an

apparent decrease in the Young's modulus. Above about half of the final failure stress, there is a rapid increase in AE and a very substantial dilatation until failure occurs (Scholz, 1968). Scholz has shown a correlation between the inelastic volumetric strain (dilatancy) and the cumulative number of AE events.

It is very likely that the onset of AE can be associated with the initiation of wing cracks (NDCs) emerging from pre-existing flaws (PECs). Making this assumption we calculated the number of NDC from<sup>1</sup>

$$N_{NDC} = \frac{4 (\theta_U - \theta_L) * V}{\pi} \gamma \quad (3.110)$$

where  $\theta_U$  and  $\theta_L$  were defined in Figure (3.3),  $\bar{a}$  is the average length of PEC being formed and  $V$  is the volume of the sample.  $\gamma$  is the number of PECs per unit volume.

In Figure 3.20 we show the number of NDC as a function of deviatoric stress for both uniaxial compression and with confining pressure. Two sets of experimental points of cumulative number of acoustic emission events (Aves, 1995) are shown for comparison.<sup>2</sup>

The theoretical curves are almost identical and present the opposite behaviour of the experiments, as the number of NDC is reduced at higher confining pressures. We could revert this tendency if we take the average length  $\bar{a}$  as inverse dependent on confining pressure, the higher  $p_0$  the lower  $\bar{a}$ . Nevertheless the exponential increase in the experiments before the peak stress can not be explained with equation (3.110).

<sup>1</sup> As we are assuming that we have an isotropic, random distribution of cracks, the number of PECs that have developed NDCs (the cracks with orientations between  $\theta_L$  and  $\theta_U$ ) is given by  $(\theta_U - \theta_L)/(\pi/2)$  multiplied by the number of original PECs. As each one of these PECs have developed 2 NDCs, equation (3.110) arises.

<sup>2</sup> During deformation of a sample, each AE event produces a signal which is observed as a wave packet. An AE hit is defined by a signal threshold and a hit definition time. From there the cumulative number of hits can be recorded. For a complete description of this kind of experiments see Aves (1995) and Stuart (1992).

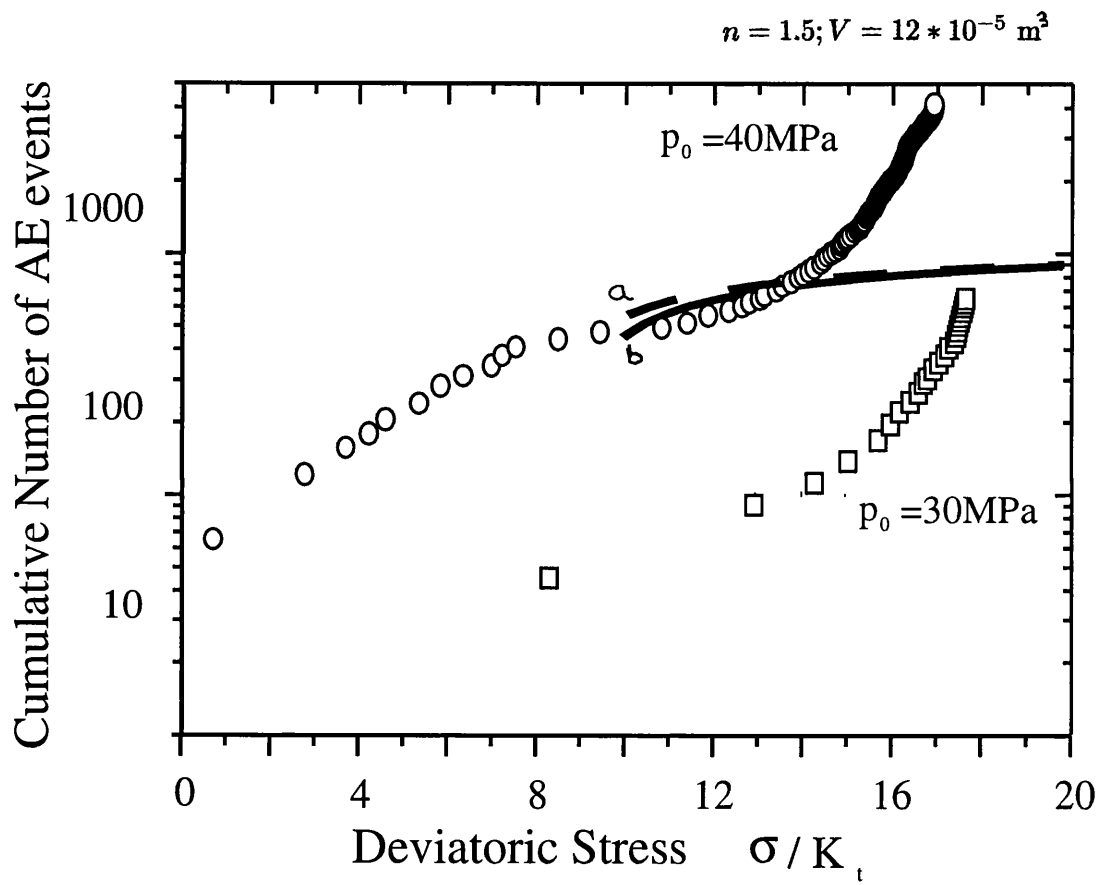


**Figure 3.20:** Semilogarithmic plot showing the number of NDCs as a function of deviatoric stress for a) uniaxial compressive case and b) with confining pressure  $= 30K_t$ . Experimental points of cumulative number of acoustic emission (AE) events are also shown.

## Chapter 4

# Effective elastic properties of cracked solids.

Ultrasonic wave velocities and velocity differences at different stress conditions may serve to indicate the existence of inhomogeneities in a rock. In this Chapter the crack density tensor concept is presented. Experimental velocities are inverted to obtain the variation of crack density and crack density anisotropy coefficients with applied stress.

### 4.1 Introduction

Clearly one of the important parameters characterising crack populations is the volumetric proportion of cracks in a body, which can be defined by a scalar crack density parameter  $\epsilon$ .

Several theoretical studies of crack-induced anisotropy have been reported in the literature. In the general 3D case a crack may be conveniently described as an ellipsoidal cavity for which one of the principal axes (the minor, or  $c$  axis) is much smaller than the other two, i.e.,  $a \geq b \gg c$ . Although the results obtained by Eshelby [1957] enable the general case to be treated (see for example, Murrell & Digby, 1970) it is convenient to treat the simpler case of penny-shaped cracks, for which the two larger principal axes ( $a, b$ ) are equal.

For low concentrations of microcracks it may be assumed that the cracks are non-interacting in their near-fields and therefore the effective elastic properties may be calculated by assuming that each crack is subjected only to the macroscopic, externally applied stress field  $\sigma$ . The contributions to the overall strain from individual cracks may then be summed to give the total strain (Bristow, 1960; Walsh, 1969). In early calculations individual cracks were assumed to be embedded in uncracked material. Hill [1965], and Budiansky

[1965] meanwhile developed the self-consistent approach to the problem of microscopically heterogeneous elastic bodies. In the self-consistent model individual cracks are assumed to be embedded in material with the mean elastic properties of the whole cracked body, and this approach was applied by Budiansky & O'Connell [1976] to cracked rocks. This scheme was extended by Hoenig [1979] to crack distributions for which the overall elastic stiffness tensor is transversely isotropic (including the planar and cylindrical kinds).

Bruner [1976] and Henyey & Pomphrey [1982] have pointed out that the self-consistent scheme may overestimate the crack interactions and have proposed an alternative, differential scheme in which the crack density is increased in small steps and the elastic properties are recalculated incrementally.

Finally, Hudson [1980, 1981, 1986] has given results for both randomly oriented and parallel cracks calculated to second order in the crack density. However, as pointed out by Sayers & Kachanov [1991], while the results of Hudson at low crack densities ( $< 0.2$  for parallel cracks, and  $< 0.6$  for randomly-oriented cracks) follow the predictions of the differential scheme, at higher crack densities Hudson's equations give an increasing stiffness as the crack density increases, contrary to what would be expected.

In their paper Sayers & Kachanov [1991] have presented a new scheme for the calculation of the elastic stiffnesses for an orientation distribution of cracks of any kind, which is a development from previous approaches but introduces a tensor measure of crack density. In this chapter we will examine the application of this scheme in experimental situations in which the orientation distribution of cracks is believed to be transversely isotropic or is not known at all.

## 4.2 The crack density tensor concept

In the earliest theoretical studies of the physical properties (e.g. elastic properties) of cracked solids a crack density parameter  $\epsilon$  was defined, as a scalar quantity. Such a parameter could obviously be measured directly in principle, by measuring the amount of fluid required to fill the cracks.

However, certain physical properties such as elastic stiffness or fluid permeability, will clearly depend on the orientation distribution function of cracks present in a body. Following Vakulenko & Kachanov [1971] and Kachanov [1980], Sayers & Kachanov [1991]

introduced a second-order crack density tensor  $\alpha$  defined by:

$$\alpha = \frac{1}{V} \sum_r \gamma_r \mathbf{n}_r \mathbf{n}_r. \quad (4.1)$$

Here  $V$  is the volume over which averaging is performed,  $\mathbf{n}_r$  is the unit vector in the direction of the (minor)  $c$ -axis of the  $r$ 'th crack and  $\gamma_r$  is a weighting factor characterising the contribution of the  $r$ 'th crack to  $\alpha$  and depending on the physical problem of interest. In the case of elastic properties  $\gamma_r = N_r a_r^3$ , where  $a_r$  is the radius of the  $r$ 'th crack for a 3D solid with penny-shaped cracks and  $N_r$  is the number of cracks with radius  $a_r$  and the  $r$ 'th orientation.

Note that the trace of the crack density tensor ( $\text{tr } \alpha = \alpha_{ii}$ ) coincides with the conventional crack density parameter  $\varepsilon = na^3$ , where  $n$  is the number of cracks per unit volume and  $a$  is the average crack radius. Then  $\alpha$  represents a tensorial generalisation of  $\varepsilon$  for an arbitrary orientation distribution of cracks.

In principle  $\alpha$  could be measured directly by making sections of the cracked body at determined orientations and counting the proportion of cracks for each orientation. For an isotropically cracked rock this proportion would be independent of the section orientation. (Note: If  $\Phi$  is the crack volume per unit volume of cracked rock, i.e., the crack porosity, then  $\Phi = \frac{4}{3}n\pi a^2 c$  for penny-shaped cracks. Thus  $\Phi = \frac{4}{3}\pi(\frac{c}{a})\varepsilon$  in this case, where  $c/a$  is the crack aspect ratio. In the case of fluid permeability, the weighting factor  $\gamma_r$ , in the crack density tensor, depends on the crack aspect ratio as well as the crack radius  $a_r$ , see Kachanov, 1980).

The effective elastic compliances  $S_{ijkl}$  for the cracked medium can be derived from an elastic potential  $f$  defined by the stress ( $\sigma$ ) and strain ( $\epsilon$ ) tensors, where:

$$\epsilon_{ij} = \partial f / \partial \sigma_{ij} = S_{ijkl} \sigma_{kl}, \quad (4.2)$$

so that the problem is reduced to finding  $f$ . For empty cracks,  $f$  can be written as a function of  $\sigma$  and (to a good approximation) of the second order crack density tensor  $\alpha$  [Kachanov, 1980]. If the material is isotropic in the absence of cracks, then  $f(\sigma, \alpha)$  must be invariant with respect to any linear orthogonal transformation applied to both  $\sigma$  and  $\alpha$ . This implies that  $\sigma$  and  $\alpha$  will enter  $f$  through their invariants only (including the simultaneous ones). Since the stress-strain relations are linear at constant  $\alpha$ ,  $f(\sigma, \alpha)$  must be quadratic in  $\sigma$ . The resulting expression for  $f$  comprises nine terms representing all independent combinations of the invariants [Vakulenko & Kachanov, 1971; Kachanov, 1980]. Kachanov [1980] and Sayers & Kachanov [1991] proposed to simplify  $f$  by retaining

only terms which are tensorially linear in  $\alpha$ , so that:

$$\begin{aligned} f(\boldsymbol{\sigma}, \boldsymbol{\alpha}) &= \frac{1}{2} S_{ijkl} \sigma_{ij} \sigma_{kl} \\ &= \omega_1 (\text{tr } \boldsymbol{\sigma})^2 + \omega_2 \text{tr}(\boldsymbol{\sigma} \cdot \boldsymbol{\sigma}) + \eta_1 \text{tr } \boldsymbol{\sigma} \text{tr}(\boldsymbol{\sigma} \cdot \boldsymbol{\alpha}) + \eta_2 \text{tr}(\boldsymbol{\sigma} \cdot \boldsymbol{\sigma} \cdot \boldsymbol{\alpha}), \end{aligned} \quad (4.3)$$

where  $\omega_1, \omega_2, \eta_1$  and  $\eta_2$  are functions of the invariants of  $\alpha$ . Kachanov [1980] shows that  $\omega_1 = -\nu^0/2E^0$ , and  $\omega_2 = (1 + \nu^0)/2E^0$  where  $\nu^0$  and  $E^0$  are the Poisson ratio and Young's Modulus for the uncracked (isotropic) solid. We can therefore write:

$$\begin{aligned} f(\boldsymbol{\sigma}, \boldsymbol{\alpha}) &= \frac{1}{2} S_{ijkl} \sigma_{ij} \sigma_{kl} \\ &= \frac{1}{2} S_{ijkl}^0 \sigma_{ij} \sigma_{kl} + \eta_1 \text{tr } \boldsymbol{\sigma} \text{tr}(\boldsymbol{\sigma} \cdot \boldsymbol{\alpha}) + \eta_2 \text{tr}(\boldsymbol{\sigma} \cdot \boldsymbol{\sigma} \cdot \boldsymbol{\alpha}), \end{aligned} \quad (4.4)$$

where  $S_{ijkl}^0$  are the compliances of the (isotropic) uncracked solid. In equations ( 4.3-4.4), a dot indicates one index contraction:  $(\boldsymbol{\sigma} \cdot \boldsymbol{\sigma})_{ij} = \sigma_{ik} \sigma_{kj}$ .

#### 4.2.1 Calculation of $\eta_1$ and $\eta_2$ for dry cracks

We will calculate how a population of non-interacting penny-shaped cracks affects the elastic compliance tensor of a body, and go on to derive values for  $\eta_1$  and  $\eta_2$ .

Following Nemat-Nasser and Hori (1993), we will consider the strain  $\epsilon^r$  due to the presence of a penny-shaped crack of surface  $S_r$  and radius  $a_r$  in a material subjected to a macroscopic stress  $\sigma_{kl}$ ,

$$\epsilon_{ij}^r = \frac{1}{a_r^3} \int_{S_r} \frac{1}{2} \{ \bar{n} \otimes [\bar{u}] + [\bar{u}] \otimes \bar{n} \} dS = H_{ijkl}^r \sigma_{kl} \quad (4.5)$$

where  $\bar{n}$  is the unit vector normal to the surface  $S_r$ , and  $[\bar{u}]$  is the crack opening displacement.  $\otimes$  is the dyadic product.

It is convenient to introduce a set of axes  $(e'_1, e'_2, e'_3)$  with origin at the centre of the penny-shaped crack, and with  $e'_3$  coinciding with the minor axis of the crack. The new basis vectors are related with the fixed ones by

$$e_i = T_{ij} e'_j \quad (4.6)$$

where

$$T_{ij} = \begin{pmatrix} \cos \theta & -\cos \phi \sin \theta & \sin \phi \sin \theta \\ \sin \theta & \cos \phi \cos \theta & -\cos \theta \sin \phi \\ 0 & \sin \phi & \cos \phi \end{pmatrix} \quad (4.7)$$

with  $0 \leq \theta \leq 2\pi$  and  $0 \leq \phi \leq \pi$ . In this coordinate system we can define

$$H_{ijkl}^{\prime r} \sigma'_{kl} = \frac{1}{a_r^3} \int_{S_r} \frac{1}{2} \{ \bar{n}' \otimes [\bar{u}'] + [\bar{u}'] \otimes \bar{n}' \} dS \quad (4.8)$$

where  $\bar{n}' = (0, 0, 1)$ , and

$$[\bar{u}'_i] = \frac{16 (1 - \nu^{02}) \sqrt{a^2 - r^2} \sigma'_{i3}}{(2 - \nu^0) \pi E^0} \quad ; \quad r \leq a (i = 1, 2) \quad (4.9)$$

$$[\bar{u}'_3] = \frac{8 (1 - \nu^{02}) \sqrt{a^2 - r^2} \sigma'_{33}}{\pi E^0} \quad (4.10)$$

for dry penny-shaped cracks.  $E^0$  and  $\nu^0$  are the Young's modulus and the Poisson ratio of the uncracked elastic solid,  $r$  measures the radial distance in the plane of the crack from its center. The only non-zero components of equation 4.8, in the case of dry cracks, are:

$$H'^r_{3333} \sigma'_{33} = \frac{1}{a_r^3} \int [\bar{u}'_3] n'_3 dS \quad (4.11)$$

$$H'^r_{2323} \sigma'_{23} = H'^r_{3232} \sigma'_{32} = H'^r_{1313} \sigma'_{13} = H'^r_{3131} \sigma'_{31} = \frac{1}{2a_r^3} \int [\bar{u}'_1] n'_3 dS \quad (4.12)$$

After making the integrations and eliminating the stress  $\sigma$  we obtain,

$$H'^r_{3333} = \frac{16 (1 - \nu^{02})}{3 E^0} \quad (4.13)$$

$$H'^r_{3131} = \frac{8 (1 - \nu^{02})}{3 (2 - \nu^0) E^0} \quad (4.14)$$

When there are many cracks with any possible orientation, a crack density function  $w(\theta, \phi)$  may be introduced such that

$$\frac{1}{4\pi} \int_0^{2\pi} \int_0^\pi w(\theta, \phi) \sin(\phi) d\phi d\theta = 1. \quad (4.15)$$

Then the overall compliance change due to the presence of the cracks is given by,

$$\Delta S_{ijkl} = \frac{\varepsilon}{4\pi} \int_0^{2\pi} \int_0^\pi H_{ijkl}(\theta, \phi) w(\theta, \phi) \sin(\phi) d\phi d\theta \quad (4.16)$$

where  $\varepsilon = na^3$  is the conventional crack density,  $n$  is the number of cracks per unit volume, and, (Nemat-Nasser and Hori, 1993.)

$$H_{ijkl}(\theta, \phi) = T_{i\alpha} T_{j\beta} T_{k\gamma} T_{l\delta} H'_{\alpha\beta\gamma\delta}. \quad (4.17)$$

We will consider three different penny-shaped crack distributions :

I) An isotropic distribution of cracks for which  $w(\theta, \phi) = 1$ ,

II) An anisotropic distribution of cracks with  $c$ -axes parallel to a fixed direction (PTI case) for which the integrating function is evaluated at  $\phi = 0$ .

III) An anisotropic distribution of cracks with  $c$ -axes all parallel to a fixed plane (CTI case) for which  $w(\theta, \phi) = 2\delta(\phi - \frac{\pi}{2})$ , where  $\delta$  is the Dirac delta function. See, Nemat-Nasser and Hori, 1993.

**I) Isotropic case, RDC.**

For randomly orientated cracks  $\alpha = \frac{\varepsilon}{3}\mathbf{I}$ , where  $\varepsilon = na^3$  is the conventional scalar crack density and  $\mathbf{I}$  is the unit tensor. From Sayers and Kachanov (1991) it is found that,

$$\Delta S_{1212} = \eta_2 \varepsilon / 3, \quad (4.18)$$

$$\Delta S_{1122} = 2\eta_1 \varepsilon / 3, \quad (4.19)$$

and calculating 4.16 with  $w(\theta, \phi) = 1$  we obtain,

$$\Delta S_{1212} = \frac{16 \varepsilon (5 - \nu^0) (1 - \nu^{02})}{45 (2 - \nu^0) E^0} \quad (4.20)$$

$$\Delta S_{1122} = \frac{-16 \varepsilon \nu^0 (1 - \nu^{02})}{45 (2 - \nu^0) E^0} \quad (4.21)$$

equating with 4.18 and 4.19

$$\eta_2 = \frac{16 (5 - \nu^0) (1 - \nu^{02})}{15 (2 - \nu^0) E^0} \quad (4.22)$$

$$\eta_1 = \frac{-8 \nu^0 (1 - \nu^{02})}{15 (2 - \nu^0) E^0} \quad (4.23)$$

therefore

$$\frac{\eta_1}{\eta_2} = \frac{-\nu^0}{2 (5 - \nu^0)} \quad (4.24)$$

and  $\eta_1 \ll \eta_2$ .

**II) Planar Transverse Isotropy, PTI.**

For cracks with  $c$ -axes all aligned in the same direction  $e_3$ ,  $\alpha_{11} = \alpha_{22} = 0$  and  $\alpha_{33} = \varepsilon$ , then, from Sayers and Kachanov (1991),

$$\Delta S_{2323} = \eta_2 \varepsilon / 2; \quad (4.25)$$

$$\Delta S_{1133} = \eta_1 \varepsilon, \quad (4.26)$$

and from 4.16 with  $w(\theta, \phi) = 4\pi\delta(\phi)$  we obtain,

$$\Delta S_{1133} = 0 \quad (4.27)$$

$$\Delta S_{2323} = \frac{8 \varepsilon (1 - \nu^{02})}{3 (2 - \nu^0) E^0} \quad (4.28)$$

equating with 4.25 and 4.26

$$\eta_1 = 0 ; \quad \eta_2 = \frac{16 (1 - \nu^{02})}{3 (2 - \nu^0) E^0} \quad (4.29)$$

This value of  $\eta_2$  coincides with the one calculated by Kachanov (1992) from different considerations.

### III) Cylindrical Transverse Isotropy, CTI.

For cracks with  $c$ -axes lying randomly in parallel planes,  $\alpha_{11} = \alpha_{22} \neq 0$  and  $\alpha_{33} = 0$ , then from Sayers and Kachanov (1991),

$$\Delta S_{1212} = \eta_2 \varepsilon / 2, \quad (4.30)$$

$$\Delta S_{1122} = \eta_1 \varepsilon, \quad (4.31)$$

and calculating 4.16 with  $w(\theta, \phi) = 2\delta(\phi - \frac{\pi}{2})$ ,

$$\Delta S_{1212} = \frac{2 \varepsilon (4 - \nu^0) (1 - \nu^{02})}{3 (2 - \nu^0) E^0} \quad (4.32)$$

$$\Delta S_{1122} = \frac{-2 \varepsilon \nu^0 (1 - \nu^{02})}{3 (2 - \nu^0) E^0} \quad (4.33)$$

equating with 4.30 and 4.31

$$\eta_2 = \frac{4 (4 - \nu^0) (1 - \nu^{02})}{3 (2 - \nu^0) E^0} \quad (4.34)$$

$$\eta_1 = \frac{-2 \nu^0 (1 - \nu^{02})}{3 (2 - \nu^0) E^0} \quad (4.35)$$

therefore

$$\frac{\eta_1}{\eta_2} = \frac{-\nu^0}{2 (4 - \nu^0)} \quad (4.36)$$

and once again  $\eta_1 \ll \eta_2$ .

It is important to mention that for a fluid-filled cavity  $\eta_1$  is, generally, not small and its impact on the effective compliances can be significant (Kachanov, 1992).

#### 4.2.2 Reduced elastic potential

In the last subsection it is shown that  $\eta_1 \ll \eta_2$  for a random distribution of dry cracks and for a transversely isotropic distribution of cracks. Therefore, it is a reasonable approximation to take  $\eta_1 = 0$  for an arbitrary crack orientation distribution and, equation (4.4) then reduces to:

$$f(\boldsymbol{\sigma}, \boldsymbol{\alpha}) = \frac{1}{2} S_{ijkl}^0 \sigma_{ij} \sigma_{kl} + \eta \text{tr}(\boldsymbol{\sigma} \cdot \boldsymbol{\sigma} \cdot \boldsymbol{\alpha}), \quad (4.37)$$

where  $\eta \equiv \eta_2$  in equation (4.4) is a function only of the elastic properties of the solid and of the invariants of  $\boldsymbol{\alpha}$  (i.e. of the scalar crack density  $\varepsilon$ ).

### 4.2.3 $\eta$ as a function of $\varepsilon$

In this section we will show how, by using the differential self-consistent-scheme  $\eta$  can be expressed as a function of  $\varepsilon$  as well as  $E^0$  and  $\nu^0$ .

From section 4.2.1, and putting  $\eta_2 = \eta$ ,

$$\frac{\eta^I}{\eta^{II}} = \frac{5 - \nu^0}{5} ; \frac{\eta^{III}}{\eta^{II}} = \frac{4 - \nu^0}{4} ; \frac{\eta^{III}}{\eta^I} = \frac{5 (4 - \nu^0)}{4 (5 - \nu^0)} \quad (4.38)$$

where the superindex indicates the corresponding crack distribution in section 4.2.1. We can see that differences between the values of  $\eta$  for the different cases is less than 10 percent for  $\nu^0 = 0.5$  and tends to disappear when  $\nu^0 \rightarrow 0$ . Therefore, as a first approximation, we can take any of the values for  $\eta$  as input to predict the crack density tensor  $\alpha$  for an arbitrary distribution of cracks.

We may take as reference the value of  $\eta$  for an isotropic distribution of cracks, namely

$$\eta^I = \frac{16 (5 - \nu^0) (1 - \nu^{02})}{15 (2 - \nu^0) E^0} \quad (4.39)$$

If we make the self-consistent assumption we should replace  $E^0$  by the effective Young's Modulus  $\bar{E}$  and  $\nu^0$  by the effective Poisson ratio  $\bar{\nu}$  of the cracked body, and we then obtain the dependence of  $\eta^I$  on scalar crack density  $\varepsilon$  as:

$$\eta^I = \frac{16 (5 - \bar{\nu}) (1 - \bar{\nu}^2)}{15 (2 - \bar{\nu}) \bar{E}} \quad (4.40)$$

Bruner [1976] showed that in fact the simple self-consistent approach in which elastic moduli of the uncracked body are replaced by the elastic moduli of the cracked body is physically unsatisfactory, and that the correct approach is to use a differential self-consistent scheme. He derived exact (but non-linear) differential equations for the dependence of  $\bar{E}$  and  $\bar{\nu}$  on  $\varepsilon$  for the isotropic case, for which an analytical solution is not available. However he showed that approximate expressions for  $\bar{E}/E^0$  and  $\bar{\nu}/\nu^0$  as a function of the crack density parameter  $\varepsilon$ , that are very near to the prediction of the differential scheme for an isotropic distribution of cracks, are given by

$$\frac{\bar{E}}{E^0} = \exp\left(-\frac{16\varepsilon}{9}\right) ; \quad \frac{\bar{\nu}}{\nu^0} = \exp\left(-\frac{8\varepsilon}{5}\right). \quad (4.41)$$

By substituting for  $\bar{E}$  and  $\bar{\nu}$  in (4.40) we obtain, a somewhat complicated relationship for  $\eta^I$  in terms of  $\varepsilon$  that can be linearised in order to obtain the value of  $\eta^I$  to the first order in  $\varepsilon$  as follows:

$$\eta = \eta' + \eta'' \varepsilon \quad (4.42)$$

where

$$\eta' = \frac{16 (5 - \nu^0) (1 - \nu^{02})}{15 (2 - \nu^0) E^0} \quad (4.43)$$

and

$$\eta'' = \frac{128 (100 - 97\nu^0 + 90\nu^{02} - 29\nu^{03} + 8\nu^{04})}{675 (2 - \nu^0)^2 E^0}. \quad (4.44)$$

#### 4.2.4 Elastic Compliances

Choosing a coordinate system with axes coincident with the principal axes of  $\alpha$ , the contributions to the non-vanishing elastic compliances  $S_{ijkl}$  due to cracks with an arbitrary orientation distribution are obtained from the derivative of equation (4.37) with respect  $\sigma_{ij}$ , and comparing with equation (4.2), the resulting equations are similar to the ones obtained by Sayers and Kachanov (1991) but with  $\eta_1 = 0$ .

$$\Delta S_{1111} = 2\eta\alpha_{11} \quad (4.45)$$

$$\Delta S_{2222} = 2\eta\alpha_{22} \quad (4.46)$$

$$\Delta S_{3333} = 2\eta\alpha_{33} \quad (4.47)$$

$$\Delta S_{1212} = \eta(\alpha_{11} + \alpha_{22})/2 \quad (4.48)$$

$$\Delta S_{2323} = \eta(\alpha_{22} + \alpha_{33})/2 \quad (4.49)$$

$$\Delta S_{3131} = \eta(\alpha_{11} + \alpha_{33})/2 \quad (4.50)$$

$$\Delta S_{1122} = \Delta S_{2233} = \Delta S_{3311} = 0 \quad (4.51)$$

where  $\Delta S_{ijkl} = S_{ijkl} - S_{ijkl}^0$ . Equations (4.45)-(4.51), with four unknowns (but note that each of these may be a function of strain), give the non-vanishing  $S_{ijkl}$  for any given orientation distribution of cracks.

The elastic stiffnesses  $C_{ijkl}$  then follow upon inversion of  $S_{ijkl}$ . In the expressions for the stiffnesses  $\eta$  is a function only of the elastic properties of the solid and of the scalar crack density  $\varepsilon$ , and the  $\alpha$  coefficients are dimensionless and depend only on the scalar crack density and on numerical factors which specify the orientation distribution of the cracks.

### 4.3 Isotropic Case

For an isotropic orientation distribution of empty cracks,  $\alpha = (\text{tr } \alpha/3)\mathbf{I} = \varepsilon\mathbf{I}/3$ , where  $\varepsilon$  is the scalar crack density parameter and therefore:

$$\Delta S_{1111} = \Delta S_{2222} = \Delta S_{3333} = 2\eta\varepsilon/3, \quad (4.52)$$

$$\Delta S_{1212} = \Delta S_{2323} = \Delta S_{3131} = \eta\varepsilon/3, \quad (4.53)$$

$$\Delta S_{1122} = \Delta S_{1133} = \Delta S_{2233} = 0. \quad (4.54)$$

where  $\eta$  is given by equation 4.42. The equations are the same as obtained by Sayers and Kachanov (1991) but with  $\eta_1 = 0$ .

A comparison of the predictions of the self-consistent scheme, the differential scheme and Hudson's second-order scheme for the case of randomly (i.e., isotropically distributed) oriented cracks was made by Sayers & Kachanov [1991]. In the following section we consider a particular case of anisotropy.

## 4.4 Transverse Isotropy

A particular case of anisotropy which is of wide occurrence in rock physics is transverse isotropy, in which properties are isotropic in all directions in a certain plane but differ from those in the direction orthogonal to the plane. This case is now considered and is subsequently used to analyse some experimental data.

For a general transversely isotropic orientation distribution of cracks let us choose the axis of symmetry to be the principal axis  $Ox_3$ . We then have  $\alpha_{11} = \alpha_{22}$  and equations (4.45)-(4.51) reduce to the following

$$\Delta S_{1111} = \Delta S_{2222} = 2\eta\alpha_{11} \quad (4.55)$$

$$\Delta S_{3333} = 2\eta\alpha_{33} \quad (4.56)$$

$$\Delta S_{1212} = \eta\alpha_{11} \quad (4.57)$$

$$\Delta S_{2323} = \Delta S_{3131} = \eta(\alpha_{11} + \alpha_{33})/2 \quad (4.58)$$

$$\Delta S_{1122} = \Delta S_{2233} = \Delta S_{3311} = 0 \quad (4.59)$$

The equations are the same as obtained by Sayers and Kachanov (1991) but with  $\eta_1 = 0$ .

Two special cases of transverse isotropy that are of interest are: i) **Planar Transverse Isotropy (PTI)**, where  $\alpha_{11} = \alpha_{22} = 0$ , and  $\alpha_{33} \neq 0$ ; and ii) **Cylindrical Transverse Isotropy (CTI)**, where  $\alpha_{11} = \alpha_{22} \neq 0$  and  $\alpha_{33} = 0$ . In the case of cracked bodies (e.g. rocks) PTI corresponds to the case in which the  $c$ -axes of the cracks lie in the same direction, and CTI corresponds to the case in which the crack  $c$ -axes lie in the same plane.

The fourth order elastic compliance tensor can be converted into a second order tensor following the convention in which pair of subscripts  $ij$  are converted to single subscripts as follows:  $11 \rightarrow 1$ ,  $22 \rightarrow 2$ ,  $33 \rightarrow 3$ ,  $23$  and  $32 \rightarrow 4$ ,  $13$  and  $31 \rightarrow 5$ , and  $12$  and  $21 \rightarrow 6$ . Then the compliance tensor  $S_{ijkl}$  is associated with a matrix element as follows:

$$S_{ijkl} \rightarrow \begin{cases} S_{mn} & m, n = 1, 2, 3 \\ S_{mn}/2 & \text{if either } m \text{ or } n = 4, 5, 6 \\ S_{mn}/4 & \text{if both } m \text{ and } n = 4, 5, 6. \end{cases} \quad (4.60)$$

And the stiffness tensor is converted to

$$C_{ijkl} \rightarrow C_{mn} \quad (4.61)$$

The stiffness tensor components  $C_{mn}$  follow upon inversion of the compliances, that for the case of transverse isotropy are given by:

$$C_{11} + C_{12} = \frac{(S_{11}^0 + 2\eta\alpha_{33})}{((S_{11}^0 + 2\eta\alpha_{33})(S_{11}^0 + S_{12}^0 + 2\eta\alpha_{11}) - 2S_{12}^{0\ 2})} \quad (4.62)$$

$$C_{11} - C_{12} = (S_{11}^0 - S_{12}^0 + 2\eta\alpha_{11})^{-1} \quad (4.63)$$

$$C_{33} = \frac{(S_{11}^0 + S_{12}^0 + 2\eta\alpha_{11})}{((S_{11}^0 + 2\eta\alpha_{33})(S_{11}^0 + S_{12}^0 + 2\eta\alpha_{11}) - 2S_{12}^{0\ 2})} \quad (4.64)$$

$$C_{44} = 1/(2(S_{11}^0 - S_{12}^0 + \eta\alpha_{11} + \eta\alpha_{33})) \quad (4.65)$$

$$C_{13} = -S_{12}^0/((S_{11}^0 + 2\eta\alpha_{33})(S_{11}^0 + S_{12}^0 + 2\eta\alpha_{11}) - 2S_{12}^{0\ 2}) \quad (4.66)$$

$$C_{66} = (C_{11} - C_{12})/2 = 1/(2(S_{11}^0 - S_{12}^0 + 2\eta\alpha_{11})) \quad (4.67)$$

In these equations  $\eta$  depends only on  $S_{11}^0$ ,  $S_{12}^0$  and  $\varepsilon$ , so the five independent coefficients depend on the five parameters  $S_{11}^0, S_{12}^0, \varepsilon, \alpha_{11}$  and  $\alpha_{33}$ .  $\eta$  is given by equation (4.42). These equations are consistent with the ones obtained by Sayers and Kachanov (1985) ignoring their fourth-rank tensor contribution.

#### 4.5 Elastic properties of an isotropic uncracked medium.

$S_{11}^0$  and  $S_{12}^0$  represent the elastic properties of an isotropic uncracked medium, and are given in terms of the Young's Modulus  $E^0$  and Poisson ratio  $\nu^0$  of the uncracked solid by:

$$S_{11}^0 = \frac{1}{E^0} \quad (4.68)$$

$$S_{12}^0 = \frac{-\nu^0}{E^0} \quad (4.69)$$

$E^0$  and  $\nu^0$  can be determined from laboratory measurements of elastic wave velocities at high confining pressures which will approach the crack-free isotropic wave velocities  $V_P^0$  and  $V_S^0$  (provided that the uncracked solid is isotropic). Using the relations between elastic constants and wave velocities for an isotropic medium, i.e.,

$$V_P^0 = \sqrt{\frac{C_{11}^0}{\rho^0}} = \sqrt{\frac{(1 - \nu^0) E^0}{(1 - 2\nu^0)(1 + \nu^0)\rho^0}} \quad (4.70)$$

$$V_S^0 = \sqrt{\frac{C_{44}^0}{\rho^0}} = \sqrt{\frac{E^0}{2(1 + \nu^0)\rho^0}} \quad (4.71)$$

we obtain,

$$E^0 = \frac{\rho^0 V_S^{0\ 2} (3V_P^{0\ 2} - 4V_S^{0\ 2})}{V_P^{0\ 2} - V_S^{0\ 2}} \quad (4.72)$$

$$\nu^0 = \frac{V_P^{02} - 2V_S^{02}}{2(V_P^{02} - V_S^{02})} \quad (4.73)$$

(where  $\rho^0$  is the density of the uncracked rock). It follows that

$$S_{11}^0 = \frac{V_P^{02} - V_S^{02}}{\rho^0 V_S^{02} (3V_P^{02} - 4V_S^{02})} \quad (4.74)$$

$$S_{12}^0 = \frac{-(V_P^{02} - 2V_S^{02})}{2\rho^0 V_S^{02} (3V_P^{02} - 4V_S^{02})}. \quad (4.75)$$

## 4.6 Elastic Wave velocities in a transversely isotropic medium.

For a transversely isotropic medium with axis of symmetry in the 3-direction, the relations between velocities and stiffnesses are:

$$V_{11} = V_{22} = \sqrt{\frac{C_{11}}{\rho^0}} \quad (4.76)$$

$$V_{33} = \sqrt{\frac{C_{33}}{\rho^0}} \quad (4.77)$$

$$V_{12} = V_{21} = \sqrt{\frac{C_{66}}{\rho^0}} \quad (4.78)$$

$$V_{31} = V_{32} = V_{13} = V_{23} = \sqrt{\frac{C_{44}}{\rho^0}} \quad (4.79)$$

where in the notation for the velocities  $V_{ij}$  the first index indicates the direction of propagation of the wave, and the second index the direction of particle motion (polarisation).

If in experimental tests  $V_{33}$  and  $V_{31}$  are measured, we can calculate  $C_{33}$  and  $C_{44}$  using equations (4.77) and (4.79), and from equations (4.64) and (4.65) we obtain the following expressions for  $\eta\alpha_{11}$  and  $\eta\alpha_{33}$ :

$$\eta\alpha_{11} = -\frac{S_{11}^0}{2} + \frac{S_{12}^0}{4} - \frac{1}{4\rho^0} \left( \frac{1}{V_{33}^2} - \frac{1}{V_{31}^2} \right) + D, \quad (4.80)$$

$$\eta\alpha_{33} = -\frac{S_{11}^0}{2} + \frac{3S_{12}^0}{4} + \frac{1}{4\rho^0} \left( \frac{1}{V_{33}^2} + \frac{1}{V_{31}^2} \right) - D, \quad (4.81)$$

where

$$D = \frac{\sqrt{(-V_{31}^2 + V_{33}^2)^2 + \rho^0 S_{12}^0 V_{31}^2 V_{33}^2 (\rho^0 S_{12}^0 V_{31}^2 V_{33}^2 + 6(-V_{31}^2 + V_{33}^2))}}{4\rho^0 V_{31}^2 V_{33}^2} \quad (4.82)$$

Alternatively if  $V_{11}$  and  $V_{12}$  are measured, we can calculate  $C_{11}$  and  $C_{66}$  using equations (4.76) and (4.78), and from equations (4.62), (4.63) and (4.67) we obtain the following expressions for  $\eta\alpha_{11}$  and  $\eta\alpha_{33}$ :

$$\eta\alpha_{11} = \frac{-S_{11}^0}{2} + \frac{S_{12}^0}{2} + \frac{1}{4\rho^0 V_{12}^2} \quad (4.83)$$

$$\eta\alpha_{33} = \frac{-S_{11}^0 + S_{12}^0}{2} + \frac{S_{12}^0 (-V_{11}^2 + 2V_{12}^2)}{2V_{11}^2 - 4V_{12}^2 + 8\rho^0 S_{12}^0 V_{12}^2 (V_{11}^2 - V_{12}^2)} \quad (4.84)$$

The scalar crack density is given by  $\epsilon (= \text{tr}\alpha = 2\alpha_{11} + \alpha_{33})$  in any of the above cases.

Writing the right-hand side of (4.80) (or (4.83)) as  $f$  and that of (4.81) (or (4.84)) as  $g$  we find:

$$\epsilon = \frac{2f + g}{\eta} \quad (4.85)$$

$$\alpha_{11} = f/\eta \quad (4.86)$$

$$\alpha_{33} = g/\eta \quad (4.87)$$

The analyses in sections 4.2.1 and 4.2.3 lead to an approximate value for  $\eta$  for low crack densities, which is given by equation 4.39, and is a function only of  $\nu^0$  and  $E^0$ . Bruner (1976) developed a differential self-consistent scheme to calculate the elastic properties of cracked solids, which gives more accurate results at higher crack densities. In 4.2.3 we showed how this leads to an expression for  $\eta$  which can be calculated to first or higher orders of the scalar crack density  $\epsilon$ . The first-order expression is given in equation 4.42. Inserting this into (4.85-4.87) and solving, we find:

$$\epsilon = \frac{-\eta' + \sqrt{\eta'^2 + 4\eta''(2f + g)}}{2\eta''} \quad (4.88)$$

$$\alpha_{11} = \frac{f}{\eta' + \eta''\epsilon} \quad (4.89)$$

$$\alpha_{33} = \frac{g}{\eta' + \eta''\epsilon} \quad (4.90)$$

where  $\eta'$  and  $\eta''$  are given in equations 4.43 and 4.44 respectively,  $f$  is the right-hand side of 4.80 (or 4.83) and  $g$  is the right-hand side of 4.81 (or 4.84).

## 4.7 Orthorhombic symmetry

The next case of interest for us is more complex, the orthorhombic symmetry, in which all the three coordinate axes are not equivalent. The stiffness tensor components follow upon inversion of equations (4.45-4.51)<sup>†</sup>, which represent an orthorhombic system. From equation (4.51) and assuming that, before the deformation the material is isotropic, it follows that,

$$S_{12} = S_{23} = S_{31} = S_{12}^0 \quad (4.91)$$

and the inversion of the orthorhombic matrix of compliances gives;

$$C_{11} = \frac{-S_{12}^2 + S_{22} S_{33}}{w}; \quad (4.92)$$

<sup>†</sup> See Sayers and Kachanov (1995).

$$C_{22} = \frac{-S_{12}^2 + S_{11} S_{33}}{w}; \quad (4.93)$$

$$C_{33} = \frac{-S_{12}^2 + S_{11} S_{22}}{w}; \quad (4.94)$$

$$C_{44} = \frac{1}{S_{44}}; \quad (4.95)$$

$$C_{55} = \frac{1}{S_{55}}; \quad (4.96)$$

$$C_{66} = \frac{1}{S_{66}}; \quad (4.97)$$

$$C_{12} = \frac{S_{12} (S_{12} - S_{33})}{w}; \quad (4.98)$$

$$C_{13} = \frac{S_{12} (S_{12} - S_{22})}{w}; \quad (4.99)$$

$$C_{23} = \frac{S_{12} (S_{12} - S_{11})}{w}; \quad (4.100)$$

$$w = 2 S_{12}^3 + S_{11} S_{22} S_{33} - S_{12}^2 (S_{11} + S_{22} + S_{33}) . \quad (4.101)$$

The shear wave velocities in each of the three orthogonal directions are given by the following equations:

$$C_{44} - \rho V_{13}^2 = 0 , \quad (4.102)$$

$$C_{55} - \rho V_{23}^2 = 0 , \quad (4.103)$$

$$C_{66} - \rho V_{12}^2 = 0 , \quad (4.104)$$

then we obtain 3 coupled equations with 3 unknowns (the  $\alpha$ 's), that can be solved exactly.

The corresponding solutions for the crack density components are:

$$\eta\alpha_{11} = \frac{-S_{11}^0}{2} + \frac{S_{12}^0}{2} + \frac{V_{12}^{-2} - V_{23}^{-2} + V_{31}^{-2}}{4\rho} \quad (4.105)$$

$$\eta\alpha_{22} = \frac{-S_{11}^0}{2} + \frac{S_{12}^0}{2} + \frac{V_{12}^{-2} + V_{23}^{-2} - V_{31}^{-2}}{4\rho} \quad (4.106)$$

$$\eta\alpha_{33} = \frac{-S_{11}^0}{2} + \frac{S_{12}^0}{2} + \frac{-V_{12}^{-2} + V_{23}^{-2} + V_{31}^{-2}}{4\rho} \quad (4.107)$$

using the shear wave velocities.

If we use the compressional wave velocities in the three orthogonal directions, the corresponding equations relating them with the stiffnesses are;

$$C_{11} - \rho V_{11}^2 = 0 \quad (4.108)$$

$$C_{22} - \rho V_{22}^2 = 0 \quad (4.109)$$

$$C_{33} - \rho V_{33}^2 = 0 \quad (4.110)$$

This time the coupling between the equations is more complicated, and I was not able to obtain an exact expression for the crack density components but had to make some approximations. First from the equation for  $V_{11}$  we obtain  $\alpha_{11}$  in terms of the other two  $\alpha$ 's. Similarly, from the equation for  $V_{22}$  we obtain  $\alpha_{22}$  and from the equation for  $V_{33}$  we obtain  $\alpha_{33}$ . These  $\alpha$ 's are then developed in series of  $\eta$  at order 0 and we obtain;

$$\eta\alpha_{11} = \frac{(-S_{11}^0 + S_{12}^0)(S_{11}^0 + 2S_{12}^0)}{2(S_{11}^0 + S_{12}^0)} + \frac{1}{2\rho V_{11}^2} - \frac{(\alpha_{22} + \alpha_{33})\eta S_{12}^{0\ 2}}{(S_{11}^0 + S_{12}^0)^2} \quad (4.111)$$

$$\eta\alpha_{22} = \frac{(-S_{11}^0 + S_{12}^0)(S_{11}^0 + 2S_{12}^0)}{2(S_{11}^0 + S_{12}^0)} + \frac{1}{2\rho V_{22}^2} - \frac{(\alpha_{11} + \alpha_{33})\eta S_{12}^{0\ 2}}{(S_{11}^0 + S_{12}^0)^2} \quad (4.112)$$

$$\eta\alpha_{33} = \frac{(-S_{11}^0 + S_{12}^0)(S_{11}^0 + 2S_{12}^0)}{2(S_{11}^0 + S_{12}^0)} + \frac{1}{2\rho V_{33}^2} - \frac{(\alpha_{22} + \alpha_{11})\eta S_{12}^{0\ 2}}{(S_{11}^0 + S_{12}^0)^2}. \quad (4.113)$$

As long as the  $\alpha$ 's remain  $\ll 1$  the coupling coefficient is small and can be neglected giving the equations;

$$\eta\alpha_{11} = \frac{(-S_{11}^0 + S_{12}^0)(S_{11}^0 + 2S_{12}^0)}{2(S_{11}^0 + S_{12}^0)} + \frac{1}{2\rho V_{11}^2} \quad (4.114)$$

$$\eta\alpha_{22} = \frac{(-S_{11}^0 + S_{12}^0)(S_{11}^0 + 2S_{12}^0)}{2(S_{11}^0 + S_{12}^0)} + \frac{1}{2\rho V_{22}^2} \quad (4.115)$$

$$\eta\alpha_{33} = \frac{(-S_{11}^0 + S_{12}^0)(S_{11}^0 + 2S_{12}^0)}{2(S_{11}^0 + S_{12}^0)} + \frac{1}{2\rho V_{33}^2}, \quad (4.116)$$

that allow the calculation of the crack density coefficients using compressional wave velocities data.

The scalar crack density is

$$\varepsilon = \alpha_{11} + \alpha_{22} + \alpha_{33}. \quad (4.117)$$

Writing the right-hand side of (4.105) (or (4.114)) as  $f1$  that of (4.106) (or (4.115)) as  $f2$  and that of (4.107) (or (4.116)) as  $f3$  we find:

$$\varepsilon = \frac{f1 + f2 + f3}{\eta} \quad (4.118)$$

$$\alpha_{11} = f1/\eta \quad (4.119)$$

$$\alpha_{22} = f2/\eta \quad (4.120)$$

$$\alpha_{33} = f3/\eta \quad (4.121)$$

Inserting equation (4.42) into (4.118-4.121) and solving, we find:

$$\varepsilon = \frac{-\eta' + \sqrt{\eta'^2 + 4\eta''(f1 + f2 + f3)}}{2\eta''} \quad (4.122)$$

$$\alpha_{11} = \frac{f1}{\eta' + \eta'' \varepsilon} \quad (4.123)$$

$$\alpha_{22} = \frac{f2}{\eta' + \eta'' \varepsilon} \quad (4.124)$$

$$\alpha_{33} = \frac{f3}{\eta' + \eta'' \varepsilon} \quad (4.125)$$

where  $\eta'$  and  $\eta''$  are given in equations 4.43 and 4.44 respectively.

An example of this kind of symmetry is given by three mutually orthogonal crack arrays.

## 4.8 Experimental Data

To test this model we use data from triaxial deformation experiments performed by researchers from the Rock & Ice Physics laboratory at University College London (Jones, 1988; Ayling, 1991; Stuart, 1992) on dry specimens of Darley Dale sandstone, a well-indurated felspathic sandstone with a siliceous cementing material (Murrell, 1965). The measurements of wave velocities during a compressive test are carried out by determining the travel time, in which ultrasonic waves are emitted and received by piezoelectric transmitters and receivers placed on opposite sides of the rock sample.

Two modes of triaxial testing have been used. In the first mode a **cylindrical geometry** is used, with two principal stresses (the minor and intermediate compressive stresses) always being equal ( $\sigma_{3'3'} = \sigma_{2'2'}$ ), so that the cylinder axis  $Ox_{1'}$  becomes the principal axis of elastic symmetry  $Ox_3$  and CTI is produced. In the second mode a **cubic geometry** is used, in which the principal stresses are in general all different from one another ( $\sigma_{3'3'} < \sigma_{2'2'} < \sigma_{1'1'}$ , compressive stress is taken positive), in which the principal axis of elastic symmetry  $Ox_3$  coincides with the minor principal compressive stress axis  $Ox_{3'}$  and **orthorhombic symmetry is produced**.

In the cylindrical geometry testing mode (Jones, 1988; Ayling, 1991), right cylindrical specimens 15mm in diameter by 45mm in length are jacketed in an impermeable plastic sleeve and deformed in compression in a cylindrical high-pressure triaxial cell described by Murrell *et al.*, (1989) and Ayling *et al.*, (1995). An all-round hydrostatic pressure ( $\sigma_{3'3'}^c = \sigma_{2'2'}^c = \sigma_{1'1'}^c$ ) is first applied to the specimen, and this is maintained at a set value (this is described conventionally as the “confining pressure”, and provides the minor and intermediate principal compressive stresses, which are equal in this case). Then an additional compressive deviatoric load  $\sigma_{1'1'}$  is applied along the cylinder axis  $Ox_{1'}$  of the rock specimen (we call this the “axial load”) by means of a servo-controlled actuator, generally operating at a constant displacement rate. For the acoustic wave measurements the pulse

transmission method (Birch, 1960) was used to measure the acoustic wave velocities  $V_{1'1'}$  and  $V_{1'3'} (= V_{2'3'})$  (parallel to the maximum principal stress) concurrently with rock deformation (Murrell *et al.*, 1989), while at the same time measuring bulk acoustic emission (AE) from the sample (Sammonds *et al.*, 1989). Compressional wave ( $P$ ) and shear wave ( $S$ ) piezoelectric transducers, with resonant frequencies of 1MHz, are mounted at each end of the rock specimen. The transducers at one end are pulsed sequentially using a square wave. Elastic wave travel times are measured using timers set to trigger on the  $P$  and  $S$  first arrivals of the amplified signals received at the other end of the sample. The experiments were carried out at a nominal strain rate of  $10^{-5}/s$ , which is a very low rate for dry samples, and is expected not to have a strong influence on crack growth. The rock samples were oven-dried at  $70^{\circ}C$  for 48 hours before the experiments.

There is a small initial anisotropy due to the bedding of the rock samples. While increasing the confining pressure reduces this anisotropy, some residual anisotropy due to plastic deformation may still be present at high confining pressures (Gueguen & Palciauskas, 1994). Application of even a modest confining pressure ( $< 200MPa$ ) closes most of the low aspect ratio cracks in the rock and increases the velocities of both, the compressional wave velocity  $V_P$  and the shear wave velocity  $V_S$  travelling through the sample. Under increasing hydrostatic pressure, both velocities increase rapidly. The highest values of the wave velocities are used then to estimate the moduli of the rock in its crack-free state.

Ayling (1991) measured  $P$  ( $V_{33}$ ) and  $S$  ( $V_{31}$ ) wave velocities as a function of confining pressure (see Figure 4.1), and subsequently measured  $V_{33}$  and  $V_{31}$  as a function of stress and strain during triaxial loading at a series of different confining pressures (see Figures 4.2 and 4.3).

From Figure 4.1 we can see that the form of the curve is concave to the increasing pressure, the highest values for  $V_P$  and  $V_S$  are taken to be the crack-free isotropic wave velocities  $V_P^0$  and  $V_S^0$  used to estimate the moduli  $S_{11}^0$  and  $S_{12}^0$  in section 4.5. Then  $V_P^0 = 4.116 \text{ Km/s}$  and  $V_S^0 = 2.278 \text{ Km/s}$ .

From Figures 4.2 and 4.3 we can see that  $V_P$  shows a markedly initial increase, and then decreases at slow rate.  $V_S$  initially increases at slower rate than  $V_P$  for  $p_0 = 30MPa$  and remains reasonably constant for increasing pressures, but as the sample becomes anelastic (higher differential stress),  $V_S$  clearly decreases at faster rate than  $V_P$ . We should notice that at certain values of differential stress there are two values of  $V_P$  and  $V_S$ , this is due to the unloading of the sample following the peak stress and failure, and this will be explained in terms of the crack population in the next section. Both the  $V_P$  and  $V_S$  decreases seem

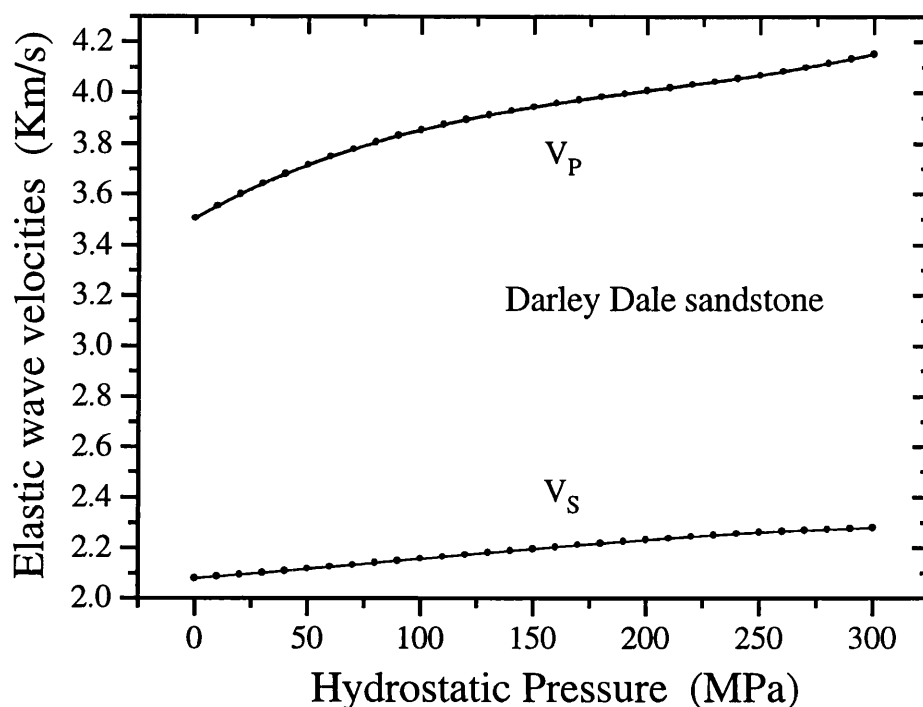


**Figure 4.1:** Elastic wave velocities  $V_P$  and  $V_S$  as a function of confining pressure in a test on a dry specimen of Darley Dale sandstone at room temperature.

to be higher for lower confining pressures. At the highest confining pressure the sample deforms by cataclastic flow, and the velocities decrease at very small rate.

Stuart (1992) performed similar experiments to those of Jones (1988) and Ayling (1991) on cubic samples of the same sandstone from Darley Dale. In this case the apparatus was designed to enable three independent principal stresses to be applied normal to the three orthogonal sets of sample faces. The strains and the  $P$  and  $S$  wave velocities in the three principal stress directions were measured, together with the bulk AE.

The apparatus is based at K.S.E.P.L. at Risjwijk. Cubic rock samples (50 mm edge length) were deformed in a three-axis stressing frame constructed of flanged steel beams, one of which is removable to allow the insertion of the sample. Three pairs of servo-controlled hydraulic jacks (300kN capacity) are used to provide the loads along orthogonal axes normal to the sample faces. There are hemi-spherical seatings and aluminium platens immediately adjacent to the rock sample, and acoustic transducers are mounted in the platens. A data acquisition and control computer was fixed both to control the loading cycle and to record the data as a function of elapsed time. Load (stress), displacement

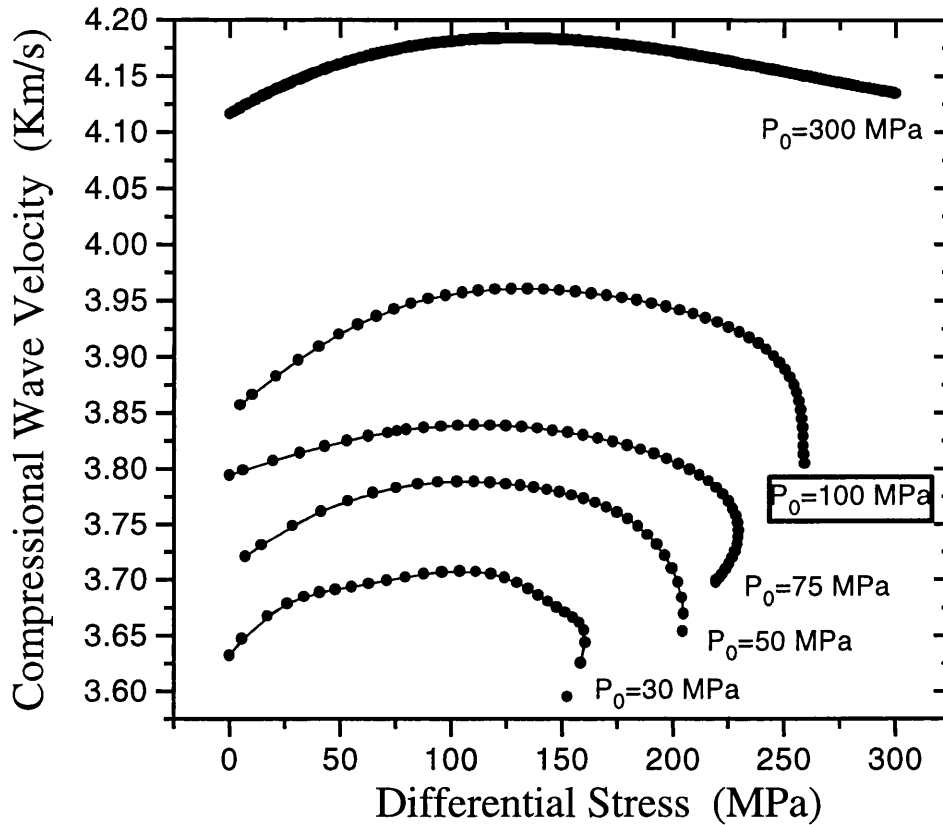


**Figure 4.2:** Compressional wave velocity versus differential stress for samples of Darley Dale sandstone deformed at different confining pressures  $p_0$ . Data from Ayling (1991).

(strain), and  $P$  and  $S$  wave travel times were logged contemporaneously (5s logging time) at pre-determined intervals (50s) throughout each test, and AE was recorded continuously between the logging periods. The  $P$  and  $S$  wave transducers had a nominal resonant frequency of 1MHz (wavelength  $\approx 3.5$ mm), and the AE transducers resonant frequency was 0.5 MHz.

In the experiments we shall discuss, two different material conditions exist depending on the experimental stress history. (1) The **elastic initial condition**. At the beginning the rock has a pre-existing crack distribution, which we take as isotropic (though there is in fact a small degree of planar transverse isotropy or orthotropy associated with sedimentary bedding). Compressive loading causes cracks to close, which results in an increase in elastic stiffness and in elastic wave velocity, in the direction of compression. This is accompanied by a small opening component in directions orthogonal to this. Under small hydrostatic or deviatoric loads the deformation is elastic, so the changes of elastic stiffness and wave

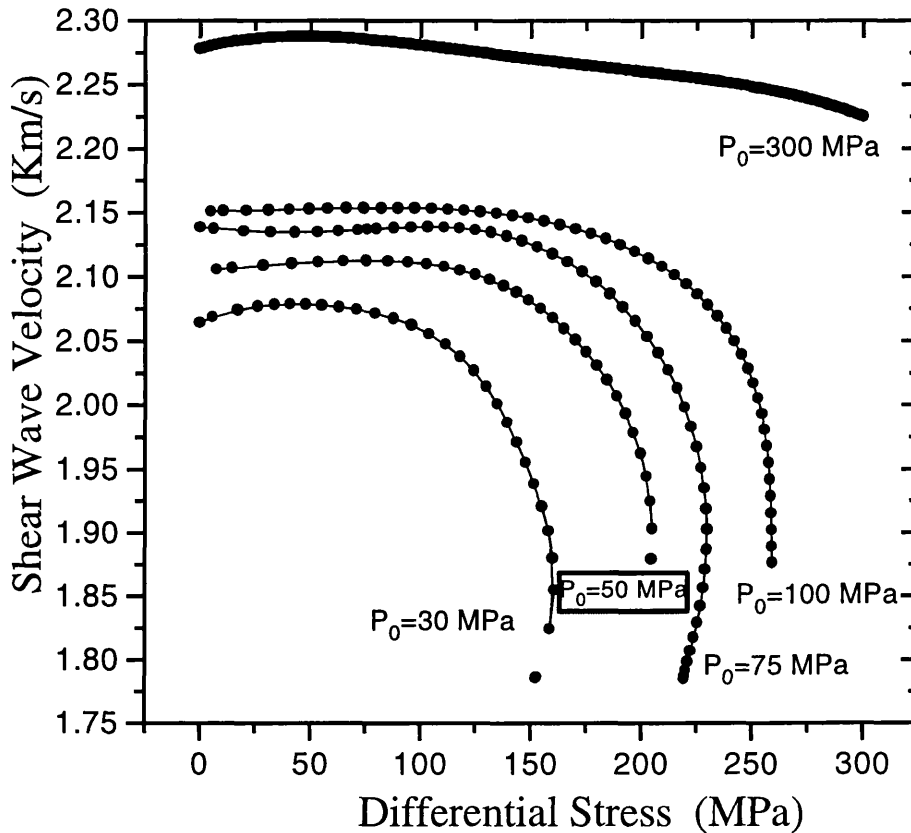


**Figure 4.3:** Shear wave velocity versus differential stress for samples of Darley Dale sandstone deformed at different confining pressures  $p_0$ . Data from Ayling (1991).

velocity are reversible. (2) The **inelastic dilatant condition**. When a critical deviatoric stress is exceeded the deformation ceases to be elastic and new dilatant cracks form and grow. This causes irreversible reductions in elastic stiffness and wave velocities. The dilatant crack population has an anisotropic distribution due to the fact that  $c$ -axes of the dilatant cracks are approximately parallel to the minor principal compressive stress axis (this follows from theoretical work by Murrell & Digby, 1970). (Inelastic pore collapse can also be produced at high hydrostatic pressures resulting in an irreversible increase of elastic stiffness and wave velocities, but this is not considered here).

In the elastic condition, application of a hydrostatic compression to a rock with an isotropic crack distribution leaves the rock in an isotropic condition, but the application of a deviatoric load results in anisotropic conditions (due to differential crack closure) and when only one principal stress ( $\sigma_{1'1'}$ ) deviates from the hydrostatic state, transverse isotropy is created in the plane normal to  $\sigma_{1'1'}$ . We use the suffix  $i$  to denote the initial

crack distribution tensor (and its components). Under zero load this tensor is taken as isotropic as already mentioned.

The inelastic dilatant condition generally results from the application of sufficiently large deviatoric loads. The new dilatant cracks have a transversely isotropic distribution, with either cylindrical transverse isotropy (CTI) where only one principal stress ( $\sigma_{1'1'}$ ) deviates from the hydrostatic state, or orthorhombic symmetry where the principal stresses are all unequal. In these two cases the symmetry axes  $Ox_3$  of the crack distributions are respectively: parallel to  $\sigma_{1'1'}$  in the former (CTI) case, with the  $c$ -axes of the dilatant cracks orthogonal to  $\sigma_{1'1'}$  ( $\sigma_{3'3'} = \sigma_{2'2'}$  in this case); and parallel to  $\sigma_{3'3'}$  in the latter (PTI) case, with the  $c$ -axes of the dilatant cracks parallel to  $\sigma_{3'3'}$ . We use the suffix  $d$  to denote the dilatant crack distribution tensor (and its components).

During any given test in general both  $i$  and  $d$  crack populations exists, and are a function of stress state and strain. However, the acoustic wave velocity changes associated with the changes in compressive stress state are opposite in sign for the two populations; increases for the  $i$ -population, and decreases for the  $d$ -population on loading, and viceversa on unloading (but remember that the  $d$ -population is associated with inelastic deformation).

## 4.9 Cylindrical Geometry Testing Results.

We begin by analysing an experimental situation in which only the P-wave velocity along the sample cylindrical axis is measured during triaxial tests (Jones, 1988; Jones & Murrell, 1989). It is not possible in this case, to determine the anisotropy of the dilatant crack distribution. However, it is possible to estimate the change in the scalar crack density parameter  $\varepsilon$  as a function of strain. In this case we have two separate crack populations (denoted  $i$  and  $d$ ) with axis of symmetry along the cylinder axis, which is the direction of the maximum principal compressive stress  $\sigma_{1'1'}$ , and  $V_{1'1'}$  was measured. In this case CTI is produced with axis of symmetry ( $Ox_3$ ) along the  $\sigma_{1'1'}$  axis. Therefore  $V_{1'1'} = V_{33}$ , where the dashed numerals refer to principal axes of the stress tensor and the undashed numerals refer to the principal axes of the rock physical properties tensor. Now from equations (4.77) and (4.64) we find:

$$\rho^0 V_{33}^2 = \frac{2\alpha_{11}\eta + S_{11}^0 + S_{12}^0}{(2\alpha_{33}\eta + S_{11}^0)(2\alpha_{11}\eta + S_{11}^0 + S_{12}^0) - 2S_{12}^0{}^2} \quad (4.126)$$

In this case  $2\alpha_{11} + \alpha_{33} = \varepsilon$ , where  $\varepsilon$  is the scalar crack density parameter, so we can write this equation in terms of either  $\alpha_{11}$  or  $\alpha_{33}$  and  $\varepsilon$ , and  $\eta$  is given by equation 4.42 in

terms of  $\varepsilon$ .  $S_{11}^0$  and  $S_{12}^0$  are functions of  $E^0$  and  $\nu^0$  (the Young's modulus and Poisson's ratio of the uncracked solid). In order to determine  $\varepsilon$  from  $V_{33}$  using (4.126) we need to find some method of eliminating one or other of the anisotropy parameters. If we assume that the cracks are always isotropically distributed then  $\alpha_{11} = \alpha_{33} = \varepsilon/3$ , and after substituting in (4.126) and neglecting terms in  $\varepsilon$  higher than  $\varepsilon^2$ , we obtain a quadratic equation that can be solved for  $\varepsilon$  in terms of  $V_{33}$  and the properties of the uncracked solid ( $\rho^0$ ,  $\nu^0$ , and  $E^0$ ). At small values of  $\varepsilon$  we can use the linear approximation, which gives:

$$\varepsilon = \frac{3 (S_{11}^0 + S_{12}^0) + 3 (-S_{11}^0 + S_{12}^0) (S_{11}^0 + 2 S_{12}^0) \rho^0 V_{33}^2}{2 \eta' (-1 + (2 S_{11}^0 + S_{12}^0) \rho^0 V_{33}^2)} \quad (4.127)$$

where  $\eta'$  is given by equation 4.43. The second order approximation gives:

$$\varepsilon = \frac{3 \left( -(\eta' (-1 + (2 S_{11}^0 + S_{12}^0) \rho^0 V_{33}^2)) + \sqrt{A} \right)}{2 \left( 2 \eta'^2 \rho^0 V_{33}^2 + \eta'' (-3 + 6 S_{11}^0 \rho^0 V_{33}^2 + 3 S_{12}^0 \rho^0 V_{33}^2) \right)} \quad (4.128)$$

where

$$A = \eta'^2 \left( 1 + 2 S_{12}^0 \rho^0 V_{33}^2 + 9 S_{12}^0{}^2 \rho^0 V_{33}^2 \right) + 6 \eta'' \times \left( -S_{11}^0 - S_{12}^0 + \left( 3 S_{11}^0{}^2 + 4 S_{11}^0 S_{12}^0 - S_{12}^0{}^2 \right) \rho^0 V_{33}^2 + (-S_{11}^0 + S_{12}^0) (2 S_{11}^0 + S_{12}^0) (S_{11}^0 + 2 S_{12}^0) \rho^0 V_{33}^2 \right) \quad (4.128b)$$

An alternative approach is to use our preliminary understanding of the nature of the anisotropy of the crack population as it changes during loading. Initially, at zero load, we assume the crack population is isotropic, so  $\alpha_{11} = \alpha_{33}$ . Isotropy is retained when a confining pressure is applied, but  $\varepsilon$  decreases. When a small deviatoric compressive load  $\sigma_{1'1'}$  is applied then  $\alpha_{33}$  should decrease and  $\alpha_{11}$  should show a small increase, as the initial crack population ( $i$ ) is deformed elastically. Eventually, at higher deviatoric loads, new dilatant cracks grow, with their  $c$ -axes orthogonal to  $\sigma_{1'1'}$ , and  $\alpha_{11}$  should show a large increase as  $\alpha_{33}$  continues to decrease (possibly at a decreasing rate).

If we assume that the largest change is in  $\alpha_{11}$  we may take as an approximation that  $\alpha_{33} = 0$ , so that  $2\alpha_{11} = \varepsilon$ . Then, from (4.126) and taking up to first order in  $\varepsilon$  we find:

$$\varepsilon = \frac{S_{11}^0 + S_{12}^0 - (S_{11}^0 - S_{12}^0) (S_{11}^0 + 2 S_{12}^0) \rho^0 V_{33}^2}{\eta' (-1 + S_{11}^0 \rho^0 V_{33}^2)} \quad (4.129)$$

where  $\eta'$  is given by equation 4.43.

The second-order approximation gives:

$$\varepsilon = \frac{-(\eta' (-1 + S_{11}^0 \rho^0 V_{33}^2)) + \sqrt{D}}{2 \eta'' (-1 + S_{11}^0 \rho^0 V_{33}^2)} \quad (4.130)$$

where

$$D = \eta'^2 - 4 \eta'' (S_{11}^0 + S_{12}^0) + 2 \left( -(\eta'^2 S_{11}^0) + 4 \eta'' (S_{11}^0{}^2 + S_{11}^0 S_{12}^0 - S_{12}^0{}^2) \right) \rho^0 V_{33}^2 + S_{11}^0 \left( \eta'^2 S_{11}^0 + 4 \eta'' (-S_{11}^0 + S_{12}^0) (S_{11}^0 + 2 S_{12}^0) \right) \rho^0 V_{33}^2 \quad (4.131)$$

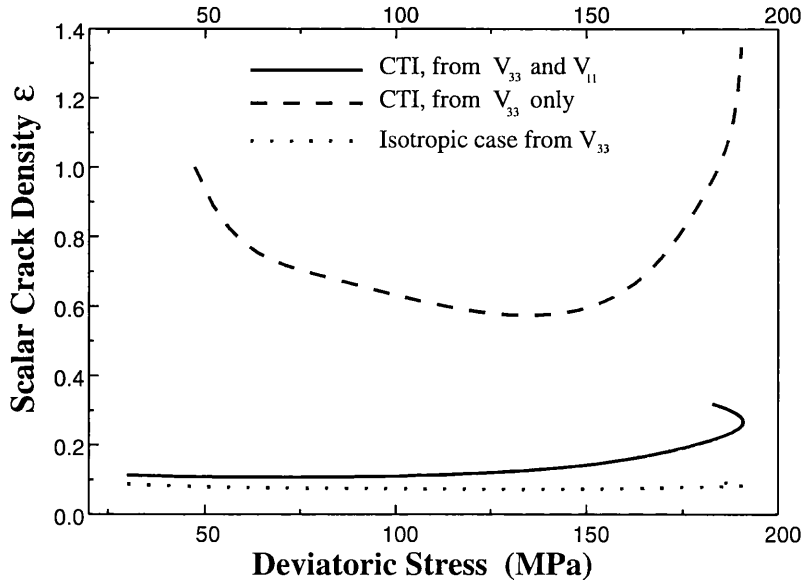


**Figure 4.4:** Scalar crack density  $\varepsilon$  as a function of deviatoric stress calculated from 3 different methods. The dotted line curve was obtained making the assumption that the crack orientation is always isotropic (eq. 4.128). The dashed curve was obtained assuming that the crack orientation is CTI (eq. 4.130). The black line curve was obtained using both  $V_P$  and  $V_S$  in eq. 4.88. The confining pressure is 30MPa. Calculated with data from Ayling (1991).  $\eta'$  and  $\eta''$  are given in equations (4.43) and (4.44).

In Figure 4.4 we show the scalar crack density  $\varepsilon$ , estimated by the two methods outlined above (equations (4.128) and (4.130)), as a function of the total axial stress  $\sigma_{1'1'}$  for one experiment, using only the axial P-wave velocity ( $V_{33}$ ). In this figure  $\varepsilon$  first decreases in response to the applied confining pressure ( $\sigma_{1'1'}^c$ ), and subsequent changes are in response to the applied deviatoric stress ( $\sigma_{1'1'} - \sigma_{1'1'}^c = \sigma_{1'1'} - \sigma_{3'3'}^c, \sigma_{3'3'}^c = \sigma_{2'2'}^c$ ). The equation (4.128) underestimates the crack density, while equation (4.130) overestimates it. The data used are not from Jones (1988) because some differences with the rock samples used by Ayling (1991) were found and it was desirable to focus only in the effects of different approximations and not in the differences between experiments. Therefore, the  $V_P$  wave data of Ayling (1991) were used instead.

If both P ( $V_{33}$ ) and S ( $V_{31}$ ) wave velocities are used, it is possible to determine both the scalar crack density ( $\varepsilon$ ) and the crack density anisotropy coefficients ( $\alpha_{11}, \alpha_{33}$ ). The equations (4.88-4.90) give  $\alpha_{11}, \alpha_{33}$ , and  $\varepsilon$ . The changes in these three parameters due to deviatoric loading alone are shown as a function of  $(\sigma_{1'1'} - \sigma_{3'3'}^c)$  in Figure 4.5 for different confining pressures, and the value of the scalar crack density parameter  $\varepsilon$  as a function of  $\sigma_{1'1'}$  for  $p_0 = 30$  MPa is plotted in Figure 4.4 for comparison with the ones obtained from P-wave velocity only.

From Figure 4.4 we can say that all three methods predict a decrease in the scalar crack density parameter upon initial differential loading, but only the methods that use the CTI

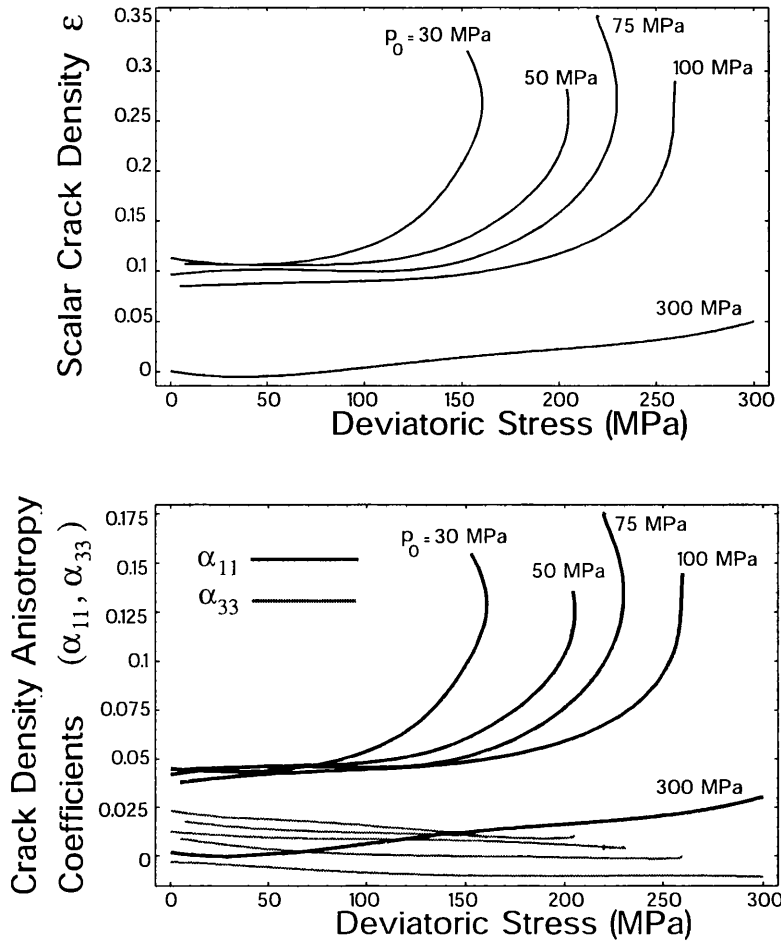


**Figure 4.5:** Variation of crack density with stress for different confining pressures  $p_0$ . a) Scalar crack density  $\varepsilon$  and b) crack density anisotropy coefficients  $\alpha_{11}$  and  $\alpha_{22}$ . Calculated with data from Ayling (1991).

simmetry show a markedly increase with higher deviatoric stress (CTI curve using both  $V_p$  and  $V_s$  increased almost a 150% ). According with the results of Chapter 3, NDC's are expected to grow quasi-parallel to the most compressive stress and therefore they will not affect significantly compressional waves propagating along that direction, but they will affect strongly shear waves propagating along the axis of loading. Therefore the P-wave methods obtained in this section are not expected to be very accurate for the cylindrical geometry testing.

In contrast, from the Figures 4.5 and 4.6, obtained using equations (4.88-4.90) applied to Ayling's data (1991), we can extract useful information concerning the microcrack population of the sample. It is apparent an initial anisotropy existed in the samples probably due to bedding. Under hydrostatic loading the anisotropy disappears at about a confining

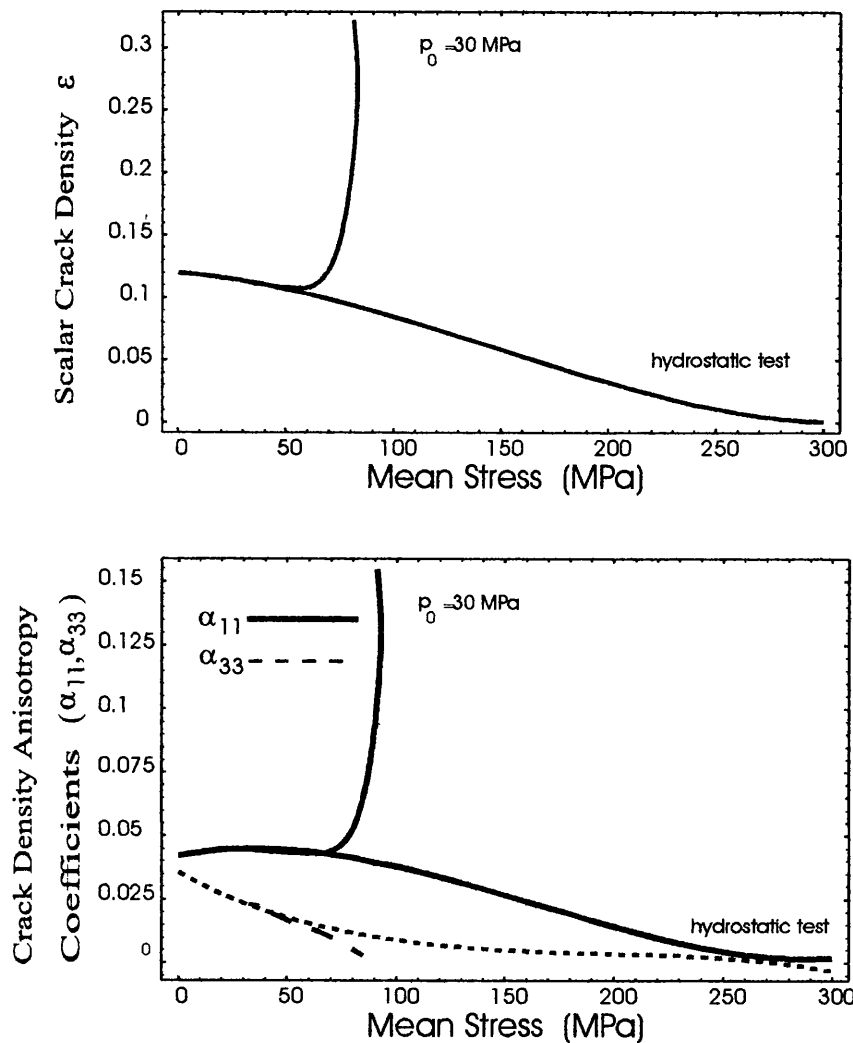


**Figure 4.6:** Variation of scalar crack density and anisotropy coefficients with mean stress, for hydrostatic test and for triaxial deformation at  $p_0 = 30$  MPa. The mean stress is  $(\sigma_{11} + \sigma_{22} + \sigma_{33})/3$ . The maximum value of the deviatoric stress is 160 MPa. pressure of 250 MPa (Figure 4.6), and almost all cracks are closed at 300 MPa.

Under differential loading all the cracks that are perpendicular to the loading axes ( $\alpha_{33}$ ) close continuously during all the test (Figure 4.5). The cracks that are parallel to the loading axis ( $\alpha_{11}$  and  $\alpha_{22}$ ) are not much affected by the initial differential loading, but there is a level of deviatoric stress (initiation of dilatancy) for which these crack populations (parallel to loading axis) start to increase markedly so that the crack growth is predominantly orientated in the axial direction in accordance with the results obtained in Chapter 3. At post-peak stresses, during partial unloading, the crack density continues to grow, this may be due to the opening and growth of some inclined cracks. At the final stage the sample

becomes highly anisotropic with a cylindrical transverse symmetry as in Figure 1.4.

As the confining pressure is increased more deviatoric stress is required to initiate dilatancy, again a result that was obtained from the crack model developed in Chapter 3 (see for example Figure 3.11 where it is clear that wing crack initiation stress is bigger for higher confining pressures). Also that the crack density rate of increase is slower for high confining pressures, is a result consistent with Figure 3.11 where it is shown that smaller cracks are produced at higher confining pressures.

### 4.10 Cubical Geometry Testing Results.

In this case, three orthogonal  $P$  wave velocities ( $V_{11}, V_{22}, V_{33}$ ) and the three orthogonal  $S$  wave velocities  $V_{12}$  ( $= V_{21}$ ),  $V_{23}$  and  $V_{31}$  ( $= V_{32}$ ) were measured (Stuart, 1992)<sup>1</sup>. This is a more complete approach as we need to assume only orthorhombic symmetry and use the most general equations (4.45-4.51) and calculate from there the three coefficients  $\alpha_{11}$ ,  $\alpha_{22}$  and  $\alpha_{33}$ . In section 4.7 we chose 3 orthogonal velocities and inverted the corresponding equations. As compressional and shear wave measurements were done with different precisions, we decided to separate the data in such a way that we reduced the compressional wave measurements separately from the shear wave ones. In doing so we assure that under inversion each velocity will make equal contribution to the precision of the crack density.

Stuart (1992) obtained expressions for crack densities applying the equations of Hudson (1981) for the velocities of stress waves impinging on an array of parallel penny-shaped cracks at an arbitrary angle. Stuart modelled the PECs by three orthogonal arrays of parallel penny-shaped cracks oriented normal to the principal stress direction, and the new dilatant cracks as separate arrays of parallel cracks oriented with their minor axes parallel to the least compressive stress. He then calculated the crack densities for each array (Stuart, 1992):

$$\alpha_{11} = (V_{23}^2 - V_{12}^2 - V_{31}^2 + V_S^{02}) / (4.63 * (V_S^{02})) , \tag{4.132}$$

$$\alpha_{22} = (-V_{23}^2 - V_{12}^2 + V_{31}^2 + V_S^{02}) / (4.63 * (V_S^{02})) , \tag{4.133}$$

$$\alpha_{33} = (-V_{23}^2 + V_{12}^2 - V_{31}^2 + V_S^{02}) / (4.63 * (V_S^{02})) , \tag{4.134}$$

$$\epsilon = \alpha_{11} + \alpha_{22} + \alpha_{33} . \tag{4.135}$$

Comparison with the results obtained using equations 4.105-4.107 shows that both models give very similar results (Figure 4.7).

<sup>1</sup> The stress in the 3-direction was raised to 81 MPa while the stress in the 2-direction was raised to 41 MPa, with the stress in the 1-direction maintained constant at 4 MPa. The mean stress is  $(\sigma_{11} + \sigma_{22} + \sigma_{33})/3$ . The mean stress is  $(\sigma_{11} + \sigma_{22} + \sigma_{33})/3$ .

The corresponding equations using the 3 orthogonal P-waves deduced in section 4.7 overestimates the values of the  $\alpha$ 's (by about a 15%), but nevertheless comparison with the values obtained from the shear wave velocities gives a very good agreement. (Figure 4.8).

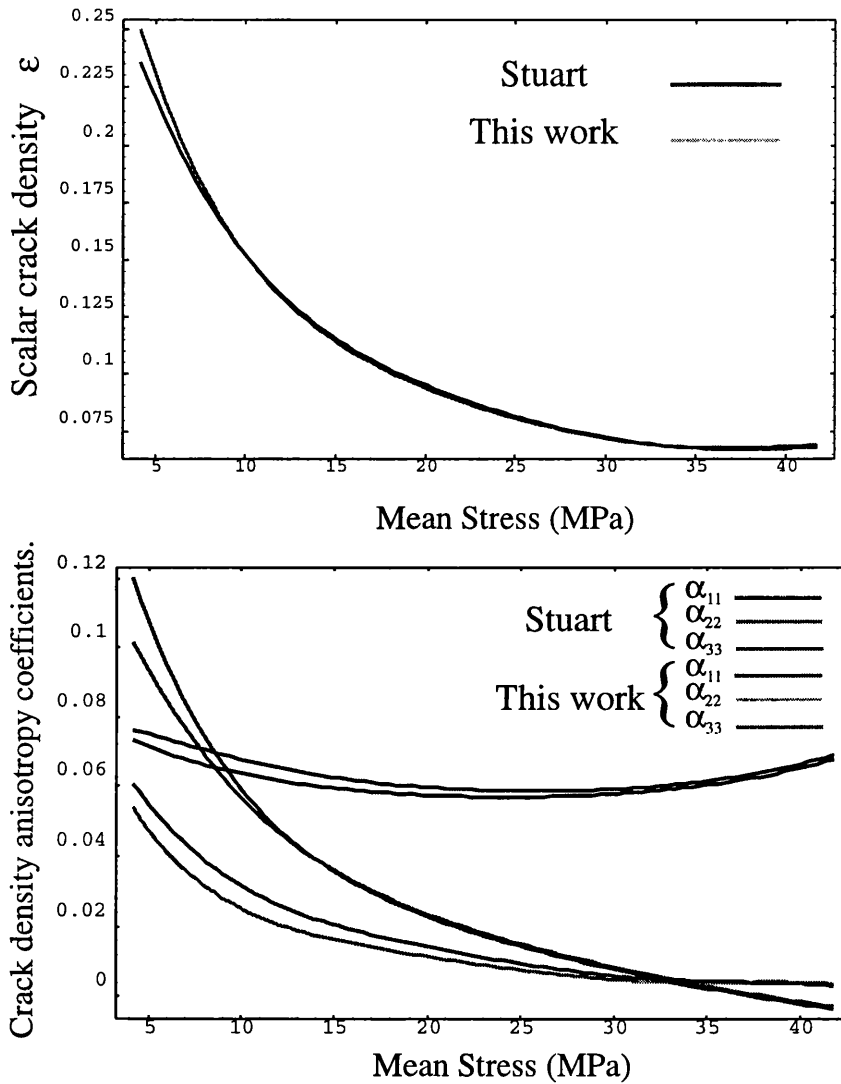


**Figure 4.7:** Scalar crack density  $\epsilon$  and coefficients of the crack density tensor  $\alpha$  as functions of the applied mean stress for a triaxial test. The decrease in the coefficients indicates closure of cracks, the increase suggests opening and generation of new cracks.

In Figures 4.7 and 4.8 we can see that the initial  $\alpha_{11}$  is greater than the other two coefficients, an effect presumably due to the bedding of the sample in the 1-direction. As the test goes on, we can see a marked decrease in  $\alpha_{11}$  and  $\alpha_{22}$  until they become practically equal meanwhile  $\alpha_{33}$  changes very little, decreasing at first but increasing after a while. These results show that the final state in the sample is nearly one of planar transverse

isotropy, because  $\alpha_{33} > \alpha_{11} \approx \alpha_{22} \approx 0$ .

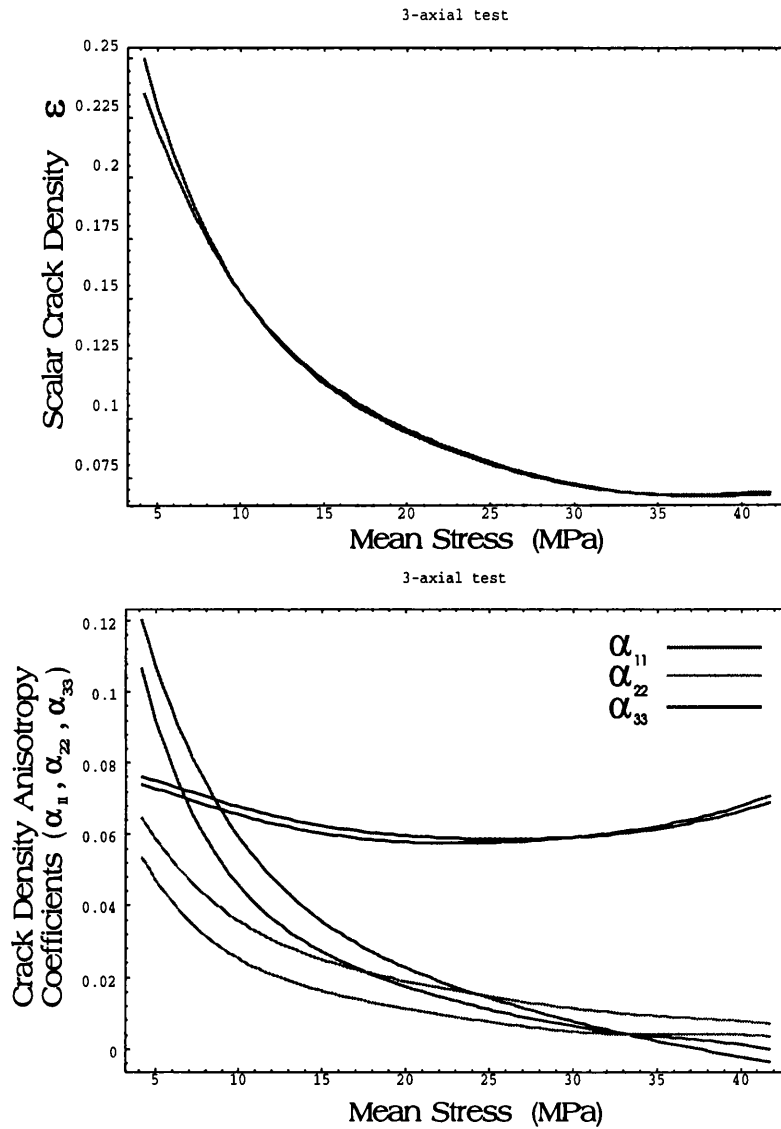


**Figure 4.8:** Scalar crack density  $\epsilon$  and coefficients of the crack density tensor  $\alpha$  as functions of the applied mean stress for a triaxial test. The decrease in the coefficients indicates closure of cracks, the increase suggests opening and generation of new cracks.

The consistency of this treatment can be seen in Figure 4.9 where the predictions of the wave velocities using the crack density tensor fit very well with the experimental data. In Figure 4.9a, the  $P$ -wave velocities are shown, where the crack density tensor was calculated using the  $S$ -wave measurements. In Figure 4.9b, the  $S$ -wave velocities are displayed, here the crack density tensor components were calculated using the  $P$ -wave data.

## 4.11 Conclusions

We have seen that the scheme developed by Sayers and Kachanov (1991) is very suitable for the interpretation of different kind of experimental data. According to the amount of data available we can either make a few simple assumptions about the symmetry of the problem and obtain very useful information about the changes of crack density, or alternatively assume an arbitrary orientation distribution and obtain the symmetry involved in the problem.

The increase in velocity in the initial stage of deformation is connected with the increase in area of contact between the grains and between discontinuities, this is due to the closure of cracks and pores under the increasing pressure. The maximum in velocity is achieved when in the wave direction this closure is perfect. The decrease following the peak velocity is due to the increase of number of cracks in one particular direction as indicated by the different behaviour of the crack density anisotropy coefficients, this may be connected to the generation of new cracks (NDCs) from PECs.

Some of the results obtained in this chapter concerning the evolution of crack population are in very good agreement with the results obtained from the crack model developed in chapter 3: i) Crack growth preferentially orientated with the major axis of compression (anisotropy), ii) the dependence of initiation of dilatancy with confining pressure, and iii) the influence of confining pressure on the stabilisation of the sample and on crack density growth.

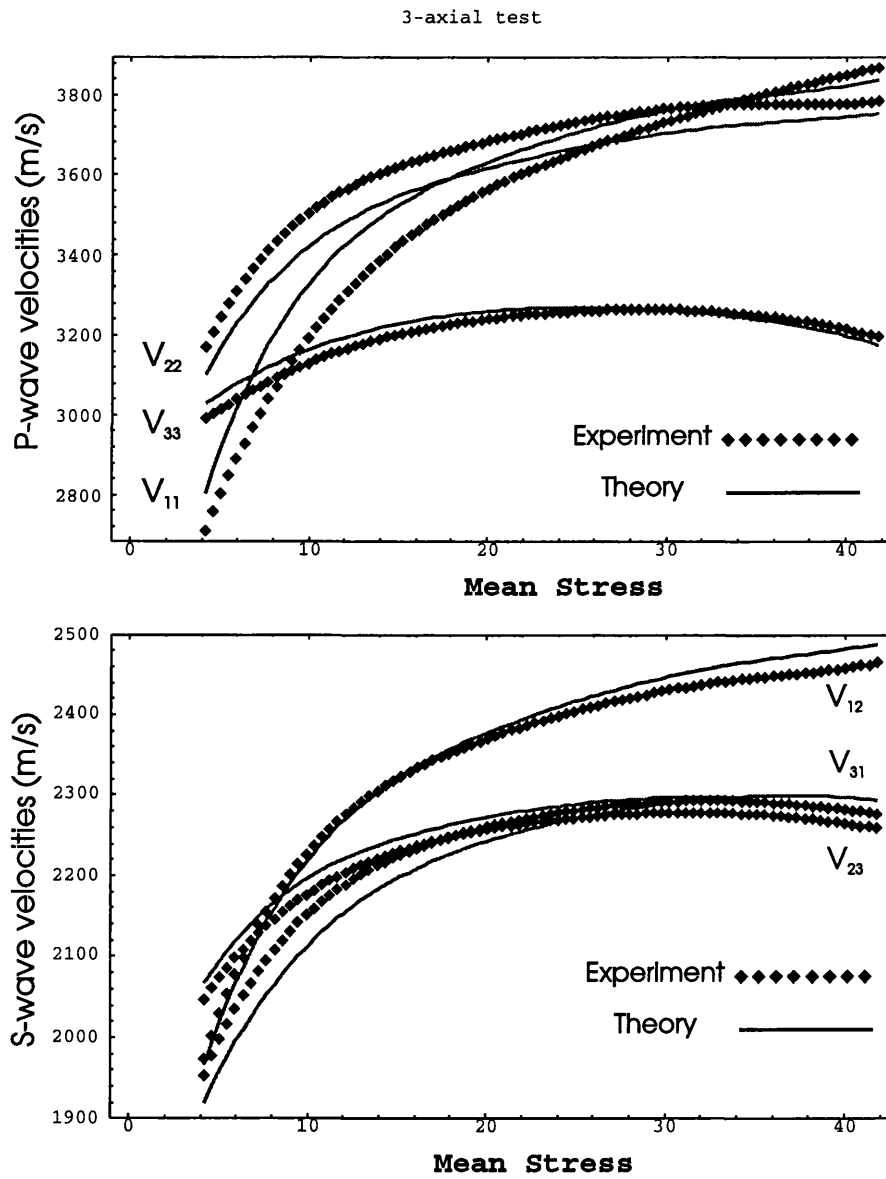


**Figure 4.9:** Changes in compressional and shear wave velocities with mean stress. The P-wave velocities in the first plot were calculated from shear wave data. The S-wave velocities in the second graph were calculated from compressional wave data.

## Chapter 5

# Discussion and Conclusions

We have seen that starting from submacroscopic considerations, it is possible to build up a macroscopic fracture criterion, *i.e.*, we were able to find a relation between the stresses that tell us when a crack will start to propagate catastrophically under the influence of the applied stresses. This criterion although sufficient to cause massive fracture may not be attainable as interaction between cracks may take place before that.

For the modelling of the massive fracture, it is necessary to know how long will a single crack grow as a function of the applied stresses, because that will define the range of the interaction between cracks. It is of interest, therefore, to study the length and stability of a wing crack branching from a pre-existing crack.

The initiation and growth of wing cracks in a body under load, has been modelled using the maximum local tensile stress criterion. The relations between applied loads and direction and magnitude of the extension of the wing crack have been found by modelling the initial flaw as a dislocation that will wedge open the wing crack. The Burgers vector of this dislocation depends on the elastic properties of the material, the size of the original cracks, and the applied stresses.

With the static wing crack model it is possible to study the system under both tensile and compressive stress fields. In the tensile case the growth is unstable, so once the wing crack is formed, it continues to grow until failure of the specimen occurs. In the compressive case, initiation of the wing crack is followed by a period of stable propagation where increasing loads are necessary to make the crack extend further. At high levels of stress the crack might be unstable but it is necessary to consider that at that level there are other cracks growing and that the interaction between them could lead to macroscopic fracture at stresses below the calculated ultimate stress of a single crack.

In the uniaxial compression case, the increasing applied stress closes more and more pre-existing cracks and as a result more than half of the NDCs are nucleated or driven open by sliding closed cracks. The presence of confining pressure closes even a bigger proportion of the pre-existing cracks, leaving open only those PECs that are quasi-parallel to the maximum compressive stress. The range of PECs nucleating wing cracks is reduced with confining pressure. Also, higher stresses are needed to nucleate NDCs as confining pressure is increased, therefore the elastic part of the deformation is increased.

Another contribution of this work is the realisation that the initial stability of NDCs emerging from PECs of the most "dangerous" orientation allows other PECS of a wider distribution of orientations being active in developing NDCs. This active population of cracks will have an impact in the mechanical properties of the material, specifically the strength.

We found that experimental data of stress at failure at different confining pressures for different rocks, falls in a line corresponding to 35% to 45% (depending on the coefficient of friction used) of PECs nucleating NDCs. This line may define a critical concentration of cracks. On the other hand we have found that the presence of confining pressure stabilise the wing cracks, and at the same time does not allow long wing cracks, making coalescence very improbable. We also found that the experimental values of failure stress for each particular rock can match with the theoretical value if we choose the right coefficient of friction.

We obtained axial, lateral and volumetric strains curves for uniaxial and biaxial compression. In them 3 regions of deformation can be appreciated. There is an initial change in the Young's modulus due to the closure of PECs, then a linear deformation region that is longer for high confining pressure, and finally there is a non-linear region that is due to the nucleation and growing of NDCs.

We have determined direction of faulting from the orientation of the first unstable NDC at the ultimate stress  $\sigma_f$ . In agreement with experimental data, this angle of fracture increase with confining pressure.

When there is an increasing population of cracks the overall properties of the material will change<sup>1</sup>, and the static and dynamic of the structure can be better analysed through statistical mechanics or under the light of continuum solid mechanics, formulating the problem in terms of constitutive equations. One of the remarkable changes that occurs is the anisotropy of this 'new' material due to the fact that these wing cracks have certain preferred orientations.

<sup>1</sup> Kachanov (1992)

In chapter 4 we analysed some specific crack orientations in terms of the crack density tensor, and explained some experimental results under the light of it. This approach is very useful to obtain the variation of crack density and anisotropy coefficients with applied stress. We can explain some features of these crack populations in terms of the crack model developed in chapter 3.

A possible important extension of the model would be to allow cracks of different sizes and aspect ratios. This could be treated in the same manner as identical cracks of different orientations. Also a 3-dimensional extension to the wing crack model is of interest though the mathematics involved is more complex.

A much more significant extension of the model would be to add a model of inelastic crack interaction, based on percolation theory. The nature of crack/pore connections is not yet well understood. Methods by which this might be experimentally studied also need to be developed. This extension of the model is needed before the physical processes of ultimate failure (fracture or cataclastic flow) can be properly modelled.

# References

- E.M. Anderson. *The Dynamics of Faulting*. Oliver and Boyd, Edinburgh, 2nd ed., 1951.
- M.F. Ashby and S.D. Hallam. The failure of brittle solids containing small cracks under compressive stress states. *Acta Metallurgica* , **34**(3):497–510, 1986.
- B.K. Atkinson and P.G. Meredith. The theory of subcritical crack growth with applications to minerals and rocks. In *Fracture Mechanics of Rock*, pages 111–166. edited by Atkinson, B.K., Academic Press Inc., London, 1987.
- P. Aves. , **Ph.D. Thesis**. University of London., 1995.
- M.R. Ayling. *An Experimental Study of Physical Property Changes in Crustal Rocks Undergoing Triaxial Deformation*, **Ph.D. Thesis**. University of London., 1991.
- M.R. Ayling, P.G. Meredith, and S.A.F Murrell. Microcracking during triaxial deformation of porous rocks monitored by changes in rock physical-properties .1. elastic-wave propagation measurements on dry rocks. *Tectonophysics* , **245**(3-4):205–221, 1995.
- M. Barquins and J.P. Petit. Kinetic instabilities during the propagation of a branch crack -effects of loading conditions and internal-pressure. *J. of Structural Geology*, **14**(8-9):139–163, 1992.
- M. Barquins, J.P. Petit, D. Maugis, and K. Ghalayini. Path and kinetics of branching from defects under uniaxial and biaxial compressive loading. *Int. J. of Fracture*, **54**(No. 2):139–163, 1992.
- R.A. Batto and E.M. Schulson. On the ductile-to-brittle transition in ice under compression. *Acta Metallurgica et Materialia*, **41**(7):2219–2225, 1993.
- C.A. Berg. The deformation of fine cracks under pressure and shear. *J. Geophys. Res.*, **70**:3447–52, 1965.

- Y. Bernabe and W.F. Brace. Deformation and fracture of berea sandstone. In *The Brittle-Ductile Transition in Rocks: the Heard volume Geophys. Monogr. Ser.*, volume **56**, pages 91–101. edited by A.G. Duba, W.B. Durham, J.W. Handin and H.F. Wang, AGU, Washington, D.C., 1990.
- F. Birch. The velocity of compressional waves in rocks to 10 kilobars. part 1. *J. Geophys. Res.*, **65**:1083–1102, 1960.
- B.P. Bonner. Shear wave birefringence in dilating granite. *Geophys. Res. Lett.*, **1**:217–220, 1974.
- W.F. Brace and Bombalakis E.G. A note on brittle crack growth in compression. *J. Geophys. Res.*, **68**:3709–13, 1963.
- P.W. Bridgman. *The Physics of High Pressure*. Bell, London, 1931.
- J.R. Bristow. Microcracks and the static and dynamic elastic constants of annealed and heavily cold-worked metals. *Fr. J. Appl. Phys.*, **11**:81–85, 1960.
- W.M. Bruner. Comment on ‘seismic velocities in dry and saturated cracked solids’ by r.j. o’connell and b. budiansky. *J. Geophys. Res.*, **81**:2573–2576, 1976.
- B. Budiansky. On the elastic moduli of some heterogeneous materials. *J. Mech. Phys. Solids*, **13**:223–227, 1965.
- B. Budiansky and R.J. O’Connell. Elastic moduli of a cracked solid. *Int. J. Solids Structures*, **12**:81–97, 1976.
- N.P. Cannon, E.M. Schulzon, T.R. Smith, and H.J. Frost. Wing cracks and brittle compressive fracture. *Acta Metall. Mater.*, **38**(10):1955–1962, 1990.
- K.J. Chang. On the maximum strain criterion- a new approach to the angled crack problem. *Eng. Fracture Mech.*, **14**:107–124, 1981.
- S. Crampin. Geological and industrial applications of extensive-dilatancy anisotropy. *Nature*, **328**:491–6, 1987.
- P.M. Davis and L. Knopoff. The elastic modulus of media containing strongly interacting antiplane cracks. *J. Geophys. Res.*, **100**(B9):18,253–18,258, 1995.

- O. Edmond and S.A.F. Murrell. Experimental observations on rock fracture at pressures up to 7 kbar and the implications for earthquake faulting. *Tectonophysics*, **16**:71–87, 1972.
- J.D. Eshelby. The determination of the elastic field of an ellipsoidal inclusion and related problems. *Proc. Roy. Soc.*, **A241**:376–396, 1957.
- R.V. Goldshtein. Fractal cracks. *PMM J. of Appl. Mathematics and Mech.*, **56(4)**:563–571, 1992.
- L. Granryd, I.C. Getting, and H. Spetzler. Path dependence of acoustic velocity and attenuation in experimentally deformed westerly granite. *Geophys. Res. Letters*, **10(1)**:71–74, 1983.
- A.A. Griffith. The phenomena of rupture and flow in solids. *Phil. Trans. Roy. Soc., Ser. A*, **221**:163–98, 1920.
- A.A. Griffith. Theory of rupture. In *Proc. First Int. Congress in Appl. Mech.*, pages 55–63. Delft, 1924.
- Y. Gueguen and V. Palciauskas. *Introduction to the Physics of Rocks*. Princeton University Press, New Jersey, 1994.
- I.N. Gupta. Seismic velocities in rock subjected to axial loading up to shear fracture. *J. Geophys. Res.*, **78**:6936–6942, 1973.
- K. Hadley.  $v_P/v_S$  anomalies in dilatant rock samples. *Pure Appl. Geophys.*, **113**:1–23, 1975.
- N. Hast. Global measurements of absolute stress. *Phil. Trans. R. Soc. London*, **274**:409–419, 1973.
- F.S. Henyey and N. Pomphrey. Self-consistent moduli of a cracked solid. *Geophys. Res. Lett.*, **9**:903–906, 1982.
- G. Herget. Variation of rock stresses with depth at a canadian iron mine. *Int. J. Rock Mech. Min. Sci.*, **10**:37–51, 1973.
- S.H. Hickman. Stress in the lithosphere and the strength of active faults. *Reviews of Geophysics, supplement*, pages 759–775, 1991.

- R. Hill. A self-consistent mechanics of composite materials. *J. Mech. Phys. Solids*, **13**:213–222, 1965.
- A. Hoenig. Elastic moduli of a non-randomly cracked body. *Int. J. Solids Structures*, **15**:137–154, 1979.
- H. Horii and S. Nemat-Nasser. Compression-induced microcrack growth in brittle solids - axial splitting and shear failure. *J. of Geophys. Res.-Solid Earth and Planets*, **90**(NB4):3105–3125, 1985.
- H. Horii and S. Nemat-Nasser. Brittle failure in compression - splitting, faulting and brittle-ductile transition. *Philosophical Transactions of the Royal Society of London Series A- Mathematical and Physical Sciences*, **319**(1549):337–374, 1986.
- J.A. Hudson. Overall properties of a cracked solid. *Math. Proc. Camb. Phil. Soc.*, **88**:371–384, 1980.
- J.A. Hudson. Wave speeds and attenuation of elastic waves in material containing cracks. *Geophys. J. Royal Astr. Soc.*, **64**:133–150, 1981.
- J.A. Hudson. A higher order approximation to the wave propagation constants for a cracked solid. *Geophys. J. Royal Astr. Soc.*, **87**:265–274, 1986.
- J.A. Hudson. Overall elastic properties of isotropic materials with an arbitrary distribution of circular cracks. *Geophys. J. Int.*, **102**:965–969, 1990.
- C.E. Inglis. Stresses in a plate due to the presence of cracks and sharp corners. *Trans. Instn. Nav. Archit, London*, **55**:219–41, 1913.
- G.R. Irwin. Analyses of stresses and strains near the end of a crack traversing a plate. *J. Appl. Mech.*, **24**:361–4, 1957.
- I.A.H. Ismail and S.A.F. Murrell. Dilatancy and the strength of rocks containing pore water under undrained conditions. *Geophys. J. R. Astronom. Soc.*, **44**:107–134, 1976.
- J.C. Jaeger and N.G.W. Cook. Pinching-off and diskings of rocks. *J. of Geophys. Res.*, **68**:1759–1765, 1963.
- J.C. Jaeger and N.G.W. Cook. *Fundamentals of Rock Mechanics*. Chapman and Hall, London, 3rd ed., 1979.

- H. Jeffreys. *The Earth*. Cambridge., 1959.
- C. Jones. *An experimental study of the relationship between P-wave velocity, acoustic emission and deformation in rocks under simulated crustal conditions*, **Ph.D. Thesis**. University of London., 1988.
- C. Jones and S.A.F. Murrell. Acoustic compressional wave velocity and dilatancy in triaxially stressed rock. *Rock at Great Depth*, 1:241–247, 1989.
- M. Kachanov. Continuum model of medium with cracks. *J. Eng. Mech. Div. ASCE*, **106**:1039–1051, 1980.
- M. Kachanov. Microcrack model of rock inelasticity, part i: Frictional sliding on pre-existing microcracks. *Mech. Mater.*, 1:3–18, 1982.
- M. Kachanov. Effective elastic properties of cracked solids: critical review of some basic concepts. *Appl. Mech. Rev.*, **45**(No. 8):304–335, 1992.
- H. Kanamori. The state of stress in the earth's lithosphere. In *Physics of the Earth's Interior, Proc. Int. School of Physics "Enrico Fermi"*, pages 531–552. North-Holland, 1980.
- H. Kanamori and D. Anderson. Theoretical basis of some empirical relations in seismology. *Bull. Seismol. Soc. Am.*, **65**:1073–95, 1975.
- S. Kanaun. Poisson's field of cracks in elastic medium. *J. Appl. Math. & Mech.*, **44**(6):808–815, 1980.
- S. Kanaun. Elastic medium with random field of inhomogeneities. In *Elastic media with microstructure*, volume **2**, pages 165–228. Springer, Berlin, 1983.
- J. Kemeny and N.G.W. Cook. Effective moduli, non-linear deformation and strength of cracked elastic solids. *Int. J. Rock Mech. Mining Sci. Geomech. Abstr.*, **23**:107–118, 1986.
- J. Kemeny and N.G.W. Cook. Micromechanics of deformation in rocks. In *Toughening Mechanisms in Quasi-Brittle Materials*, pages 155–188. Kluwer Academic Publishers, Dordrecht, 1991.
- R.L. Kranz. Microcracks in rock: A review. *Tectonophysics*, **100**:449–480, 1983.

- B.R. Lawn. *Fracture of Brittle Solids*. 2nd ed., Cambridge University Press, 1993.
- C.L. Li and E. Nordlund. Deformation of brittle rocks under compression -with particular reference to microcracks. *Mech. of Materials*, **15**(3):223–239, 1993.
- D.A. Lockner, J.B. Walsh, and J.D. Byerlee. Changes in seismic velocity and attenuation during deformation of granite. *J.Geophys. Res.*, **82**:5374–5378, 1977.
- I.G. Main, P.G. Meredith, P.R. Sammonds, and C. Jones. Influence of fractal flaw distributions on rock deformation in the brittle field. In *Deformation Mechanisms, Rheology and Tectonics*, volume **54**, pages 81–96. Geol. Soc. Lond. Spec. Pub., 1990.
- D. Maugis. Stresses and displacements around cracks and elliptic cavities-exact-solutions. *Eng. Fracture Mech.*, **43**(2):217–255, 1992.
- K. Mogi. Some precise measurements of fracture strength of rocks under uniform compressive stress. *Rock Mech. Eng. Geol.*, **4**:41–55, 1966.
- S.A.F. Murrell. The theory of the propagation of elliptical griffith cracks under various conditions of plane strain or plane stress. part i. *Br. J. Appl. Phys.*, **15**:1195–1210, 1964. Part II and III, *ibid*, 1211-1223.
- S.A.F. Murrell. The effect of triaxial stress systems on the strength of rocks at atmospheric temperatures. *Geophys. J. R. Astron. Soc.*, **10**:231–281, 1965.
- S.A.F. Murrell. Mechanics of tectogenesis in plate collision zones. In *Collision Tectonics*, pages 95–111. Geological Society Special, Publication No.19, 1986.
- S.A.F. Murrell. General report: The measurements of the properties at greath depth of rocks and rock masses. In *Rock at Greath Depth, Vol. III*, pages 1219–1229. Balkema, Rotterdam, 1990.
- S.A.F. Murrell and P.J. Digby. The theory of brittle fracture initiation under triaxial stress conditions. part i. *Geophys. J. R. Astron. Soc.*, **19**:309–334, 1970. Part II, *ibid*, 499-512.
- S.A.F. Murrell and I.A.H. Ismail. The effect of decomposition of hydrous minerals on the mechanical properties of rocks at high pressures and temperatures. *Tectonophysics*, **31**:207–258, 1976.

- S.A.F. Murrell, P.G. Meredith, P.R. Sammonds, M.R. Ayling, and C. Jones. High temperature triaxial apparatus for acoustic measurements. In *Rock at Great Depth*, volume 1, pages 291–296. Balkema, Rotterdam, 1989.
- N.I. Muskhelishvili. *Some Basic Problems of the Mathematical Theory of Elasticity*. Groningen: Noordhoff, 1953. 3rd edn.
- S. Nemat-Naser and M. Hori. *Micromechanics: Overall properties of heterogeneous materials*. Elsevier, 1993.
- S. Nemat-Nasser and H. Deng. Strain-rate effect on brittle failure in compression. *Acta Metallurgica et Materialia*, **42**(3):1013–1024, 1994.
- A. Nur and G. Simmons. Stress-induced velocity anisotropy in rock: an experimental study. *J. Geophys. Res.*, **74**:6667–6674, 1969.
- R.J. O'Connell and B. Budiansky. Seismic velocities in dry and saturated cracked solids. *J. Geophys. Res.*, **79**:5412–5426, 1974.
- E. Orowan. The fatigue of glass under stress. *Nature*, **154**:341–43, 1944.
- E. Orowan. Fundamentals of brittle behaviour in metals. In *Fatigue and Fracture in Metals*, pages 139–67. Wiley, New York, 1952.
- Z. Ouyang and D. Elsworth. A phenomenological failure criterion for brittle rock. *Rock Mech. and Rock Eng.*, **24**(3):133–153, 1991.
- M.S. Paterson. *Experimental Rock Deformation - The Brittle Field*. Springer, Berlin, 1978. 254 pp.
- T. Pöschl. Über eine particular lösung des biharmonischen problems für den anbeuraum einer ellipse. *Math. Z.*, **11**:89–96, 1921.
- M.A. Rist and S.A.F. Murrell. Ice triaxial deformation and fracture. *J. of Glaciology*, **40**(135):305–318, 1994.
- P.R. Sammonds, M.R. Ayling, C. Jones, P.G. Meredith, and S.A.F. Murrell. A laboratory investigation of acoustic emission and elastic wave velocity changes during rock failure under triaxial stresses. In *Rock at Great Depth*, volume 1, pages 233–240. Balkema, Rotterdam, 1989.

- C.M. Sayers and M. Kachanov. A simple technique for finding effective elastic constants of cracked solids for arbitrary crack orientation statistics. *Int. J. Solids Structures*, **27(6)**: 671-680, 1991.
- C.M. Sayers and J.G. van Munster. Microcrack-induced seismic anisotropy of sedimentary rocks. *J. Geophys. Res.-Solid Earth*, **96(NB10)**:16529-16533, 1991. accepted for publication in.
- C.M. Sayers, J.G. van Munster, and M.S. King. Stress-induced ultrasonic anisotropy in Berea sandstone. *Int. J. Rock Mech.*, **27**:429-436, 1990.
- C.H. Scholz. Microfracturing and the inelastic deformation of rock in compression. *J. Geophys. Res.*, **73**:1417-32, 1968.
- C.H. Scholz. *The mechanics of earthquakes and faulting*. Cambridge University Press, 1990.
- C.H. Scholz, G. Boitnott, and S. Nemat-Nasser. The Bridgman ring paradox revisited. *PAGEOPH*, **124**:587-599, 1986.
- T.R. Smith and E.M. Schulson. The brittle compressive failure of fresh-water columnar ice under biaxial loading. *Acta Metallurgica et Materialia*, **41(1)**:153-163, 1993.
- P.S. Steif. Crack extension under compressive loading. *Eng. Fracture Mech.*, **20(3)**:463-473, 1984.
- C.E. Stuart. *Evolution of Anisotropic Microcrack Damage in Cyclically Stressed Rock, Characterized By Contemporaneous Acoustic Emission and Elastic Wave Velocity Measurements*, **Ph.D. Thesis**. University of London., 1992.
- C.E. Stuart, P.G. Meredith, S.A.F. Murrell, and J.G. VanMunster. Anisotropic crack damage and stress-memory effects in rocks under triaxial loading. *Int. J. of Rock Mech. and Mining Sciences & Geomechanics Abstracts*, **30(7)**:937-941, 1993.
- D.L. Turcotte. Mechanisms of crustal deformation. *J. Geol. Soc. London*, **140**:701-724, 1983.
- D.L. Turcotte and G. Schubert. *Geodynamics: Applications of Continuum Physics to Geological Problems*. John Wiley and Sons, New York, 1982.

- A.A. Vakulenko and M. Kachanov. Continuum theory of medium with cracks. *Mehanika Tverdogo Tela*, 6:159–166, 1971.
- J.B. Walsh. The effect of cracks on the compressibility of rocks. *J. Geophys. Res.*, 70(2):381–389, 1965.
- J.B. Walsh. New analysis of attenuation in partially melted rock. *J. Geophys. Res.*, 78:4333–4337, 1969.
- T.F. Wong. A note on the propagation behaviour of a crack nucleated by a dislocation pileup. *J. of Geophys. Res.*, 95:8639–8646, 1990.
- H.C. Wu and K.J. Chang. Angled elliptic notch problem in compression and tension. *ASME J. of Appl. Mech.*, 45:258–262, 1978.
- C. Zener. *Fracturing of metals*. New York: Amer. Soc. Metals, 1948.
- B. Evans, J.T. Fredrich and T.-f. Wong. The Brittle-Ductile Transition in Rocks: Recent Experimental and Theoretical Progress. In *The Brittle-Ductile Transitions in Rocks: The Heard volume, Geophys. Monogr. Ser.*, volume 56, pages 1-20, edited by A.G.Duba, W.B. Durham, J.W. Handin and H.F. Wang, AGU, Washington, D.C., 1990.
- S.A.F. Murrell. Natural faulting and the mechanics of brittle shear failure. *J. Geol. Soc. Lond.* 133:175-189, 1977.
- C.M. Sayers and M. Kachanov. Microcrack-induced elastic wave anisotropy of brittle rocks. *J. Geophys. Res.*, 100(B3):4149-4156, 1995.
- S. Timoshenko and J.N. Goodier, *Theory of Elasticity*, 3rd. ed., McGraw-Hill, Kogakucha, 1970.
- D. Lockner. The role of Acoustic Emission in the Study of Rock Fracture. *Int. J. Rock Mech. Min. Sci. & Geomech. Abstr.* 30(7):883-899, 1993.